

Climate Change Initiative Extension (CCI+) Phase 1  
New Essential Climate Variables (NEW ECVS)  
High Resolution Land Cover ECV (HR\_LandCover\_cci)

Climate Assessment Report  
(CAR)

Prepared by:

Università degli Studi di Trento  
Fondazione Bruno Kessler  
Université Catholique de Louvain  
Università degli Studi di Pavia  
Università degli Studi di Genova  
Politecnico di Milano  
Université de Versailles Saint Quentin  
CREAF  
e-GEOS s.p.a.  
Planetek Italia  
GeoVille



	Ref	CCI_HRLC_Ph1-CAR		
	Issue	Date	Page	
	3.0	28/10/2022	1	

## Changelog

Issue	Changes	Date
1.0	First version.	16/07/2020
2.0	Second version.	20/10/2021
3.0	Third version	28/10/2022

## Detailed Change Record

Issue	RID	Description of discrepancy	Sections	Change

	Ref	CCI_HRLC_Ph1-CAR		
	Issue	Date	Page	
	3.0	28/10/2022	2	

## Contents

<b>1</b>	<b>Introduction.....</b>	<b>5</b>
1.1	Executive summary.....	5
1.2	Purpose and scope .....	6
1.3	Applicable documents .....	6
1.4	Reference documents.....	6
1.5	Acronyms and abbreviations .....	6
<b>2</b>	<b>Land Cover from MRLC on our 3 study regions (static and historical): analysis and potential issues .....</b>	<b>8</b>
2.1	LC and LCC (1992-2018) over Amazonia.....	8
2.2	LC and LCC (1992-2018) over Sahel .....	9
2.3	LC and LCC (1992-2018) over Siberia.....	10
<b>3</b>	<b>Use of Biomass products to improve the interpretation of MRLC classes in terms of Plant Functional Types for land surface models.....</b>	<b>11</b>
3.1	Using biomass product with land cover data in ORCHIDEE.....	11
3.2	Refinement of the description of LC classes in terms of PFTs with Biomass data.....	13
<b>4</b>	<b>New Cross-Walking tables (CWTs) to convert HRLC classes to Generic PFTs and to ORCHIDEE PFTs .....</b>	<b>14</b>
<b>5</b>	<b>HRLC in ORCHIDEE: PFT building and comparisons with MRLC.....</b>	<b>17</b>
<b>6</b>	<b>Coherence of MRLC and surface albedo changes in satellite products and comparison to ORCHIDEE ....</b>	<b>20</b>
6.1	GlobAlbedo product .....	20
6.2	Albedo changes observed.....	20
6.3	Comparison with ORCHIDEE .....	21
<b>7</b>	<b>Use of MRLC in ORCHIDEE to assess LCC impacts on carbon, water and energy surface budgets .....</b>	<b>23</b>
7.1	Analysis.....	24
7.1.1	Globally.....	24
7.1.2	South Brazil.....	24
<b>8</b>	<b>First use of HRLC in ORCHIDEE to assess the improvements or deteriorations on the carbon, water and energy budgets with respect to MRLC.....</b>	<b>25</b>
<b>9</b>	<b>Implementation and validation of LMDZ IPSL ESM on our 3 studied regions .....</b>	<b>27</b>
9.1	LMDZ description.....	27
9.2	Zoom implementation in the 3 study regions .....	28
9.3	Simulations performed .....	28
<b>10</b>	<b>New albedo optimization in ORCHIDEE.....</b>	<b>31</b>
<b>11</b>	<b>Analysis of land cover – atmosphere feedbacks with ORCHIDEE-LMDZ .....</b>	<b>32</b>
11.1	Amazonian region.....	32
11.1.1	PFT maps used in the simulations.....	33
11.1.2	Impacts of HRLC-MRLC differences on surface variables .....	34
11.1.3	Land cover – atmosphere feedback analysis .....	34
11.1.4	Comparison with observations .....	35
11.2	Africa.....	36

11.2.1	PFT maps used in the simulations.....	36
11.2.2	Land cover impacts on surface variables .....	37
11.2.3	Land cover – atmosphere feedback analysis .....	38
11.2.4	Comparison with observations .....	39
11.3	Siberia .....	39
11.3.1	PFT maps used in the simulations.....	39
11.3.2	Land cover impacts on surface variables .....	41
11.3.3	Land cover – atmosphere feedback analysis .....	41
11.3.4	Comparison with observations .....	44
<b>12</b>	<b>Analysis of the land cover change product on 3 regions.....</b>	<b>44</b>
<b>13</b>	<b>Sensitivity of ORCHIDEE to LCC on Amazonia .....</b>	<b>45</b>
<b>14</b>	<b>Ecosystem changes model using VI time series, Medium Resolution (MR) land cover maps and climate variables .....</b>	<b>48</b>
14.1	Materials.....	49
14.1.1	Remote sensing images and derived products .....	49
14.1.2	Land cover maps .....	49
14.1.3	Drought climate models and its derived variables .....	49
14.2	Methodology .....	50
14.2.1	Spatio-temporal selection.....	50
14.2.2	EFT generation .....	52
14.2.3	Selected Land Cover Changes .....	55
14.3	Analysis and conclusions .....	56
14.3.1	Tree loss analysis .....	58
14.3.2	Tree gain analysis.....	60
14.3.3	Urban growth.....	61
14.3.4	Crop expansion .....	63
<b>15</b>	<b>Ecosystem changes model with HR land cover final product.....</b>	<b>64</b>
15.1	Materials.....	64
15.1.1	Remote sensing images and derived products .....	64
15.1.2	Land cover maps .....	64
15.2	Methodology and results.....	64
15.2.1	EFT generation .....	65
15.2.2	Correlation between LC changes and EFT changes at HR.....	67
15.2.3	Tree/shrub loss analysis.....	69
15.2.4	Tree/shrub gain analysis .....	71
15.2.5	Urban growth analysis .....	72
15.2.6	Crop expansion analysis.....	73
15.3	Discussion .....	74
<b>16</b>	<b>Comparison between MR and HR LC products .....</b>	<b>75</b>
16.1	KPIs on ORCHIDEE.....	75

	Ref	CCI_HRLC_Ph1-CAR		
	Issue	Date	Page	
	3.0	28/10/2022	4	

16.2	KPIs on Landscape metrics .....	75
16.2.1	Shannon diversity index.....	75
16.2.2	Edge density.....	77
16.3	KPI's on Ecosystem functional metrics .....	77
16.3.1	Confusion matrix.....	77
16.3.2	Detrended Correspondence Analysis .....	78
<b>17</b>	<b>References .....</b>	<b>78</b>
	<b>Appendix A: CWT-ORCH v2 .....</b>	<b>82</b>
	<b>Appendix B: EFT components at MR.....</b>	<b>83</b>
	<b>Appendix C: EFT maps at HR.....</b>	<b>86</b>
	<b>Appendix D: Land Cover Changes Mapping priorities .....</b>	<b>87</b>

	Ref	CCI_HRLC_Ph1-CAR		
	Issue	Date	Page	
	3.0	28/10/2022	5	

## 1 Introduction

### 1.1 Executive summary

This CAR document reports the work that has been done during the three years of the ESA HRLC project within the “Product Assessment” work packages (WP1510L&M, WP2510L&M), by the LSCE and CREAM climate teams. Given that the HRLC products were not available to the climate users during the first two years of that period, part of the studies are based either on the MRLC maps and MERIS data at 300 m resolution, or on higher resolution satellite products like Landsat and aerial imagery available through Google Earth Engine platform. These works helped firstly, to better diagnose some of the deficiencies of the MRLC product and of the methods developed to use the land cover maps in climate modeling (especially the mapping of the land cover classes into Plant Functional Types used by global land surface models), secondly to develop the modeling tools that will be used for the HRLC product assessment. As a result, we have carried out preliminary developments in the ORCHIDEE land surface model and the LMDZ atmospheric model, in order to better describe the land cover heterogeneity in every grid cell and improve some of the biophysical parameterizations linked to the surface-atmosphere coupling. A first version of the HRLC products which were only available over selected tiles, have also been used to assess the contribution of HRLC compared to MRLC in ORCHIDEE and helped to define the key performance indices that will be used in the final step of the project to compare both products. Finally, we present the simulations and analysis performed with the HRLC final production (static maps and historical products). In summary, this first version of the CAR document presents the following results:

- some guidelines to improve the interpretation of the MRLC land cover classes in our studied regions and to revise it regionally,
- the methodology developed to refine the Cross Walking Table used to translate land cover classes into Plant Functional Types,
- the added value of auxiliary products like satellite derived Above Ground Biomass products (ABG) to improve woody/herbaceous coverage fractions,
- some guidelines to revise the surface albedo calibration in ORCHIDEE and to better account for water bodies, the set-up of the optimization process and the results obtained globally,
- some guidelines to use the upcoming HRLC dataset in an optimal way and some first highlights of its expected contribution for climate modeling, i.e., a better characterization of the croplands, in particular of its woody character, a better separation between croplands and grasslands, a better characterization of the vegetation organisation within the grid cell, a better characterization of the land cover changes (class transitions and localisation),
- the ORCHIDEE and LMDZ simulations performed based on the final HRLC production and the results obtained highlighting the crucial role of land cover and albedo on the land-atmosphere feedbacks,
- a methodology for identifying the coupled role of land cover and climate change in the dynamics of ecosystem functionality. This methodology was prepared with MR products and it was adapted to the HR product version 1.
- the analysis of the relationship between the presented Ecosystem Functional Types (EFT) model and selected interesting land cover transitions
- the use of the quality layers of the HR product (first and second best classes and corresponding probabilities) for filtering LC changes
- the KPIs evaluation of the benefits of changing spatial resolution from MR to HR

	Ref	CCI_HRLC_Ph1-CAR		
	Issue	Date	Page	
	3.0	28/10/2022	6	

## 1.2 Purpose and scope

In this document, we report the methods/tools that we have developed to prepare the assessment of the HRLC products for climate modeling and the results obtained with preliminary products. The different axis/questions that have been studied are the following:

- how MRLC products allow to assess land cover (LC) and land cover changes (LCC) on our 3 study regions, their deficiencies and the expected contribution of HRLC to better interpret the land cover classes in terms of ORCHIDEE Plant Functional Types (PFTs)
- a complementary study on the potential of Above Ground Biomass data (estimated from satellite observations) to improve the split of land cover classes in terms of tree versus short vegetation PFTs.
- the new CWTs developed for the HRLC products
- the coherence with the satellite albedo products and the capacities of ORCHIDEE to simulate the observed values and time evolution
- the results of a new albedo optimization method
- the sensitivity of ORCHIDEE simulated energy, water and carbon (e-w-c) fluxes to LCC
- how the IPSL LMDZ climate model has been settled and performs in the studied regions and what are the expected surface/atmosphere retroactions
- the results of the simulations performed with the final HRLC production on the 3 studied regions,
- the dynamics of Ecosystem Functional Types (EFTs) as a result of an integrated model of climate and land cover changes
- the discrimination between climate and LCC drivers in the main detected EFT changes
- the inclusion of quality layers of HR products for refinement of the LC change analysis
- the design elaboration for the climate assessment of HR products

## 1.3 Applicable documents

**Ref. Title, Issue/Rev, Date, ID**

[AD1] CCI HR Technical Proposal, v1.1, 16/03/2018

[AD2] CCI Extension (CCI+) Phase 1 – New ECVs – Statement of Work, v1.3, 22/08/2017, ESA-CCI-PRGM-EOPS-SW-17-0032

[AD3] Data Standards Requirements for CCI Data Producers, v2.0, 17/09/2018, CCI-PRGM-EOPS-TN-13-0009

[AD4] CCI\_HRLC\_Ph1-D1.1\_URD, latest version

[AD5] CCI-LC-PUGV2, 2017-04-10

## 1.4 Reference documents

**Ref. Title, Issue/Rev, Date, ID**

[RD1] The Global Climate Observing System: Implementation Needs, 01/10/2016, GCOS-200

## 1.5 Acronyms and abbreviations

AGB	Above Ground Biomass
CCI	Climate Change Initiative
CRS	Coordinate Reference System
CRU	Climate Research Unit
CWT	Cross Walking Table
EFT	Ecosystem Functional Type
EO	Earth Observation

	Ref	CCI_HRLC_Ph1-CAR		
	Issue	Date	Page	
	3.0	28/10/2022	7	

ESM	Earth System Models
EVI	Enhanced Vegetation Index
GCOS	Global Climate Observing System
GCM	General Circulation Model
HR	High Resolution
IPSL	Institut Pierre Simon Laplace
JRA	Japanese ReAnalysis
KPI	Key Performance Indicators
LAI	Leaf Area Index
LC	Land Cover
LCC	Land Cover Change
LCCS	Land Cover Classification System
LMD	Laboratoire de Météorologie Dynamique
LSCE	Laboratoire des Sciences du Climat et de l'Environnement
MR	Medium Resolution
MMAX	Phenology, EFT component
NDVI	Normalized Difference Vegetation Index
NDVI-I	Productivity, EFT component
PFT	Plant Functional Type
RS	Remote Sensing
sCV	Seasonality, EFT component
SPEI	Standardized Precipitation Evapotranspiration Index
URD	User Requirements Document

	Ref	CCI_HRLC_Ph1-CAR		
	Issue	Date	Page	
	3.0	28/10/2022	8	

## 2 Land Cover from MRLC on our 3 study regions (static and historical): analysis and potential issues

The CCI MRLC product has been processed all over the available period (1992-2018) to characterize the various ecosystems present in our 3 studied regions and to analyse the class transitions, especially over the historical region where the HRLC product will be focused. This analysis was performed with a critical eye, to highlight the potential uncertainties/biases. Therefore, the maps were in some regions compared to HR images and pictures with the help of Google Earth platform, in order to assess the future contribution of the HRLC maps to better interpret the mosaic classes and better translate the land cover classes into the Plant Functional Type (PFT) categories used by the climate modelers to represent the land surface heterogeneity and the related processes in their model grid.

### 2.1 LC and LCC (1992-2018) over Amazonia

Figure 2.1 presents the LC maps and transitions derived from the MRLC product over the static and the historical regions. The land cover is mapped for the year 1992 and the transitions are calculated between the two extreme years of the study period to illustrate the changes observed in 2018 compared to 1992. The conversion of the evergreen forests into crops, grasslands or shrublands is clearly visible in the southern part of the Amazonian Brazilian forest (Mato Grosso and Gran Chaco) as well as in Bolivia and Paraguay. The afforestation in protected areas is also visible at different places, and in the historical zone in Cerrado province with an intensification of this process since 2015. The water bodies class also shows some changes around the river beds, explained both by various dams implementation and the new flooded areas generated upstream, and by the well-known dynamics of Amazonian rivers with moving river beds because of the flat terrain and their high sediment load. In the historical region, the observed changes mainly concern the decrease of the evergreen broadleaf forests in the northern part of the domain and of the deciduous broadleaf forests in the south-western part (Bolivia, Paraguay), by about 6% in favour of the increase of croplands, grasslands and shrublands, all by around 2%. The classification review against Google Earth HR data allowed to diagnose some issues of the MRLC product particularly in the interpretation of the croplands/grasslands mosaic classes: managed grasslands for bovine farming being classified sometimes as crops although their functioning regarding the e-w-c cycles is closer to grasses and shrubs, and some tree crops like palm trees being classified as crops, although they should be considered as evergreen trees/shrubs in the land surface model. The interpretation of the mosaic classes in terms of fractions of PFTs is thus associated with potential large uncertainties as it depends on the regions and the type of crops / grasses and their usage. A regional interpretation seems thus to be highly needed, as opposed to the global interpretation used so far during the ESA-CCI MRLC projects. The future HRLC product will therefore certainly help to better characterize the land cover in these areas.

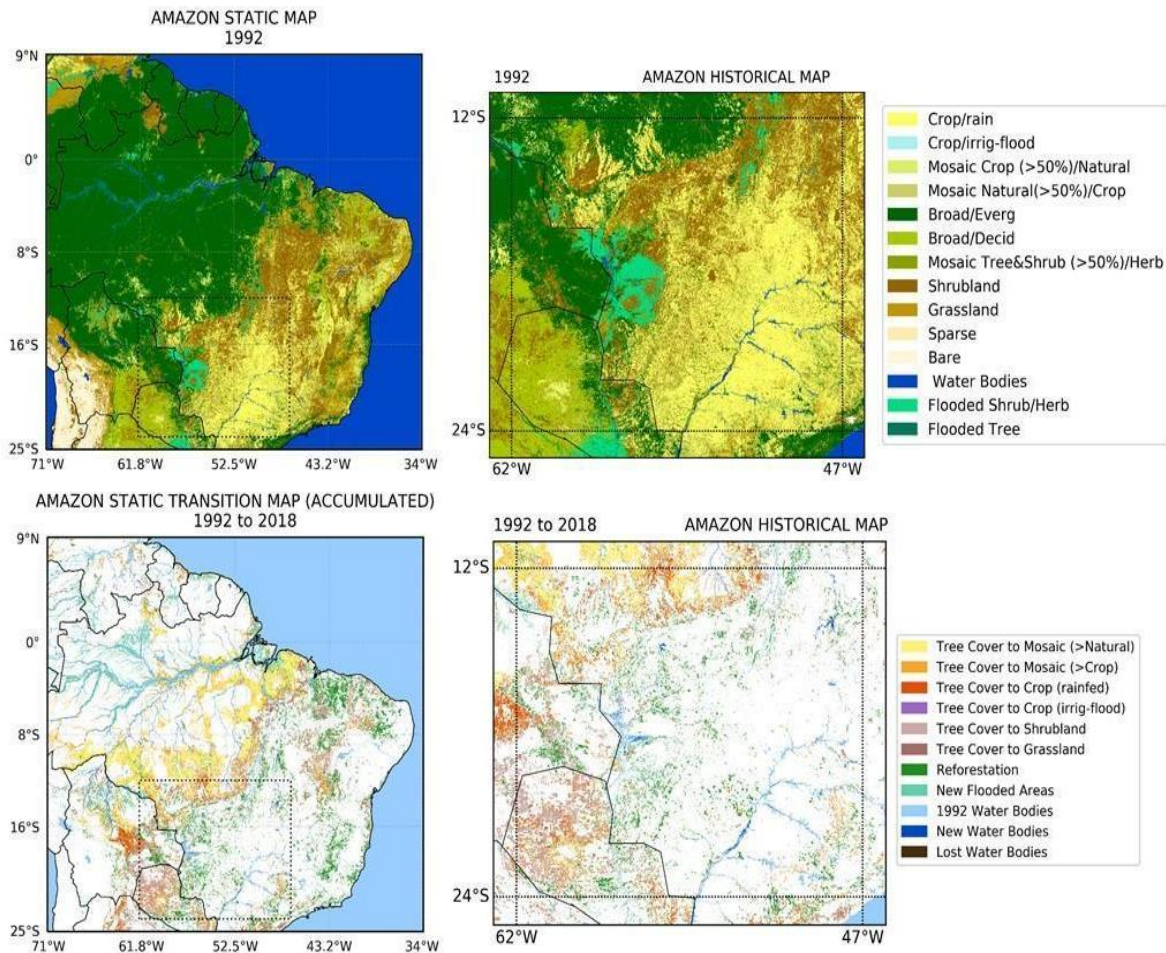


Figure 2.1: MRLC classification and land cover transitions between 1992 and 2018, over the static and historical regions of Amazonia and South Brazil.

## 2.2 LC and LCC (1992-2018) over Sahel

Figure 2.2 presents the same results over the Sahel static and historical regions, with the LC map of 1992 over the static and historical regions and the transitions accumulated over the (1992 - 2018) period. Here, the pattern of the Great Green Wall afforestation project to combat the increasing desertification of Sahel is clearly seen in the north of Sahel in the transition maps. Reforestation in the southern part of Sahel as well as intensification of croplands are also clearly visible. In some places, like in Center Mali, Niger or Soudan, land degradation can be seen with the conversion of grasslands and shrublands to sparse or bare soils. The vegetation recovering since 2003 after the severe droughts of the last century, can be clearly seen on the yearly transitions. In the historical region, the largest changes concern the decrease of shrublands in the north-western part by 3%, the afforestation in Ethiopia and Eastern Sudan by 2% and a slight increase of croplands by 0.6%. It can be noted that the afforestation is mainly done with deciduous tree species (Fetene et al., 2016), less water demanding than the evergreens, in order to preserve the water resources. The fact that the HRLC product will be able to separate evergreen from deciduous tree species will be very interesting to study the impacts of these replanting choices on climate trends and future resources. The product will also help to see the density of the afforestation (tree per hectare), an important characteristic for modeling aspects.

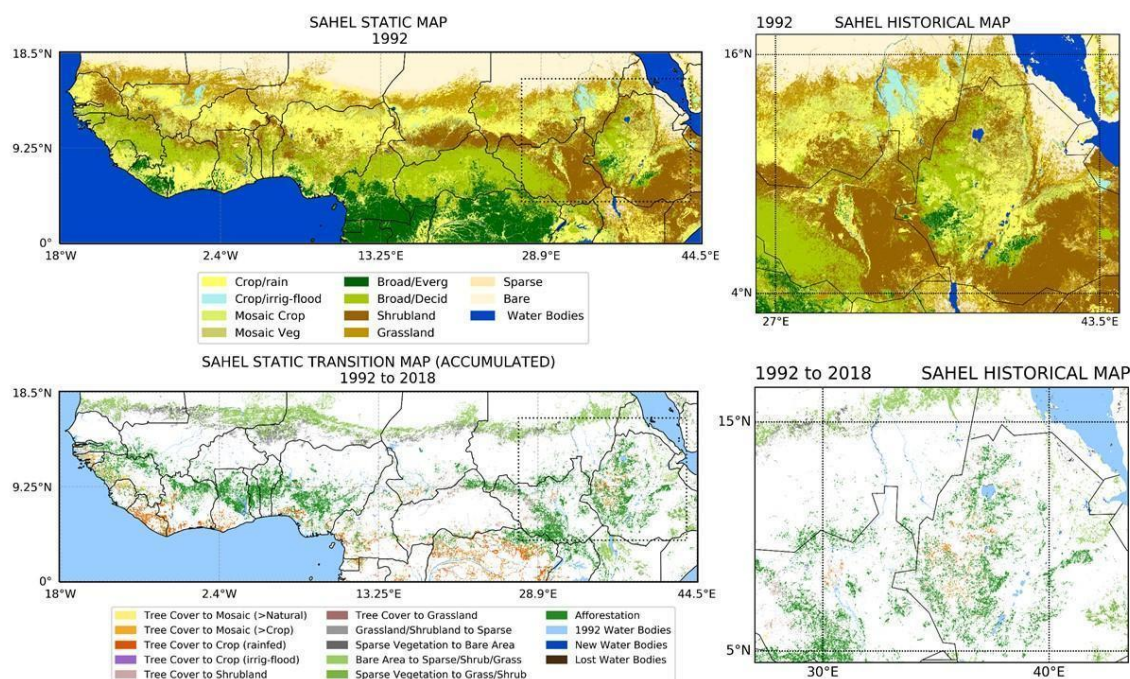


Figure 2.2: MRLC classification and land cover transitions between 1992 and 2018, over the static and historical regions (right column) of Sahel and Ethiopia.

### 2.3 LC and LCC (1992-2018) over Siberia

Over our static region of Siberia, as shown in Figure 2.3, the main land cover features concern the large flooded area of the downstream part of the Ob river on the western part of the study region and the large part of Central Siberia covered by the needleleaf deciduous trees (mainly larches). The northern part with extreme weather conditions sees mainly shrubs, grasslands which move into lichen and mosses northern. In the 28-year study period, the land cover transitions show some forest loss in favour of grasslands and shrubs on both sides of the large Taiga forest which could be the signature of land drying and browning and fire disturbances increase (Dyukarev, 2011, Miles, 2016). As described by Miles and Esau, 2016, the Taiga browning is species and spatially dependent, affecting more evergreen coniferous trees compared to needleleaf deciduous (larches) more tolerant to warmer temperatures and water deficit. More to the North, forest/shrubs gain is observed, probably a consequence of the Arctic tundra greening already observed by numerous works (Macias-Faura, 2012, Miles & Esau, 2016). In the historical region, the main transitions concern the significant decrease of flooded shrubs by 2% in favour of forested areas, which could be explained by the drying of the region because of the increased temperatures. Parallel increase of flooded shrubs could be the result of increased floods because of the larger precipitation over the region. These transitions are expected to be better identified with the HR products with the benefit of the higher spatial resolution and the SAR imagery. Such transitions from flooded grasslands and shrubs to trees (and the other way round) is expected to have a significant impact on the land surface processes simulated by ORCHIDEE. The HR products will also help to characterize the water bodies especially the thermokarst lakes due to the melting of soil ice in the permafrost regions.

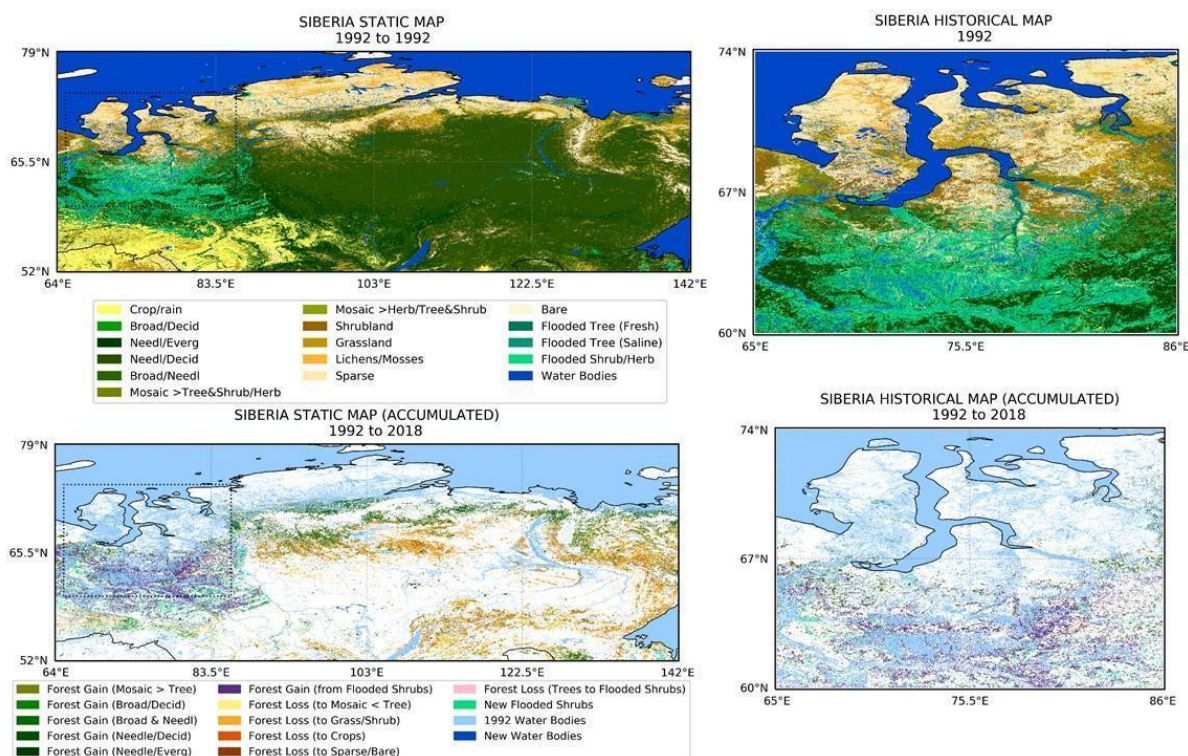


Figure 2.3: MRLC classification and land cover transitions between 1992 and 2018, over the static and historical regions of Siberia.

### 3 Use of Biomass products to improve the interpretation of MRLC classes in terms of Plant Functional Types for land surface models

#### 3.1 Using biomass product with land cover data in ORCHIDEE

ORCHIDEE describes the heterogeneity of the vegetation in each grid cell by combining fractions of PFTs (15 PFTs in the standard configuration) that share the same equations (with exceptions for the calculation of leaf phenology) but differ in their parameters. The PFTs distribution usually comes from historical land cover reconstructions and/or contemporary remote sensing products. Since the release of the ESA-MRLC product, the land cover maps have been used by the ORCHIDEE group to derive the PFT distribution. The original 38 land cover classes (DiGregorio et al., 2005) of the MRLC are re-mapped onto a set of generic PFTs at 0.25° resolution. Re-mapping for the years 1992 to 2015 is guided by a so-called cross-walking table (CWT, Poulter et al., 2015) defining the correspondence between the land cover classes and the generic PFTs. The fraction of each generic PFTs for each land cover classes can be visualised under the web page: <https://orchidas.lscce.ipsl.fr/dev/lccci/tools.php>

However, the CWT has been defined globally and there are large uncertainties in terms of PFT fractions especially for specific LCCs like: mixed vegetation, cropland, mosaic vegetation, etc. In this context, several actions were initiated to revise / improve the CWT and to define specific CWTs per region (by large ecosystems). Before using the upcoming HRLC products, we started to revise the CWT for the African ecosystems, using an independent product: satellite driven estimates of above ground biomass data (AGB).

The main objective of this parallel project is to assimilate AGB data into ORCHIDEE in order to improve the simulation of forest carbon stocks and their fate under climate change. Assimilating AGB is a complicated task, because simulating forest C stocks combine not only the uncertainties linked to C input, C allocation, mortality and recruitment over the history of the forest ecosystem but also the uncertainties in land cover description.

More specifically the partition between tree and short vegetation is likely to be a first order driver of the AGB distribution (C stocks in trees are two orders of magnitude larger than in grasses). In this context, we propose to test a stepwise approach for Africa with the Bouvet et al. (2018) AGB maps, as described in Figure 3.1, below:

- In a first step we use the satellite AGB map to refine the fraction of tree / grass / bare soil PFTs of each grid cell in Africa, given the uncertainties in the current PFT map derived from the standard CWT presented above and applied to the MRLC product (Bontemps et al., 2013).
- Second, we will define at the resolution of the model (0.5 degree) the maximum AGB for each grid cell (ABGmax, using the 95 percentile of the raw AGB values) as a function of mean annual precipitation (MAP), as in Yang et al. (2020). The AGBmax - MAP relationship will be the target of the ORCHIDEE parameter optimisation, i.e. the potential AGB that ORCHIDEE should simulate without large disturbances. The maps in Figure 3.2 illustrate the approach with a preliminary comparison of the AGB estimates.
- Finally, the simulated AGB from the optimised model will be compared to the raw EO AGB of Bouvet et al. (2018). Remaining differences will primarily inform on all processes not simulated in ORCHIDEE.

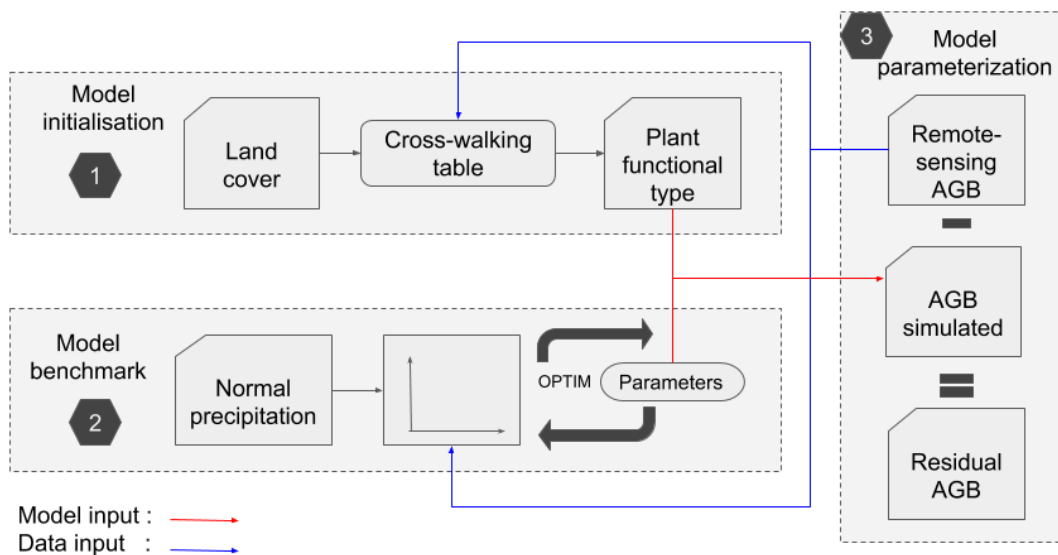
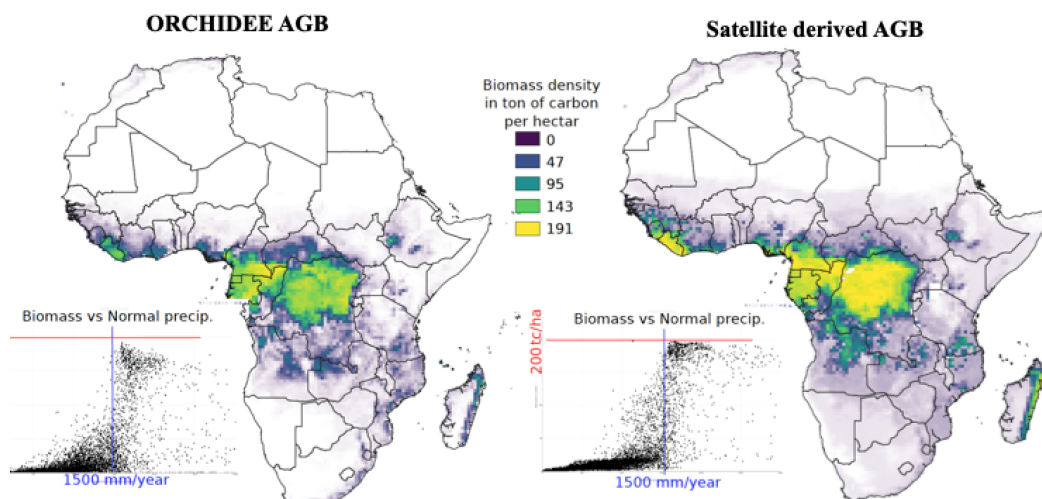


Figure 3.1. Overview of the three model applications with the AGB product, i.e., (1) model initialization, (2) parameter optimization, and (3) model evaluation, that are explored in this study.



	Ref	CCI_HRLC_Ph1-CAR		
	Issue	Date	Page	
	3.0	28/10/2022	13	

Figure 3.2: (from G. Marie, personal communication). Spatial distribution of the AGB simulated by the ORCHIDEE model and from satellite observations (Bouvet et al., 2018) together with a diagram for each product of the AGB versus Mean Annual Precipitation for the whole of AFRICA. Such relation will be the observation operator in the Data Assimilation step.

### 3.2 Refinement of the description of LC classes in terms of PFTs with Biomass data

The first objective is thus to improve the CWT linking the 43 land cover types of the ESA MRLC product to the 15 PFTs distinguished by ORCHIDEE, using the information contained in the AGB product (and also from an annual mean precipitation data).

Because of the large difference in biomass between woody and herbaceous biological entities, the biomass observed at each pixel,  $p$ , ( $B_p$ ) can be written as:

$$B_p = F_{p,tree} \cdot Bref_{tree} + F_{p,herb} \cdot Bref_{herb} \quad (1)$$

where  $F_{p,tree}$  and  $F_{p,herb}$  are the fractions of the surface area of a given pixel  $p$  covered by woody and herbaceous vegetation respectively.  $Bref_{tree}$  and  $Bref_{herb}$  are the reference biomass of the tree and the herbaceous vegetation respectively. Equation (1) can be further simplified:

$$B_p = F_{p,tree} \cdot Bref_{tree} + (1 - F_{p,tree}) \cdot Bref_{herb} \quad (2)$$

Equation (2) will be used to refine the existing CWT that links 38 land cover types to 15 PFTs. We thus simply express the biomass of each land cover type,  $lc$ , ( $B_{p,lc}$ ) as a function of the mean tree cover of each  $lc$  type ( $\overline{F}_{lc,tree}$ ) and the mean reference biomass for tree and herbs ( $\overline{Bref}_{lc,tree}$  and  $\overline{Bref}_{lc,herb}$ ) following:

$$B_{p,lc} = \overline{F}_{lc,tree} \cdot \overline{Bref}_{lc,tree} + (1 - \overline{F}_{lc,tree}) \cdot \overline{Bref}_{lc,herb} \quad (3)$$

The estimation of  $\overline{F}_{lc,tree}$  will be then used to update the CWT and thus the PFTs of ORCHIDEE. Equation (3) assumes that the reference biomasses are constant across space for a given land cover type. This is true only if land cover types are restricted in a narrow range of climatic characteristics. In a further refinement of this approach (ongoing) we will make the reference biomass a function of the mean annual precipitation.

The different terms of Eq. 3 are associated with an uncertainty that was accounted for in the method used to fit this model to the AGB data. A Bayesian approach was used to estimate the 95% confidence interval of  $\overline{F}_{lc,tree}$  for each LC. The approach requires to set prior values and statistical distributions for each unknown of the equation, which were chosen to follow a normal or gamma distribution.

The first results that we obtained are:

- On average the crop or mosaic-crop land cover classes (classes 10, 11, 12, 20, 30) appear to need more tree PFTs than the original assessment in the CWT. The main reason is that there are vegetation classified as crops in the MRLC product that correspond more to trees (avocado, palm tree, ...) for the carbon cycle.
- The split of the mosaic and shrubland classes (classes 40, 100, 110, 120, 121, 122) into tree and short vegetation PFTs is also slightly modified compared to the original split, with less trees.

We are currently finalising this regional CWT following the information provided by the AGB data. We will apply the CWT to the MRLC product in order to create a new PFT map for the year 2010 and to simulate the African biomass. This work also prepares the use of the upcoming HRLC products as we will try to combine the information for the HRLC maps and the information from the AGB map to better define the fraction of trees for each class of the MRLC product.

## 4 New Cross-Walking tables (CWTs) to convert HRLC classes to Generic PFTs and to ORCHIDEE PFTs

The following tables show the Generic PFTs and the ORCHIDEE PFTs (used as an input for ORCHIDEE's simulations):

Table 4.1: Generic PFTs (left) and ORCHIDEE PFTs (right).

<b>TREES</b>	Broadleaved Evergreen	PFT1 : Bare Soil
	Broadleaved Deciduous	PFT2 : Tropical Evergreen
	Needleleaved Evergreen	PFT3 : Tropical Raingreen
	Needleleaved Evergreen	PFT4 : Temperate Needleleaf Evergreen
<b>SHRUBS</b>	Broadleaved Evergreen	PFT5 : Temperate Broadleaf Evergreen
	Broadleaved Deciduous	PFT6 : Temperate Broadleaf Summergreen
	Needleleaved Evergreen	PFT7 : Boreal Needleleaf Evergreen
	Needleleaved Evergreen	PFT8 : Boreal Broadleaf Summergreen
<b>GRASSES</b>	Natural Grasses	PFT9 : Boreal Needleleaf Deciduous
	Crops	PFT10 : Temperate Natural Grassland (C3)
<b>Bare Soil</b>		PFT11 : Natural Grassland (C4)
<b>Water</b>		PFT12 : Crops (C3)
<b>Snow and Ice</b>		PFT13 : Crops (C4)
<b>Urban</b>		PFT14 : Tropical Natural Grassland (C3)
<b>No Data</b>		PFT15 : Boreal Natural Grassland (C3)

### 4.1 CWT-HRLC: HRLC-to-Generic PFTs

In contrast with the MRLC classification, the HRLC pixels in most cases tend to represent more homogeneous classes due to the higher resolution, and thus, the legend is different. For this reason we needed to revise the previous interpretation of the land cover classes in terms of PFTs and we had to adapt our previous MRLC CWT.

We decided to build regional HRLC CWTs, one for Amazonia and Sahel and another for Siberia, because the vegetation features (species, density, phenology) are different when comparing tropical and boreal regions.

Given that ORCHIDEE lacks from shrub PFTs, the shrub classes are converted already in this stage into trees PFTs, prioritizing their seasonality (evergreen/deciduous) and assigning 100% of them to broadleaved PFTs in Amazonia and Sahel and 25% to broadleaved/75% to needleleaved PFTs in Siberia. The flooded vegetation was treated in a similar way: 20% water in every region and 80% broadleaved evergreen trees in Amazonia and Sahel and 80% needleleaved evergreen in Siberia.

-HRLC can be found here: [https://orchidas.lsce.ipsl.fr/dev/lccci/hr\\_regions.php](https://orchidas.lsce.ipsl.fr/dev/lccci/hr_regions.php)

Table 4.2. CWT-HRLC (Amazonia and Sahel): HRLC classes to Generic PFTs

Source: [https://orchidas.lsce.ipsl.fr/dev/lccci/hr\\_regions.php](https://orchidas.lsce.ipsl.fr/dev/lccci/hr_regions.php)

CCI CLASS	NAME	TREES				SHRUBS				GRASSES		Bare Soil	Water	Snow and Ice	Urban	No Data
		TrBrEv	TrBrDe	TrNeEv	TrNeDe	ShBrEv	ShBrDe	ShNeEv	ShNeDe	NatGr	Crops					
0	No Data															100
1	Tree/Everg-Broad	100														
2	Tree/Everg-Needle			100												
3	Tree/Decid-Broad		100													
4	Tree/Decid-Needle				100											
5	Shrub/Everg	100														
6	Shrub/Decid		100													
7	Grassland									100						
8	Cropland										100					
9	Woody/flooded	80											20			
10	Herb/flooded									80			20			
11	Lichens-Mosses									85		15				
12	Bare area											100				
13	Built-up														100	
14	Water/Season												100			
15	Water/Permanent												100			
16	Snow-Ice													100		

Table 4.3. CWT-HRLC (Siberia): HRLC classes to Generic PFTs

Source: [https://orchidas.lsce.ipsl.fr/dev/lccci/hr\\_regions.php](https://orchidas.lsce.ipsl.fr/dev/lccci/hr_regions.php)

CCI CLASS	NAME	TREES				SHRUBS				GRASSES		Bare Soil	Water	Snow and Ice	Urban	No Data
		TrBrEv	TrBrDe	TrNeEv	TrNeDe	ShBrEv	ShBrDe	ShNeEv	ShNeDe	NatGr	Crops					
0	No Data															100
1	Tree/Everg-Broad	100														
2	Tree/Everg-Needle			100												
3	Tree/Decid-Broad		100													
4	Tree/Decid-Needle				100											
5	Shrub/Everg			100												
6	Shrub/Decid		25		75											
7	Grassland									100						
8	Cropland										100					
9	Woody/flooded			80									20			
10	Herb/flooded									80			20			
11	Lichens-Mosses									85		15				
12	Bare area											100				
13	Built-up														100	
14	Water/Season												100			
15	Water/Permanent												100			
16	Snow-Ice													100		

## 4.2 CWT-ORCH v2: Generic-to-ORCHIDEE PFTs

### 4.2.1 New Köppen-Geiger map

ORCHIDEE's PFTs are separated according to their distribution among different climate zones and C3/C4 classification (for crops and grasses). The climate zones are defined using a Köppen-Geiger map adapted from *Peel, M. C., Finlayson, B. L., and McMahon, T. A (2007)*.

In order to fix possible biases due to an oversimplification of the previously used Köppen-Geiger map (needed to distribute the Generic PFTs among different climate regions), the "Tropical" climate zone extension was excessive, so we decided to include the "Arid Warm" and "Arid Cool" classes (Figs. 4.1 and 4.2). Also, we redistributed the previous extensions of "Boreal Warm" and "Boreal Cool".

With this new classification we intend to have a more realistic split and global distribution of PFTs after the conversion from Generic-to-ORCHIDEE PFTs.

This new Köppen-Geiger map is currently used for the PFT construction, and it could eventually be used to regionalize the albedo optimization in the future (Section 10).

### Köppen-Geiger climate map

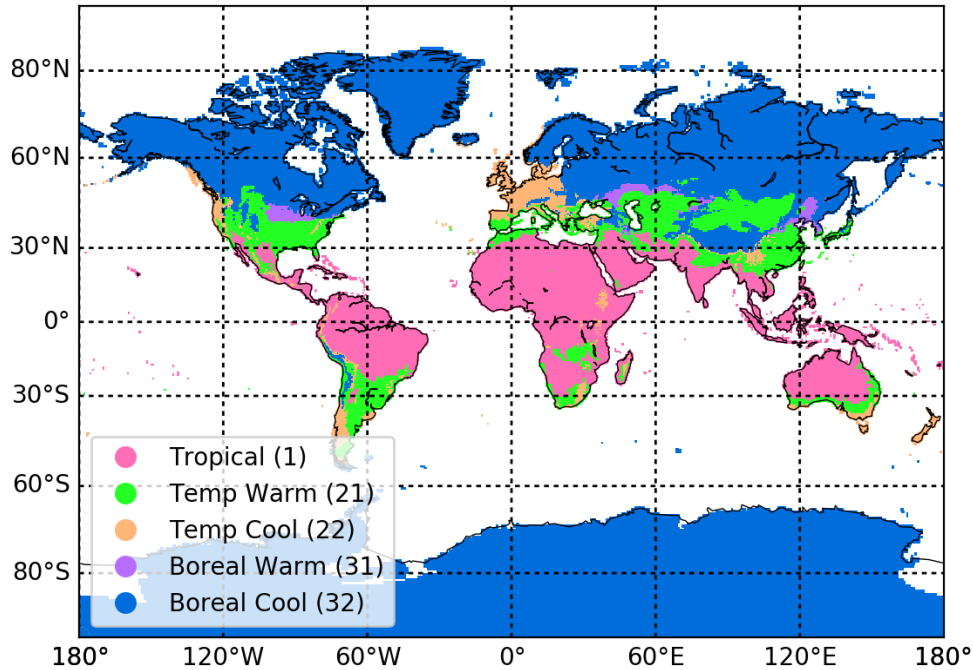


Figure 4.1: Previous Köppen-Geiger climate zone map (300 m resolution, 5 climate zones). Original data: Peel, M. C., Finlayson, B. L., and McMahon, T. A (2007).

### Köppen-Geiger climate map

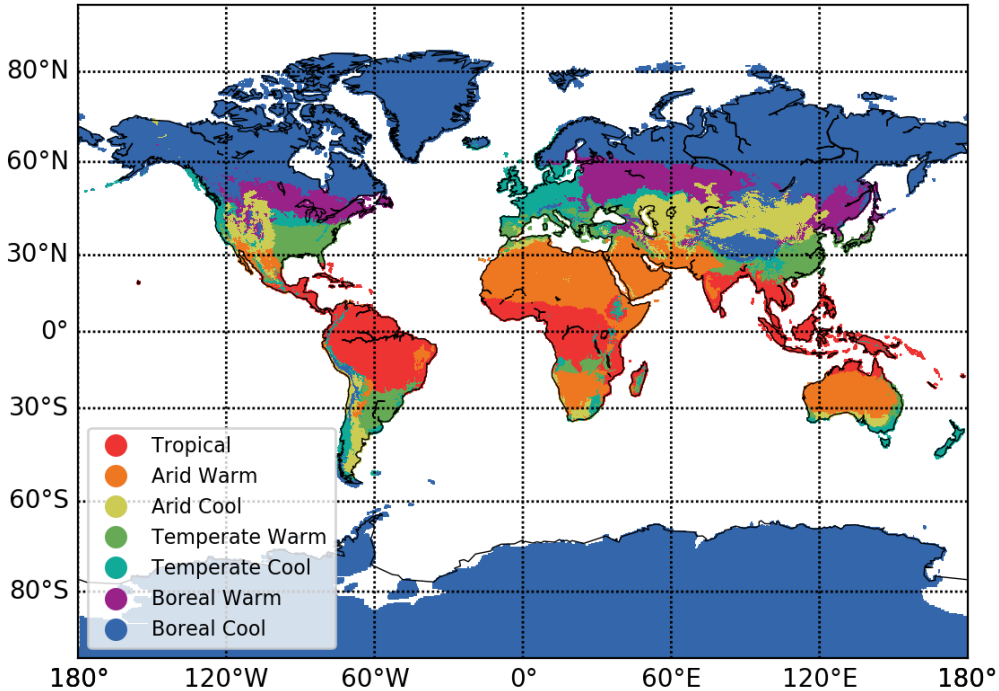


Figure 4.2: New Köppen-Geiger climate zone map (300 m resolution, 7 climate zones). Original data: Peel, M. C., Finlayson, B. L., and McMahon, T. A (2007).

	Ref	CCI_HRLC_Ph1-CAR		
	Issue	Date	Page	
	3.0	28/10/2022	17	

#### 4.2.2 C3/C4 classification

The distinction between C3 and C4 for grasses and crops was improved through the combination of two detailed products with higher resolution:

- Grasses: product provided by C.Still at  $1/6=0.166^\circ$  for 3 classes: C3 herbaceous cover, C4 herbaceous cover and C3 tree cover
- Crops: product provided within TRENDY2020 (land use harmonization data) at  $0.25^\circ$  for 12 classes: primf (forested primary land), primn (non-forested primary land), secdf (potentially forested secondary land), secdn (potentially non-forested secondary land), urban (urban land), c3ann (C3 annual crops), c4ann (C4 annual crops), c3per (C3 perennial crops), c4per (C4 perennial crops), c3nfx (C3 nitrogen-fixing crops), pastr (managed pasture), range (rangeland)

#### 4.2.3 CWT-ORCH v2

Using the new Köppen-Geiger map, the C3/C4 map by *Still et al. (2009 and 2018)* and the Land-Use Harmonization data (LUH2, 2020), we built a new CWT (CWT-ORCH v2; Tables A.1, A.2 and A.3 in Appendix A) to convert the Generic PFTs into the ORCHIDEE PFTs solving some biases found using CWT-ORCH v1. The future implementation of this new CWT will bring the following changes and improvements to the PFT translation:

- Arid classes are added. Arid Warm assigns the same PFTs as Tropical, while Arid Cool behaves as Temperate Warm.
- Temperate Broadleaved Evergreen (PFT 5) in Boreal areas (warm or cool) are converted to Boreal Needleleaved Evergreen (PFT 7).
- Temperate Needleleaved Evergreen (PFT 4) in Tropical areas are converted to Tropical Broadleaved Evergreen (PFT 2).
- Tropical areas only present tropical PFTs (PFT 2 or 3) and Boreal Cool areas only present boreal PFTs (PFT 7, 8 or 9) prioritizing the seasonal properties (evergreen or deciduous) coming from the generic PFTs.

## 5 HRLC in ORCHIDEE: PFT building and comparisons with MRLC

### 5.1 Maps for 2019 over the historical regions

We built and compared ORCHIDEE-PFTs maps using HRLC and MRLC as an input over the three historical regions for 2019. In order to build the MRLC and HRLC maps for the first comparisons presented below, we used for each dataset its respective LandCover-to-Generic PFTs CWT (CWT-MRLC or CWT-HRLC), and then, the same CWT from Generic-to-ORCHIDEE PFTs (CWT-ORCH v1) for both datasets. In this way, the main differences between the two are related to the changes introduced by the HRLC product and its improved land cover classification: better bare soil detection, higher distinction between grasses and shrubs (which are included in the trees PFTs in ORCHIDEE), no mosaic classes (in the MRLC dataset, mosaic classes are distributed in a generic way globally, bringing biases and unrealistic distributions of PFTs, such as broadleaved evergreen trees in boreal regions).

#### 5.1.1 Amazon

In Figure 5.1 we can see the HRLC-based ORCHIDEE's PFTs for the Amazonian historical region, and the comparison with the MRLC PFTs, presented as the fraction differences (HRLC-MRLC). The differences are mapped for each PFT (upper plot) and summarized in the bar plots below. The results show a reclassification of an important fraction of broadleaved evergreen trees to broadleaved summergreen trees, possibly showing an improvement in the seasonality detection by HRLC. We can also find an important amount of MRLC croplands that are detected as grasses and bare soils by the HRLC, as well as a reclassification of the MRLC needleleaved trees as broadleaved trees.

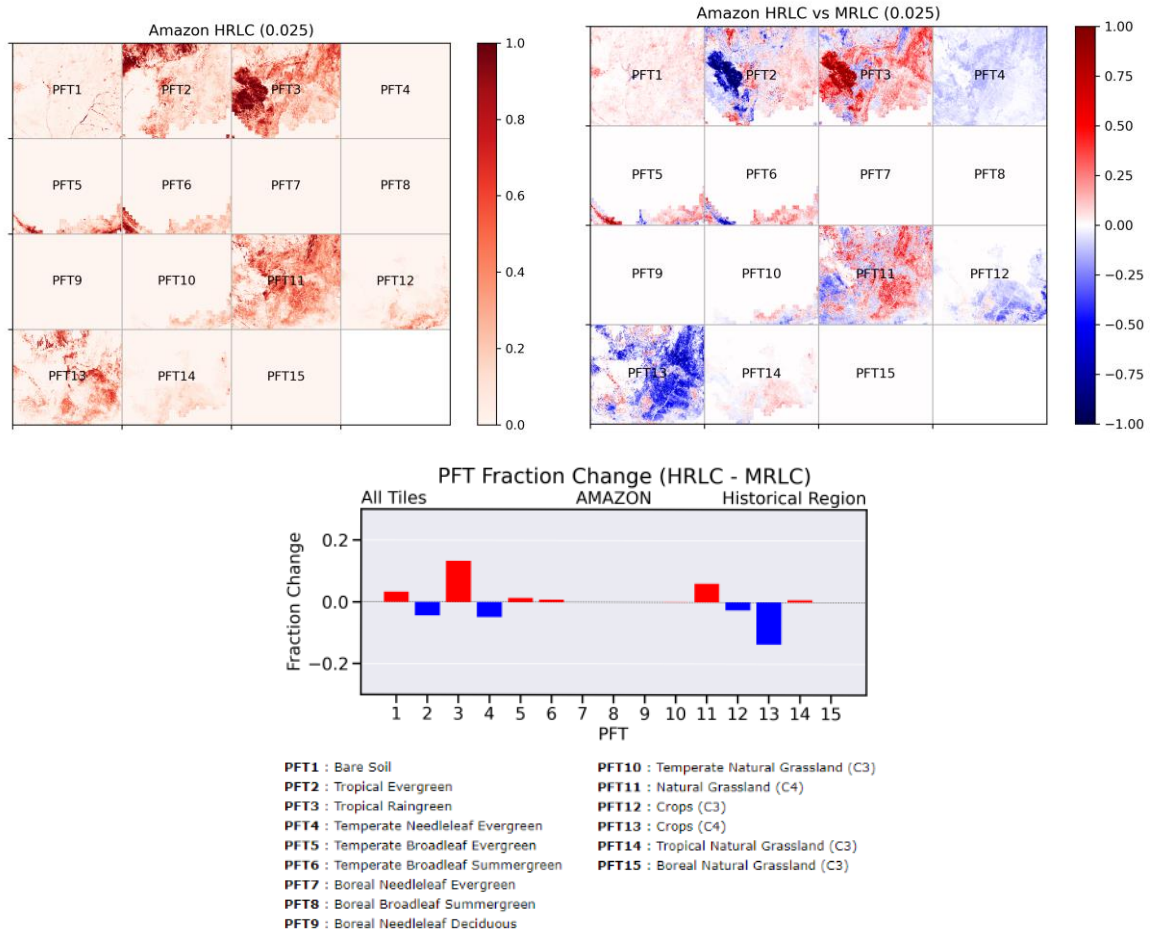
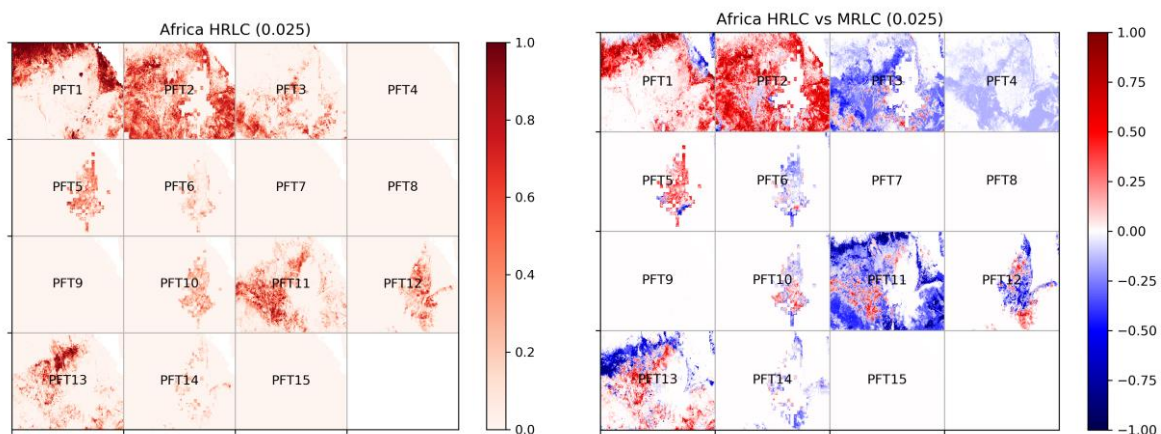
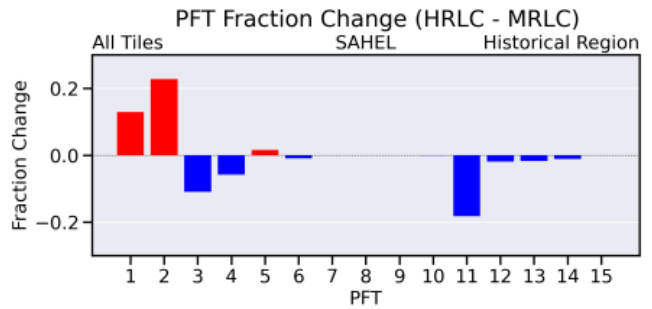


Figure 5.1. ORCHIDEE-PFTs maps built with HRLC first production over Amazonia (top left), maps comparison between HRLC's and MRLC's ORCHIDEE-PFTs (top right) and bar plots showing fraction differences (bottom).

### 5.1.2 Sahel

The same analysis has been performed for the Ethiopian historical region and Figure shows the results obtained. They clearly show an improvement in the detection of bare soil and shrubs (which are translated to trees' PFTs in ORCHIDEE).



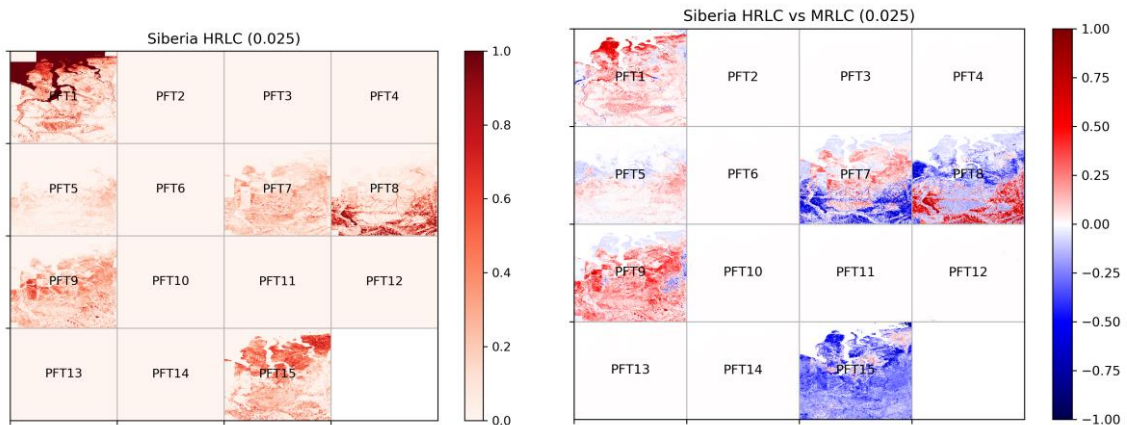


- |   |   |
|---|---|
| <b>PFT1</b> : Bare Soil                       | <b>PFT10</b> : Temperate Natural Grassland (C3) |
| <b>PFT2</b> : Tropical Evergreen              | <b>PFT11</b> : Natural Grassland (C4)           |
| <b>PFT3</b> : Tropical Raingreen              | <b>PFT12</b> : Crops (C3)                       |
| <b>PFT4</b> : Temperate Needleleaf Evergreen  | <b>PFT13</b> : Crops (C4)                       |
| <b>PFT5</b> : Temperate Broadleaf Evergreen   | <b>PFT14</b> : Tropical Natural Grassland (C3)  |
| <b>PFT6</b> : Temperate Broadleaf Summergreen | <b>PFT15</b> : Boreal Natural Grassland (C3)    |
| <b>PFT7</b> : Boreal Needleleaf Evergreen     |   |
| <b>PFT8</b> : Boreal Broadleaf Summergreen    |   |
| <b>PFT9</b> : Boreal Needleleaf Deciduous     |   |

Figure 5.2. ORCHIDEE-PFTs maps built with HRLC first production over Sahel (top left), maps comparison between HRLC's and MRLC's ORCHIDEE-PFTs (top right) and bar plots showing fraction differences (bottom).

### 5.1.3 Siberia

The LC differences in the two maps in Western Siberia concern mainly a redistribution of grasses PFTs to trees and bare soil. In reality, the increase of the trees' PFTs are mostly coming from an increase in shrublands (interpreted as trees in ORCHIDEE PFTs).



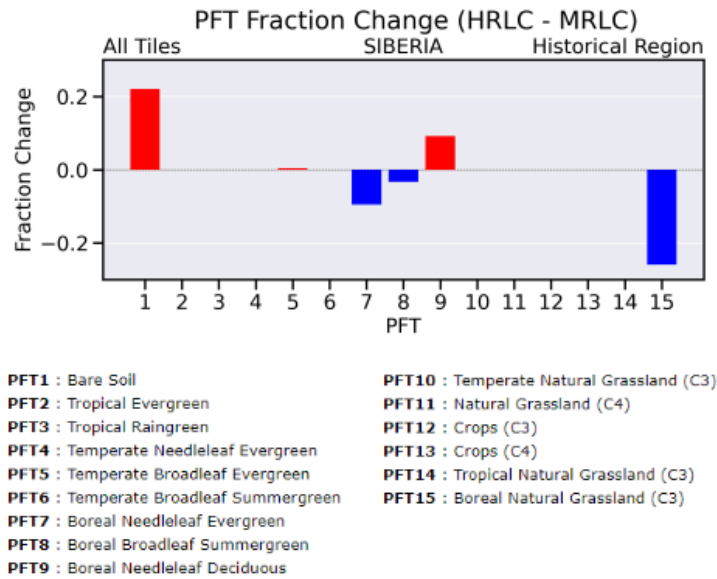


Figure 5.1. ORCHIDEE-PFTs maps built with HRLC first production over Siberia (top left), maps comparison between HRLC's and MRLC's ORCHIDEE-PFTs (top right) and bar plots showing fraction differences (bottom).

## 6 Coherence of MRLC and surface albedo changes in satellite products and comparison to ORCHIDEE

Surface albedo is critical in land surface and climate modeling since it determines the surface net radiation, i.e., the part of the solar radiation that will be available to heat the soil and the atmospheric boundary layer or to evaporate land water (from soil and vegetation surfaces). In ORCHIDEE, it is calculated at each timestep according to the vegetation and snow coverage. The parameterisations used for this calculation have been calibrated against MODIS albedo products (in the visible and near infrared domains) acquired during the (2001-2010) period. Since the albedo can vary significantly with land cover (a bare soil presents generally higher values compared to a vegetated area and forest covers present lower albedo than grassland covers), drastic land cover changes as deforestation or afforestation could produce high changes. In this work, we wanted to see if the land cover changes detected in MRLC have impacted the surface albedo, quantify these changes, compare with ORCHIDEE and diagnose potential albedo issues in our parameterizations that would need prior corrections. For that purpose, it was important to use a product which has not been used in our calibration process. The GlobAlbedo time series available at <http://globalbedo.org/> have therefore been used.

### 6.1 GlobAlbedo product

GlobAlbedo has been derived from European satellites (ATSR2, SPOT4-VEGETATION and SPOT5-VEGETATION-2 as well as AATSR and MERIS) and is available for a 15-year period from 1998 to 2011 (Muller et al., 2012). It is produced at different spatial resolutions at 0.05° and 0.5° and also at different time scales (8-day and monthly). In this work, we used the monthly dataset and the 0.5° resolution to assess the time evolution and the links with land cover changes.

### 6.2 Albedo changes observed

Figure 6.1 shows the albedo changes derived from the GlobAlbedo dataset (annual averages for the Amazonia and Africa regions, summer monthly minimum for Siberia to avoid potential snow effects), calculated over the time period (1998 - 2011). The differences have about the same order of magnitude in the 3 regions and the spatial variations are close to the LCC patterns. The transitions from forests to crops or shrublands in Amazonia

or Sahel show higher albedo values (values around 0.04 but up to 0.2 higher), (the opposite is observed in the afforested regions), and an overall small decrease is observed in Siberia northern of the larch forest (values around 0.02 lower), corresponding to the observed intensification of shrubs. In the extreme Arctic regions, the albedo seems to have increased and we have to confirm if this is not the result of remaining snow impacts or/and potential directional effects not correctly removed in the satellite product.

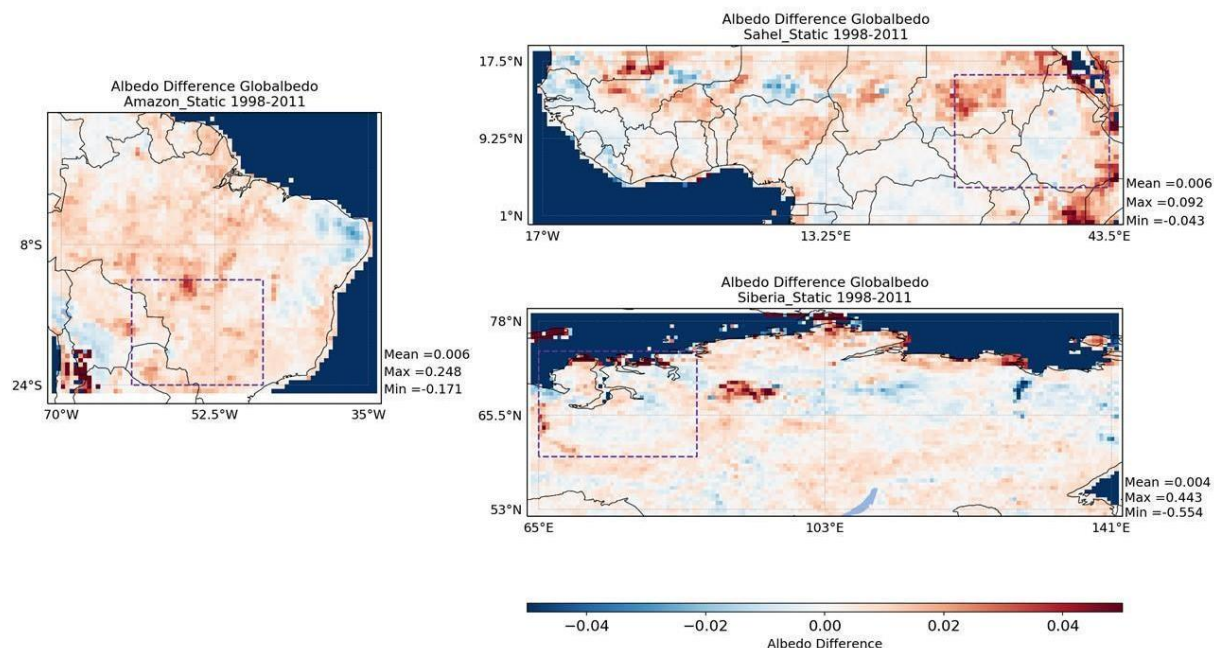


Figure 6.1: Albedo differences/changes extracted from GlobAlbedo product between 1998 and 2011 on Amazonia, Sahel (both in annual mean) and Siberia (monthly minimum)

### 6.3 Comparison with ORCHIDEE

To assess the capacities of ORCHIDEE to reproduce the observed albedo trends and patterns, we have performed a model simulation over the same time period. In ORCHIDEE, the surface albedo is calculated at each time step according to the land cover type and fraction (which evolves daily with the seasonal evolution of the biomass/LAI) and the variations of the snowpack (mass, temperature, coverage and aging) if any. The parameterization was calibrated against MODIS albedo datasets using the ORCHIDAS data assimilation tools developed at LSCE (<https://orchidas.lsce.ipsl.fr/>, Bastrikov et al., in preparation). The calibration was done with one albedo value (for the visible and for the near infrared) for each vegetation PFT and with one albedo for each grid cell for the bare soil PFT. The performed simulation (called in the following ORCHIDEE-LUC) used the CRU-JRA reanalysis (Kobayashi et al., 2015, Harris, 2019) as atmospheric forcing over the period (1992-2018) with a 6-hourly time step and at a resolution of 0.5°. In this simulation, the MRLC land cover product is used to map the Plant Functional Types (PFTs) used in ORCHIDEE to prescribe the vegetation properties and is updated yearly as described in Lurton et al., 2020.

Figure 6.2 illustrates the albedo differences simulated by the ORCHIDEE model between the two years 1998 and 2011. As for GlobAlbedo dataset, the annual mean has been used for Amazonia and Sahel, the monthly minimum value has been extracted for Siberia, in order to remove the perturbing effects of snow cover. The comparison with ORCHIDEE shows the same patterns already seen in GlobAlbedo, confirming that the vegetation trends and changes are correctly accounted for. However, the differences are significantly lower than in the GlobAlbedo product, with differences generally lower than 2%, suggesting that the variations are underestimated even if the trends are correctly represented. This underestimation points to the need for a better calibration of the different vegetation PFT albedo coefficients. It is noteworthy also to highlight that the positive trend observed in the north of Siberia at the limit with the coastline is not present in ORCHIDEE simulations. In the historical region, the

region which shows significant transitions between flooded and non- flooded forests and shrubs, show also different trends in ORCHIDEE compared to the satellite observations. A positive trend is simulated in ORCHIDEE in this region showing an increase of flooded vegetation. This incorrect variation could be the consequence of one of the deficiencies of ORCHIDEE (like most of the climate models) which represent land water as bare soils. In ORCHIDEE, the flooded class 180 of CCI-MRLC, assigns a fraction of 30% to water, therefore to the bare soil PFT. Such an increase of the bare soil fraction could have led to an unrealistic increase of the surface albedo. This point which has to be confirmed with a deeper analysis of the bare soil values assigned to bare soil in ORCHIDEE in this region, highlights the importance of the land cover mapping for climate modeling and the expected improvements that will be brought by the HRLC dataset which will allow to better identify the flooded areas and their dynamics.

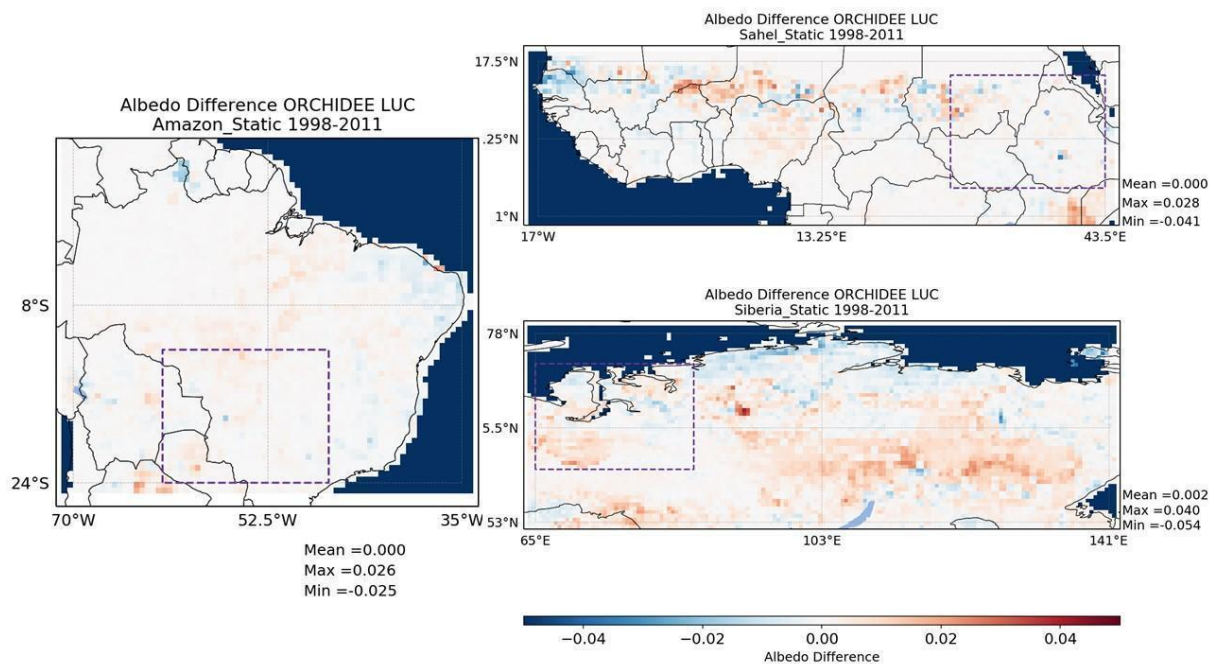


Figure 6.2: Albedo differences modeled by ORCHIDEE-LUC on the time period (1998 - 2011)

In Figure 6.3, the mean errors between ORCHIDEE-LUC albedos and GlobAlbedo time series have been calculated for the 3 study regions and are plotted at 0.5° resolution. The mountainous areas show the larger errors because of the variability of the snow coverage which could differ from model to observations on the monthly time series. Apart from these regions, we see some interesting features starting from the Amazon (showing the lower RMSE), where the rivers and surrounding flooded areas (e.g., Pantanal in South Brazil) show significant underestimation in ORCHIDEE, suggesting that the albedo of bare soil/water is not well calibrated. Positive errors also appear in the transition regions from forests to croplands and shrublands, suggesting that the vegetation albedo could be slightly overestimated for these ecosystems. In Sahel, the RMSE are slightly larger compared to Amazonia (0.032 compared to 0.023) and a positive bias is clearly seen on the bare areas highlighting that the bare soil albedo in this area could be overestimated. A negative bias is observed in the north of the Sahelian band, showing that the albedo is underestimated in ORCHIDEE for shrublands and croplands contrary to the Amazonian case. This could be the result of too large fractions of bare soils assigned to these ecosystems by the CWT or to calibration issues, both assumptions suggesting that regional CWTs and/or PFTs parameterizations are necessary to improve the representation of the surface albedo in ORCHIDEE.

Finally, in Siberia, apart from the mountainous area of Central Siberia Plateau contaminated by snow, the albedo seems to be underestimated overall with a mean error of about 2%, suggesting either incorrect albedo calibration or incorrect land cover fractions assigned by the CWT. In the south, the albedo could be overestimated in some

places mostly covered by crops. All these discrepancies have to be analyzed more in depth, in line with other satellite datasets like biomass and LAI to confirm and drive the revision of the CWT as well as the calibration process.

Note finally that part of these model - GlobAlbedo differences can be due to the fact that for ORCHIDEE the albedo parameters and especially all grid-point bare soil albedo values were calibrated with a different albedo product, i.e., from MODIS instruments.

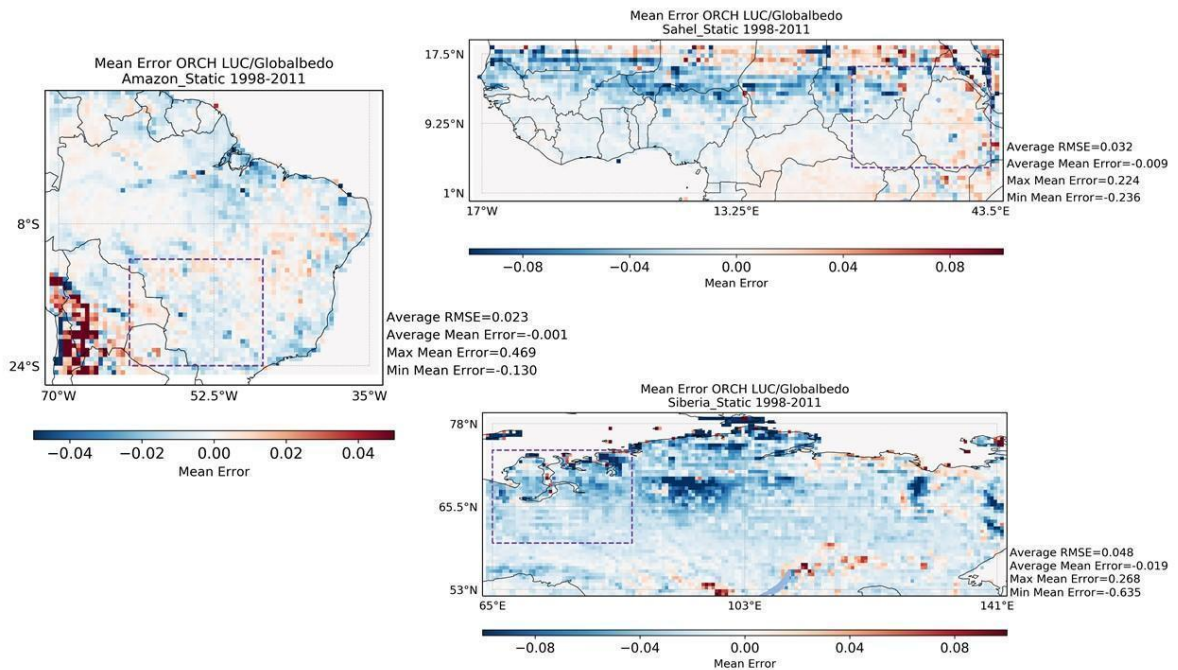


Figure 6.3: Albedo errors ORCHIDEE-LUC / GlobAlbedo (average RMSE, biases, max and min errors) calculated over the period (1998 - 2011) at monthly time step.

## 7 Use of MRLC in ORCHIDEE to assess LCC impacts on carbon, water and energy surface budgets

To assess the impacts of land cover changes on the e-w-c budgets and the contribution of yearly updated land cover maps for climate modeling, we proposed to compare 2 simulations performed with ORCHIDEE based on either a static land cover map representative of the nineties (ORCHIDEE-FIX), or a dynamic one, updated each year accounting for the land cover changes observed (ORCHIDEE-LUC, simulation already presented in section 4.3). For this task, we performed the second simulation (ORCHIDEE-FIX), forced with the same atmospheric forcing CRU-JRA than for the ORCHIDEE-LUC simulation, the only difference being the not updating of the LC map, therefore of the PFT fractions. Both simulations were done at a scale of 0.5° and for the period 1992-2018. A spin up period of 10 years was chosen for the initialisation of the model variables with the static map of 1992 for the prescription of the land cover.

## 7.1 Analysis

### 7.1.1 Globally

Figure 5.1 presents at global scale and in annual mean, the differences between the two simulations (ORCHIDEE-LUC minus ORCHIDEE-FIX), for different prognostic variables: surface albedo, LAI, latent and sensible heat fluxes, GPP and surface temperature.

The plots show clearly how the LCCs translate in albedo changes, the conversion of forest to croplands/grasslands in Amazonia leading to albedo increase, and in the contrary, the gain of forests in Siberia to albedo decrease. But even if these changes are the consequence of similar amplitude of variations on vegetation coverage (LAI, i.e., LAI decrease in Amazonia and increase in western Siberia by about 0.4), these changes do not translate on surface fluxes in the same way and with the same amplitude: in Amazonia, the lower LAI values impacts negatively the evapotranspiration but positively the GPP and the sensible heat flux leading to larger surface temperatures. In western Siberia, the increase of flooded areas translates into lower albedo values, larger surface water and carbon fluxes and slightly lower temperatures. Note that the increase of GPP with a reduction of evapotranspiration is due to the fact that grass/crop PFTs have a larger maximum photosynthetic capacity than tree PFT, on average.

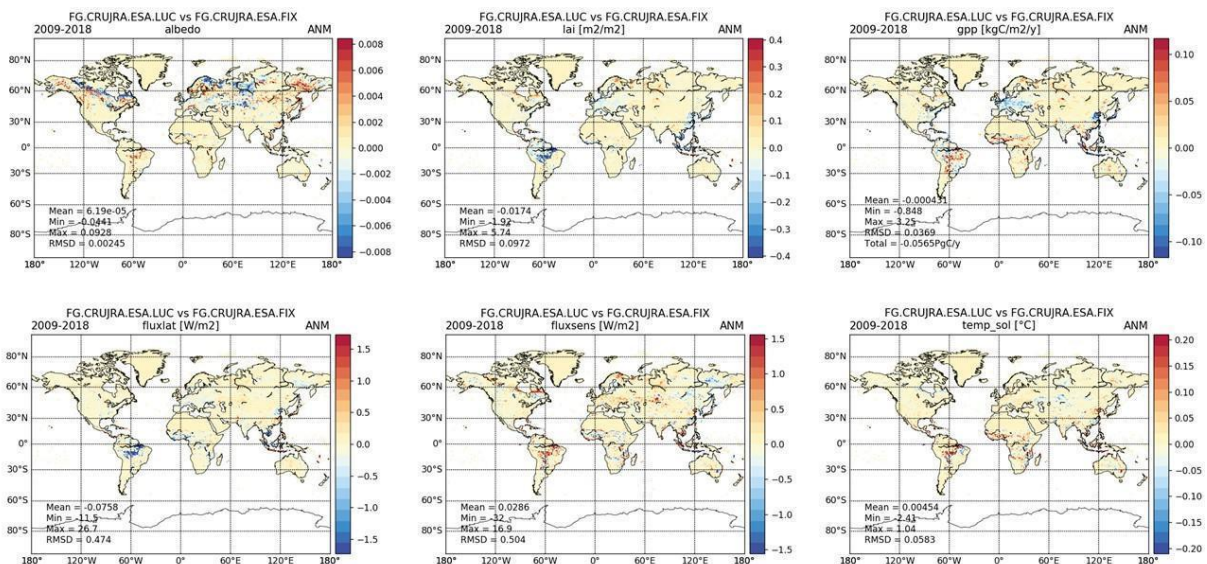


Figure 7.1: Differences between the 2 ORCHIDEE simulations (ORCHIDEE-LUC minus ORCHIDEE-FIX) forced by the same CRU-JRA atmospheric forcing.

### 7.1.2 South Brazil

To better understand how the LCC impacts the surface e-w-c transfers, Figure 5.2 shows summer averages (December to February) over the historical region of South Brazil. In the north-western part of the domain, the conversion of evergreen forest to crops translate in higher albedo values, lower LAIs (around 0.5), lower evapotranspiration (latent heat flux lower by a few W/m<sup>2</sup>) but higher GPP (around 0.3 KgC/m<sup>2</sup>/yr) because crops and grasslands are more productive than forests in the ORCHIDEE model, and larger surface temperatures up to 0.6°C because of the reduction of the evapotranspiration. In Paraguay, the conversion of evergreen forests to mosaic of croplands in the northern part and the conversion of deciduous forest to mosaic of shrublands in the southern part, produce opposite impacts on LAI, surface fluxes and finally surface temperatures, with higher temperatures on the shrublands compared to the croplands (a few tens of degrees). The different phenology of deciduous trees compared to evergreen species, combined with the two different climates (warmer and dryer in the South with lower soil water availability), result in opposite effects on LAI, evapotranspiration and surface

temperature. This point highlights the importance of land characterization in land surface models and of the cross-walking table that will interpret the land cover classes in terms of PFTs. The uncertainties already highlighted in this region where managed grasslands are mostly classified as crops and where mosaic classes are difficult to interpret, show the improvements that will be brought by the HRLC product, by a better mapping of the vegetation and an improved translation in terms of PFTs.

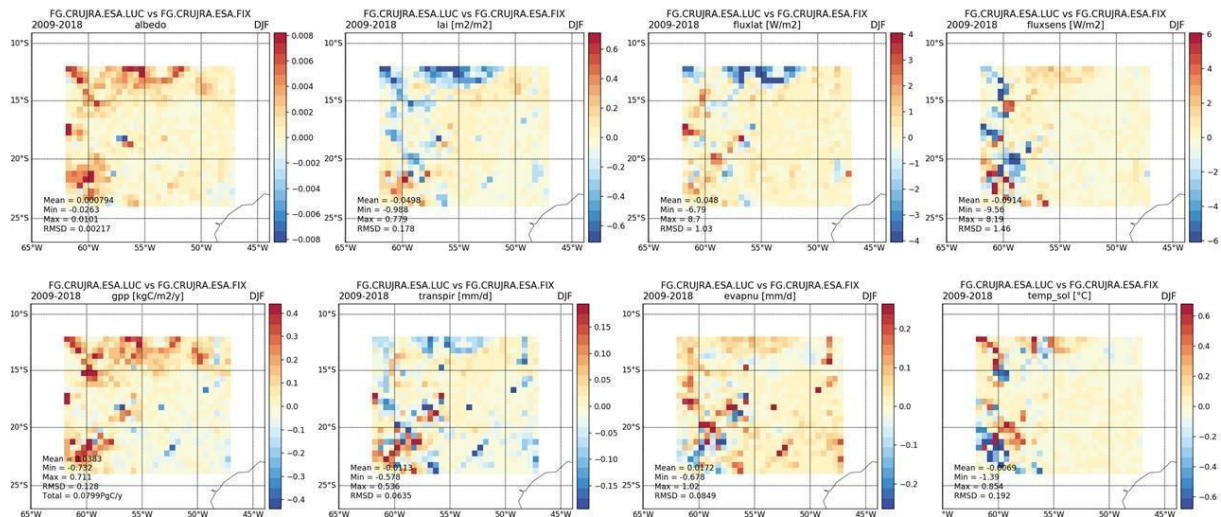


Figure 7.2: Albedo, LAI, surface fluxes (Latent and Sensible Heat, GPP, transpiration, soil evaporation) and soil temperature differences between the 2 ORCHIDEE simulations (ORCHIDEE-LUC minus ORCHIDEE-FIX) over South Brazil

## 8 First use of HRLC in ORCHIDEE to assess the improvements or deteriorations on the carbon, water and energy budgets with respect to MRLC

ORCHIDEE model was run on 4 regions of Amazonia, Ethiopia and Siberia, corresponding to the 4 tiles processed for the round-robin (RR) task, at the first production delivery. The climate and evaluation teams reported some deficiencies in the classification results, e.g., overestimation of water/flooded areas in Amazonia or some confusions between grasslands and croplands in Sahel. However, these HRLC maps have been used to assess the impacts of the land cover changes (compared to MRLC maps), on the surface fluxes and states simulated by ORCHIDEE. This preliminary assessment allowed us in addition, to set up some evaluation metrics, to quantify the changes and be able to show further improvements or deteriorations in the simulations. These metrics, named KPIs (Key Performance Indices) in the following, have been defined according to the observations available to evaluate the simulations. They are presented in Section 13.1, the analysis of the new maps and their contribution in ORCHIDEE are discussed in the following.

### 8.1 New vs MRLC land cover maps

The 4 regions which were studied correspond to the 4 RR tiles shown in Figure 8.1, i.e., 2 tiles in South-America, named in the following Amazon (21KXT) and Amazon2 (21KUQ), 1 tile in Ethiopia (37PCP) named Sahel and 1 tile in Siberia (42WXS). In this work, only the most likely class provided in the files was used to map LC and generate the PFTs maps required for ORCHIDEE, following the methodology presented in Section 4.2.

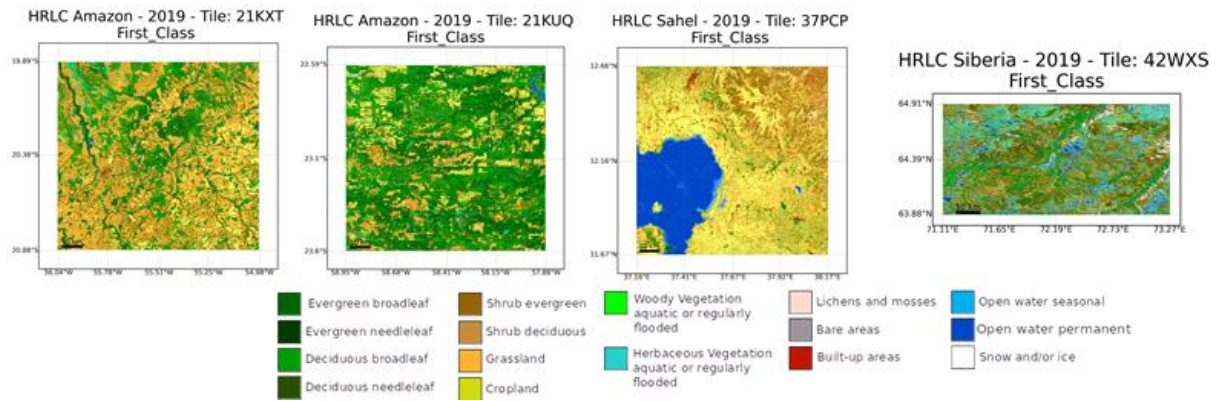


Figure 8.1 Land cover mapping of the 4 regions/tiles studied

In each of these regions, the PFT comparison with the previous MRLC-derived PFT maps, highlighted discrepancies summarized in Figure 8.2.

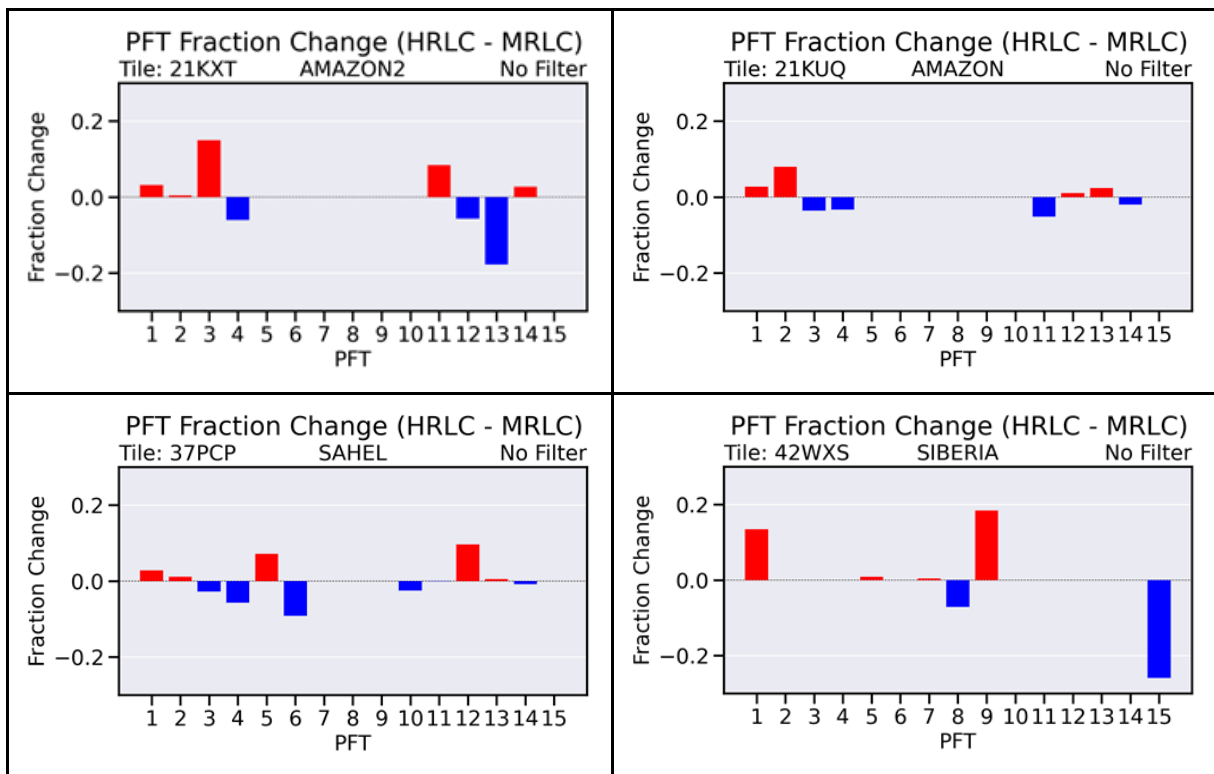


Figure 8.2: Changes in ORCHIDEE PFTs fractions for the 4 RR tiles studied.

The main changes for each region are:

- in Amazon tile: different fractions of broadleaf evergreen/raingreen trees, less needleleaf evergreen species, larger fractions of bare soil and grasslands and lower fractions of crops
- in Amazon2 tile: different fractions of broadleaf evergreen/raingreen trees, larger fractions of bare soil and crops and lower fractions of grasslands
- in Sahel tile: lower fractions of trees, except for temperate broadleaf evergreen species, larger fractions of bare soil and crops and lower fractions of grasslands

- in Siberia tile: larger fractions of bare soil and needleleaf deciduous trees, lower fractions of grasslands. Many differences in the tree species identification (needleleaf/broadleaf, evergreen/summergreen) were noted.

## 8.2 ORCHIDEE results

The model was run over the period (1992-2018) over the 4 different tiles, at three different resolutions (0.025°, 0.1° and 0.25°) forced by the same atmospheric forcing (CRU-JRA reanalysis).

As expected, the PFT changes highlighted previously, translated into changes in the albedo, vegetation momentum, thermal and hydrological properties, leading to significant differences in the surface fluxes and variables simulated. However, similar changes do not impact the surface fluxes in the same way. For example, an increase of trees in Siberia would negatively impact the albedo, increase the available energy at the surface, the turbulent fluxes and lead to lower temperatures in summer but larger temperatures the rest of the year. This is explained by the larger contribution of the sensible heat flux compared to the latent heat flux, part of the year. In the Sahelian tile, the larger fractions of bare soil and lower fractions of trees, explained the higher values simulated, the lower evapotranspiration and the increased surface temperatures consequently. Figure 8.3 illustrates the results obtained on the Amazon tile where the larger fractions of evergreen trees impact the LAI seasonality negatively, with lower agreement with the observations provided by the Eumetsat SAF-Land. The effect of the latent heat flux appears however very small when averaged on the south-eastern part of the tile with a quite good agreement with the observations.

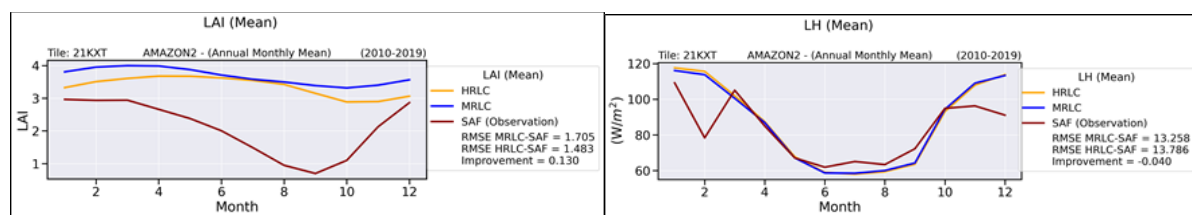


Figure 8.3: Comparison of the LAI and latent heat flux (mean seasonal cycles averaged over the period 2010-2019), simulated by ORCHIDEE with the two land cover maps MRLC and HRLC, compared to the observations from the SAF-Land. The values were averaged over the south-eastern part of the tile.

Given the small size of the new tiles and the deficiencies of the albedo parameterization in these ORCHIDEE simulations, we did not go further in the analysis of these preliminary simulations, seeing them as a way to prepare the work on the whole historical regions, i.e., set up of the most relevant observational datasets and development of the visualization and data processing tools.

## 9 Implementation and validation of LMDZ IPSL ESM on our 3 studied regions

We have seen previously how LC impacts the land surface variables simulated by ORCHIDEE (albedo, surface fluxes, soil water content and surface temperature); the objective in this project is to go further in order to understand the relationships between changes in surface properties induced by LCC and changes in the atmosphere (physics and dynamics) and the possible feedbacks. For that purpose, we need to work with an interactive atmosphere, fully coupled with the land surface, therefore with a climate model like LMDZ. In this part, we show the work which has been performed to settle the model on our 3 regions using the zoomed configuration of the coupled LMDZ - ORCHIDEE model.

### 9.1 LMDZ description

LMDZ is the atmospheric General Circulation Model (GCM) that has been developed for about thirty years at the "Laboratoire de Météorologie Dynamique (LMD)". The "Z" in "LMDZ" stands for "zoom" capabilities, indicating

that the horizontal grid is stretchable in both longitude and latitude. The model is composed of two parts: i) a dynamical core in which the three dimensional primitive equations are discretized on a longitude-latitude horizontal grid, and ii) a physical part in which the vertical transfers of heat, moisture and momentum associated with physical parameterizations are computed. The mass and energy transfers at the land interface are calculated by the ORCHIDEE land surface model (Cheruy et al., 2020).

## 9.2 Zoom implementation in the 3 study regions

LMDZ (version 6.1.9) has been implemented in 3 configurations zoomed in the historical regions. Figure 6.1 presents the grid structure zoomed over South Brazil, Ethiopia and Western Siberia. In these configurations, the dimension of the grid is 142x144 boxes horizontally and 79 levels vertically. For all the configurations, a zoom factor of 5 was used, meaning that the grid cell is divided by 5 at the center of the zoomed area. As a consequence, the size of the grid cell is equal to 54.8 km x 28.2 km at zoom center in Ethiopia, to 52.9 km x 28.2 km in Brazil and to 21.7 km x 28.2 km in Siberia.

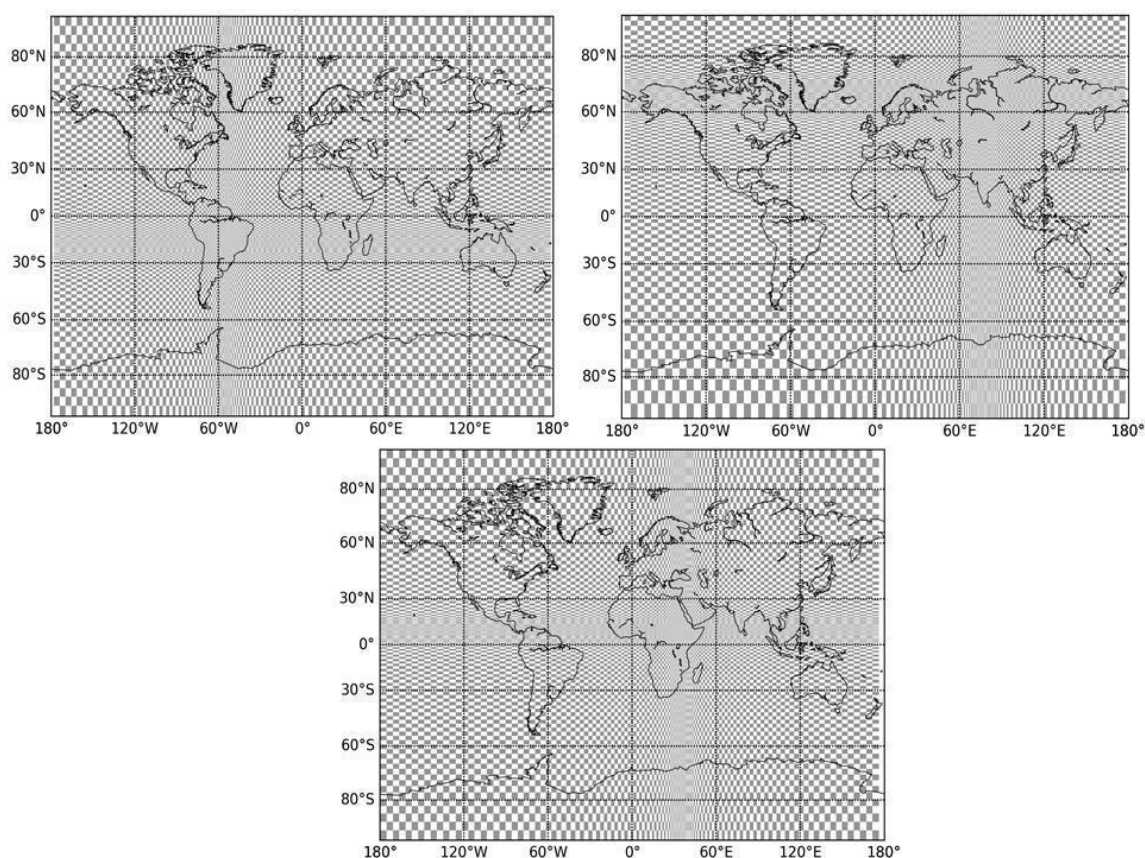


Figure 9.1: LMDZ grid for the three zoomed configurations over South Brazil, Ethiopia and Western Siberia

## 9.3 Simulations performed

Three simulations were performed over the time period (1966 - 2015) with each configuration, all of them were done using the nudging capacity of the model to constrain the large scale dynamics of the winds. In practice wind-nudging consists in relaxing the horizontal winds of the model towards those of the reanalysis produced by numerical weather forecast centers with a typical time constant of several hours (in our case a reanalysis from ECMWF). By constraining large scale features (dynamics) to be close to the observed ones, nudging allows to derive meteorological time series which can be confronted on a day-by-day basis to observations with much smaller errors than using a free GCM (Coindrau et al., 2007, Cheruy et al., 2013).

The three LMDZ simulations performed were compared to the independent CRU-JRA atmospheric reanalysis on a five-year period (2011 - 2015), in order to verify that the model configurations are correctly defined and that the simulated atmospheric variables are realistic. The idea here is to validate the model dynamics and quantify the systematic errors and internal model noise in order to allow the interpretation of differences between simulations. We recall that the objective is to run the model with different land cover maps to separate the respective roles of the land surface and of the global climate patterns on the simulated surface variables.

Figure 9.2 shows the comparison of various atmospheric and surface variables (rainfall, shortwave and longwave radiations, LAI, sensible and latent heat fluxes, air temperature and total soil water content) simulated by LMDZ in the African configuration with the CRU-JRA forcing resampled at 0.5° on the time period (2011-2015). The differences (coupled GCM minus CRU-JRA reanalysis) in annual mean are plotted here. Given that the 3 configurations give the same results, we present only one model configuration (the simulation zoomed on Ethiopia).

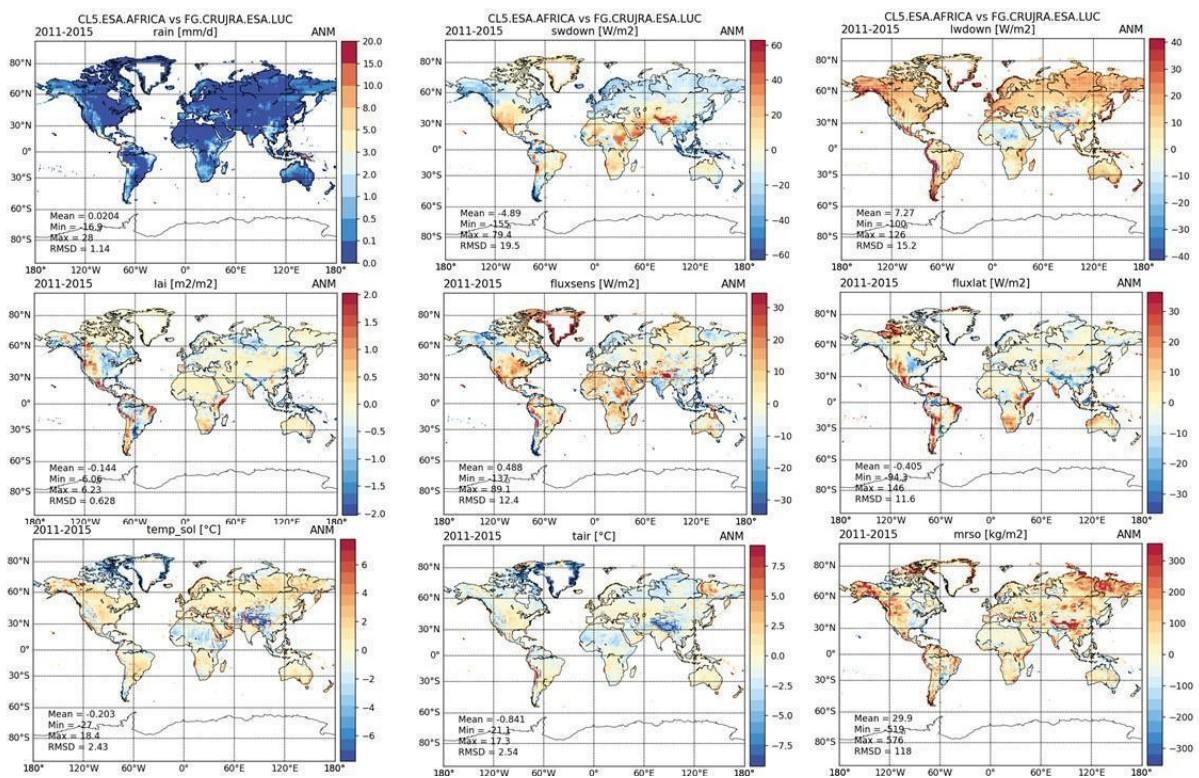


Figure 9.2: From left to right and top to bottom: rainfall, downward shortwave, longwave radiations, LAI, sensible and latent heat fluxes, soil and air temperatures and total soil water content simulated by LMDZ and compared to CRU-JRA reanalysis. The differences (LMDZ minus CRU-JRA) are plotted globally and on annual mean over the time period (2011- 2015).

The plots confirm that LMDZ with its zoomed capacity and with a simple nudging of the winds with reanalysis, is able to correctly reproduce the atmosphere dynamics and the global climate. The albedo comparison (not shown here) shows that the surface albedo is slightly overestimated in the northern latitudes, explaining the bias observed on the shortwave radiation. The snowfall comparison shows that in the same area, the snowmass is larger in the coupled simulations leading to higher albedo values. A moderate bias of about 20 W/m2 is also observed in the atmospheric longwave radiation, probably linked to larger cloudiness (to be confirmed with more analysis). Spatial differences in the rainfall can also be noted, for example over the north of America. These

differences explain the differences in the LAI and in water and carbon fluxes, and the resulting surface temperatures.

Looking at the monthly time series of air temperature, rainfall and LAI averaged on the three historical regions for the 3 model configurations (Figure 9.3), shows that the seasonal cycles are well represented and well phased compared to the reanalysis. Over Ethiopia, a negative bias on the air temperature (around 1°C) is highlighted, probably linked to the excess of cloudiness and storms on the high reliefs, but the monthly rainfall and LAI present very good agreement. Over South Brazil, the air temperature is positively biased, especially during the start of the rainy season (above 1 °C). This bias corresponds to a positive bias on the shortwave radiation; LAI time series show larger seasonal amplitude but lower values especially in the dry season (up to 1 lower) which may be linked to the higher air temperatures which induce larger hydric stress. Over Siberia, rainfall and air temperatures are correctly represented, snowfall differences (not shown here) which is larger in the coupled model, explain the larger soil water capacity and the larger productivity of the vegetation (forest, shrubs and grasslands) present in this area. All this comparison and the overall good agreement between CRU-JRA and our LMDZ-ORCHIDEE simulation shows that LMDZ in the 3 configurations that we have developed in our study regions is really reliable and can be used in later experiments to understand the impacts of LCC on the regional climate.

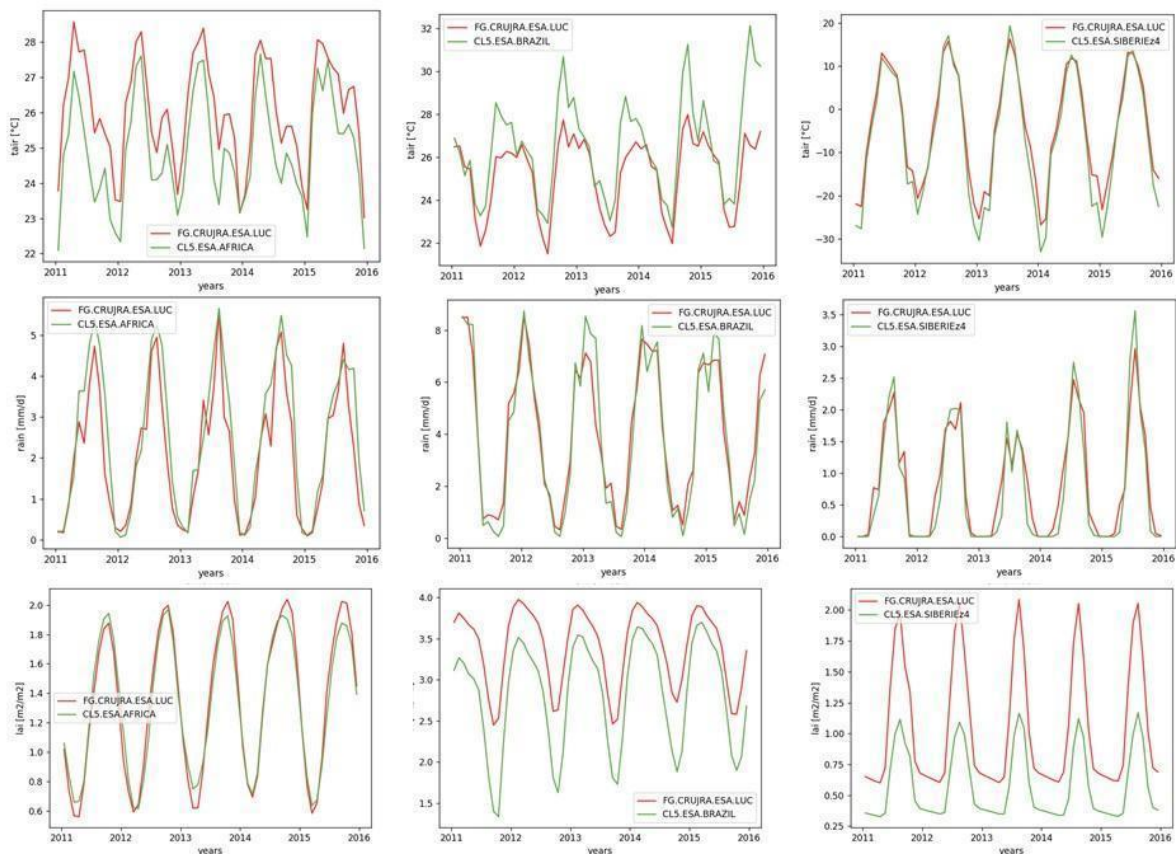


Figure 9.3: Monthly time series of air temperature, rainfall and LAI over the five years (2011 - 2015), averaged over the 2 historical regions (from left to right: Ethiopia, South Brazil and Western Siberia).

## 10 New albedo optimization in ORCHIDEE

Before launching the final ORCHIDEE-LMDZ coupled simulations with HRLC's first production, a new albedo optimization scheme has been developed and implemented.

The optimization is carried out in three steps, aiming to successively calibrate the PFT's leaf albedo, the PFT-dependent snow albedo and the soil background albedo (bare soil albedo).

The full description of the procedure is described in: [https://orchidas.lscce.ipsl.fr/dev/albedo/3\\_steps.php](https://orchidas.lscce.ipsl.fr/dev/albedo/3_steps.php)

The evaluation work performed during the project, in the evaluation against GlobAlbedo and MODIS products as well as the revision of the CWTs, allowed us to define more realistic ranges of variations of the parameters (intervals assigned to constrain the optimization process) and to use higher resolution and more recent auxiliary products like the prior background albedo whose resolution has been increased by a factor 50, from 0.5° to 0.01°. The optimization was performed at the global scale and also regionally on our 3 study static regions. The final results for the leaf albedos are given in Table 10.1

We can see that the albedo difference between trees and grasses PFTs has increased (Table 10.1), and we expect that this effect, together with that of the improved snow and soil background albedo, will bring a global improvement to ORCHIDEE's simulated albedo, specially over the areas with deforestation processes such as Amazonia and areas where the background albedo has a high impact on the overall albedo, such as in the Sahelian grasslands and shrublands.

Table 10.1: Global vegetation albedos obtained at the end of the optimization process

LEAF_ALB (NIR)	PFT2	PFT3	PFT4	PFT5	PFT6	PFT7	PFT8	PFT9	PFT10	PFT11	PFT12	PFT13	PFT14	PFT15
<i>prior</i>	0.23	0.18	0.18	0.2	0.24	0.15	0.26	0.2	0.24	0.27	0.28	0.26	0.24	0.24
<i>min</i>	0.17	0.17	0.1	0.1	0.16	0.1	0.1	0.16	0.1	0.17	0.1	0.15	0.1	0.2
<i>max</i>	0.25	0.24	0.23	0.24	0.24	0.19	0.33	0.23	0.36	0.36	0.46	0.36	0.29	0.35
<i>post</i>	0.204	0.189	0.15	0.176	0.228	0.129	0.263	0.178	0.296	0.258	0.259	0.292	0.222	0.323
LEAF_ALB (VIS)	PFT2	PFT3	PFT4	PFT5	PFT6	PFT7	PFT8	PFT9	PFT10	PFT11	PFT12	PFT13	PFT14	PFT15
<i>prior</i>	0.04	0.04	0.04	0.04	0.03	0.03	0.03	0.03	0.06	0.06	0.06	0.06	0.06	0.06
<i>min</i>	0.02	0.02	0.01	0.01	0.02	0.01	0.02	0.02	0.02	0.04	0.02	0.05	0.02	0.04
<i>max</i>	0.06	0.08	0.09	0.08	0.07	0.05	0.04	0.04	0.18	0.18	0.23	0.15	0.16	0.1
<i>post</i>	0.022	0.02	0.023	0.023	0.02	0.023	0.02	0.02	0.046	0.048	0.051	0.060	0.02	0.04
	5		1	1		4			4	5	3	6		
LEAF_ALB (VIS+NIR)	PFT2	PFT3	PFT4	PFT5	PFT6	PFT7	PFT8	PFT9	PFT10	PFT11	PFT12	PFT13	PFT14	PFT15
<i>prior</i>	0.14	0.11	0.11	0.12	0.14	0.09	0.15	0.12	0.15	0.17	0.17	0.16	0.15	0.15
<i>post</i>	0.11	0.10	0.09	0.10	0.12	0.08	0.14	0.10	0.17	0.15	0.16	0.18	0.12	0.18
<i>Difference (%)</i>	-2.18	-0.55	-2.35	-2.05	-1.10	-1.38	-0.35	-1.60	<b>+2.12</b>	-1.18	-1.49	<b>+1.63</b>	-2.90	<b>+3.15</b>

Table 10.2: Global calibration of snow albedo parameters

Full spectra	PFT1	PFT4/5/7	PFT6/8/9	PFT10-15
<i>snow_aged_prior</i>	0.50	0.30	0.30	0.50
<i>snow_aged_post</i>	0.60	0.15	0.32	0.61
<i>Difference</i>	<b>+0.1</b>	-0.15	<b>+0.02</b>	<b>+0.11</b>
<i>snow_dec_prior</i>	0.15	0.15	0.15	0.15
<i>snow_dec_post</i>	0.18	0.01	0.03	0.09
<i>Difference</i>	<b>+0.03</b>	-0.14	-0.12	-0.06

	Ref	CCI_HRLC_Ph1-CAR		
	Issue	Date	Page	
	3.0	28/10/2022	32	

Snow albedo parameters have been also revised using daily MODIS albedo products and the new values are given in Table 10.2. The two parameters that have been calibrated are related to the albedo of aged snow and a parameter controlling the decay of snow albedo with age. The new values of aged snow are larger for bare soil (PFT1) and short vegetations (PFT 6 to 15) and lower for tree PFTs. The decay parameters are lower for all the vegetation types except for bare soils. Such values should lead to larger simulated albedos during the snow periods with consequences on the duration of the snow cover (increased duration with lower melting rates).

## 11 Analysis of land cover – atmosphere feedbacks with ORCHIDEE-LMDZ

We used the HRLC products to analyse the impacts of a better characterization of the vegetation and related properties such as the surface albedo, on the surface energy-water and carbon budgets and the boundary atmosphere. For that task, we run our land surface model ORCHIDEE in 6 different configurations: with a prescribed atmosphere given by atmospheric reanalysis (CRUJRA dataset, similar as in the previous simulations) and fully coupled with the atmospheric model LMDZ and using 3 different land cover maps: the former MRLC product for 2 different years 1995 and 2019 and the new HRLC product (static map for year 2019). The analysis of the simulations performed with 2019 HRLC and MRLC maps allowed to analyse the benefit of the HRLC developments, whereas, the comparison of the simulations performed with 1995 et 2019 MRLC maps allowed to assess the impacts of the LC net change that occurred between 1995 and 2019 on the regional climate. Finally, the comparison of forced and coupled simulations allowed assessing the atmospheric feedbacks in our study regions for which these feedbacks are known to be important. To summarize, the six simulations performed for each of the 3 studied regions are the following:

- Forced ORCHIDEE simulation with the static MRLC 2019 map and CRUJRA atmospheric reanalysis
- Forced ORCHIDEE simulation with the static MRLC 1995 map and CRUJRA atmospheric reanalysis
- Forced ORCHIDEE simulation with the static HRLC 2019 map and CRUJRA atmospheric reanalysis
- Coupled ORCHIDEE-LMDZ simulation with the static MRLC 2019 map and CRUJRA reanalysis
- Coupled ORCHIDEE-LMDZ simulation with the static MRLC 1995 map and CRUJRA reanalysis
- Coupled ORCHIDEE-LMDZ simulation with the static HRLC 2019 map and CRUJRA reanalysis

The forced simulations have been done at the resolution of the CRU-JRA dataset (i.e., with a grid mesh of 0.5°), and the LMDZ-ORCHIDEE simulations have been performed in the same zoomed configuration presented in section 9.2, but after refocusing the zoom on the center of the static region (accounting for the new limits defined during the project) and relaxing the wind nudging inside the zoom (no nudging in the boundary layer and upper in the atmosphere using a nudging frequency of 10 days). The wind nudging outside the zoom was kept to the default value of the time step of the ERA5 reanalysis used to constrain LMDZ (i.e., 6 hours). The simulations were done on the time periods (1975-2014 in forced mode, and 1995-2014 in coupled mode) and the results are analysed on the same time period (2005-2014).

In this report, given that the static maps were available only for year 2019, we focus on the analysis of the simulations performed with the maps of 2019. The analysis of the simulations performed in 1995 will be part of the next section on the historical regions. Then, for each region, we present first the differences between the PFT maps used in the MRLC and HRLC simulations, the impacts of the PFT differences on the surface fluxes and variables in forced mode and the atmospheric feedbacks identified.

### 11.1 Amazonian region

The static HRLC map covers the region limited by the following coordinates (0 - 23.5S, 62W - 43W). The new CWT presented in section 4 was used to interpret the LC classes in terms of ORCHIDEE PFTs. To generate the global PFT maps needed to run ORCHIDEE-LMDZ, we used the MRLC-PFT global maps and replace the data where the HRLC-PFT data where available.

### 11.1.1 PFT maps used in the simulations

The PFT maps are all available on our website at <https://orchidas.lsc.ipsl.fr/mapper/>. Figure 11.1 presents for each of the ORCHIDEE PFTs its fraction in the HRLC product and the fraction of changes when moving from MRLC to HRLC maps. The study region covers a part of the Amazonian broadleaf evergreen forest in the north-eastern part, some broadleaf raingreen trees southern shared with grasslands and croplands (mainly C4 types) (Figure 11.1, left). Compared to the former MRLC product, we observed in the HRLC dataset, that there is slightly more broadleaf evergreen (PFT2) and less raingreen trees (PFT3) at the benefit of grasslands (PFT11), slightly less crops and a rearrangement between C3 and C4 crops, because of the revising of the Land Cover-PFT Cross Walking Table. If we look only to the variation in tree amount (after aggregating the various tree species) and in order to get a global picture of the dominant changes, we can see in Figure 11.2 that the tree fraction has significantly decreased along a diagonal SW-NE up to 20% and increased in the region of the Amazon delta and along the 50°W meridian. If we compare those changes to the ones that can be related to the forest deforestation between 1995 and 2019 (Figure 11.1, central plot), we can see that the changes are of the same order of magnitude and present a larger extension. We will see in the following that the impacts on the surface processes and the atmosphere are coherent and can be used to better understand the vegetation-atmosphere feedbacks in this region.

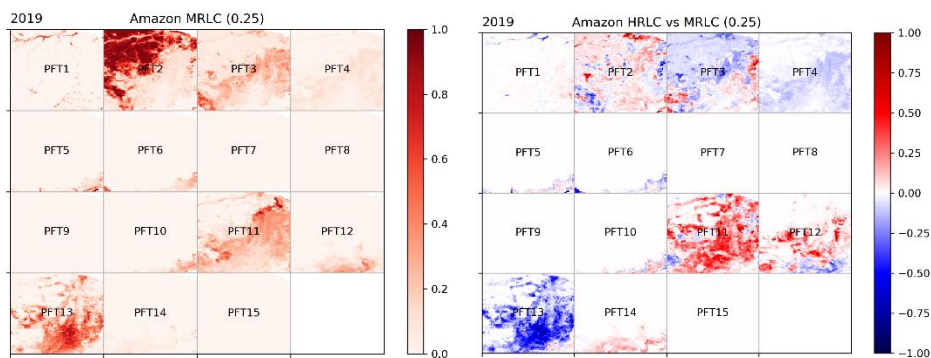


Figure 11.1: ORCHIDEE PFT fractions derived from HRLC product (left) and differences between the HRLC and MRLC products aggregated at 0.25° (right).

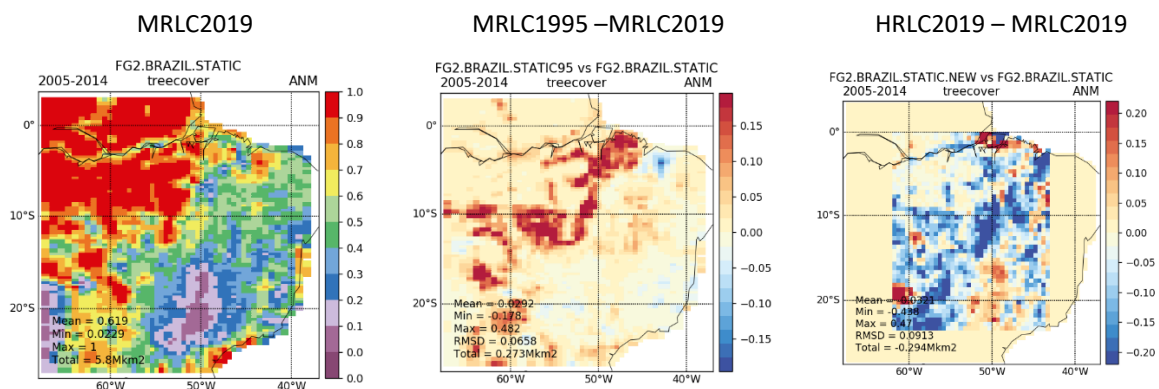


Figure 11.2: from left to right, tree cover fraction from MRLC2019 and differences (MRLC1995- MRLC2019) and (HRLC2019-MRLC2019)

### 11.1.2 Impacts of HRLC-MRLC differences on surface variables

The analysis of the simulations performed with a prescribed atmosphere show the impacts of moving from the MRLC to HRLC product in ORCHIDEE. Changes of albedo are seen in the regions where LC is different but also elsewhere because of the refinement of the albedo model. We observe an overall decrease of the surface albedo up to 0.02% (in absolute value) and a slight increase on the diagonal where the tree cover decreased. These albedo changes translate in a larger amount of available energy where albedo decreased (and the other way round where albedo increased), a decrease of the surface latent heat flux where tree cover decreased compensated by an increase of sensible heat flux, leading to more water in the soils (not shown here) and lower simulated LAI and GPP values in these regions. The differences in C3/C4 crop fractions (less C4, more C3 in the SE quarter) and in grasses/crops fractions (more grasslands and less crops) explained also part of the LAI and GPP impacts, since C4 crops are more productive than grasslands in ORCHIDEE. As a result, surface temperature shows variations explained by the variations in the turbulent fluxes partition with larger surface temperatures where sensible heat decreased, all these processes strongly related to the amount of soil water available. Thus, a similar variation of tree cover in the humid northern part has more impact on the transpiration and sensible heat fluxes and surface temperature (especially in summer season) than in the more arid south region.

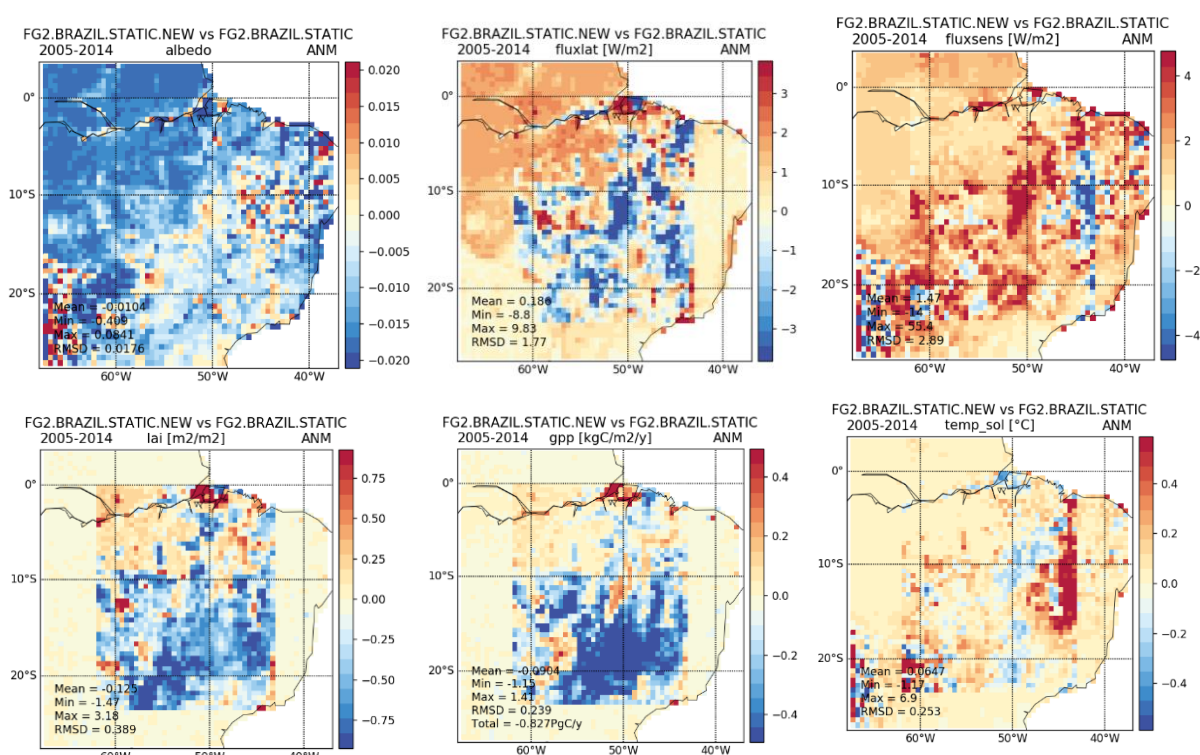


Figure 11.3: Upper panel: surface albedo, latent heat and sensible heat fluxes simulated by ORCHIDEE; Lower panel: LAI, GPP and soil temperature; all variables are annual averages for the period (2005-2014)

### 11.1.3 Land cover – atmosphere feedback analysis

The atmospheric impacts of the land cover and albedo changes between MRLC and HRLC simulations can be seen on Figure 11.4 which display the same surface variables (surface temperature, sensible and latent heat fluxes) as well as air temperature, wind speed and total rainfall. The same features identified using a prescribed atmosphere can be seen but amplified in annual mean. Surface temperature for example show larger amplitudes in annual mean, with maximum differences in summer (JJA) up to 7°C in daily mean (compared to 1.4°C in forced mode). This amplification is probably the result of the increased wind speed in the regions where tree amount

decreased leading to an increase of the turbulence and of the surface fluxes. The increased surface temperatures in the less forested regions, lead to larger air temperatures that will themselves amplify the surface fluxes. Rainfall is slightly impacted with lower precipitation (up to 0.4 mm/jour in annual mean) where tree amount decreased, mainly linked to a decrease of convective precipitation and larger rainfall elsewhere resulting from the increase of large scale precipitation due to the larger winds and land-sea temperature gradients.

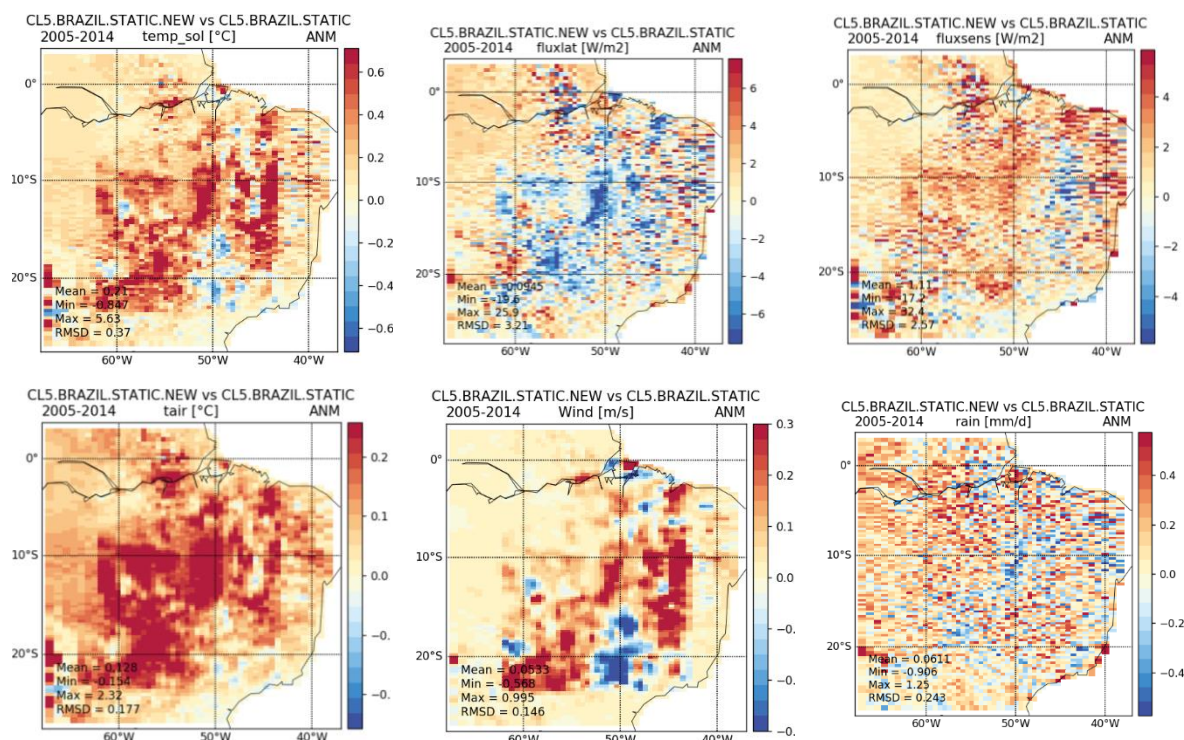


Figure 11.4: Upper panel: soil temperature, latent heat and sensible heat fluxes simulated by LMDZ; Lower panel: air temperature, wind speed and rainfall; all variables are annual averages for the period (2005-2014)

### 11.1.4 Comparison with observations

Comparison to observations allow to see if the HRLC changes compared to MRLC lead to improvements in the simulation of surface variables by ORCHIDEE. Here, we used various satellite products for LAI, albedo, evapotranspiration, soil moisture, surface temperature as well as surface fluxes, to quantify the model improvements or degradations. The products used are the following:

- Albedo products:

MODIS MCD43C3 16 days global dataset at 0.05° from 2000 to 2020 (Schaaf and Wang, 2015)

GLOBALBEDO, 8-daily, 0.05°, from 1998 to 2011 (Muller et al., 2011)

GLASS-AVHRR, daily, 0.05°, from 1981 to present (Liang et al., 2020)

- LAI:

GIMMS

Copernicus, SPOT/VEGETATION, PROBA-V, 1 km, 1999-2020, v2.0, (Verger et al., 2014)

- LST :

SAF-Land, 0.05°, 2004-2019, Trigo et al., 2011

- Latent, sensible heat fluxes, GPP

FluxNET- MTE, 0.25°, Jung et al., 2009

- Evapotranspiration, Soil moisture

GLEAM, V3., 0.25°, 1980 – 2021, Martens et al., 2016

Figure 11.5 presents the comparison of the 2 coupled simulations (MRLC based) and HRLC based with the observations in annual mean. The model errors show about the same amplitudes but some slight improvements may be seen in some parts of the domain. For example, we can see that the LAI and GPP errors have decreased in the center of the domain (between 10°S and 20°S, 60°W and 50°W) a region where tree amount and crops are lower to the benefit of grasslands in HRLC compared to MRLC. Improvements are less visible on the albedo and the other surface fluxes (latent and sensible heat fluxes, not shown here), but it is important to note that the albedo data are not independent since they were used to calibrate the former MRLC version. More datasets are then needed to evaluate the simulations.

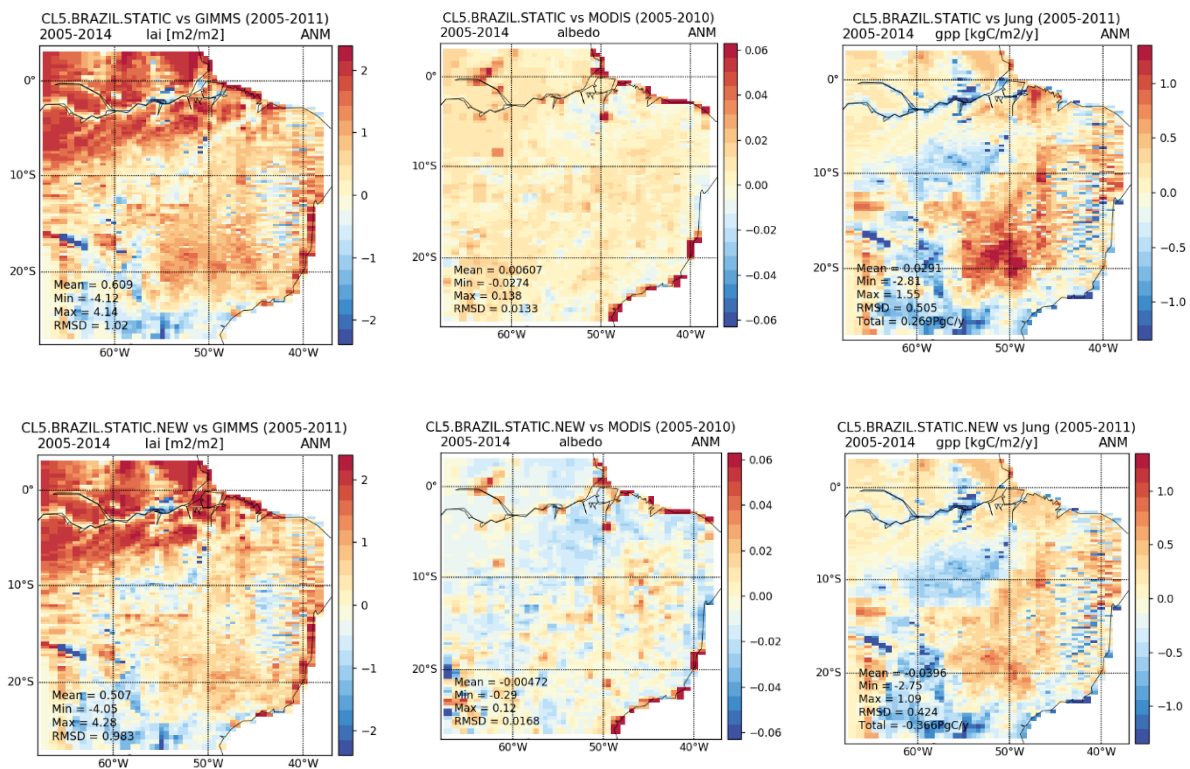


Figure 11.5: Differences (simulated- observations) for LAI, albedo and GPP obtained for 2 LMDZ simulations based on the former MRLC land cover map (upper panel) and with the new HRLC product (lower panel).

## 11.2 Africa

The resized African static map covers the region 18°N – 0°, 10°E – 43°25E. Same protocol and methodology was used to perform the simulations in prescribed atmosphere and coupled to LMDZ and with the 3 different LC maps (MRLC1995, MRLC2019 and HRLC2019).

### 11.2.1 PFT maps used in the simulations

In this region, the vegetation ranges from tropical rainforest in the south-western part to broadleaf raingreen trees, grasslands and crops northern. Further north, the southern part of the Sahara presents large fractions of bare soils (Figure11.6 left). The same figure shows the differences between the HRLC and MRLC derived PFT maps aggregated at the resolution of 0.25°. Tree PFTs fractions are generally lower in the northern part of Sahel but larger southern. More grasslands and different partition of C3 and C4 crops is also seen. The fraction of bare soil has also changed in the northern part of the region (more for longitudes larger than 20°E and less below) and translated to grasslands changes. Considering only the variations of tree coverage in Figure11.7, we see that tree fractions decreased up to 20% in the northern part of Sahel and increased in about the same proportions in the south-western part of the domain and that extreme values can be up to 58%. If we compare to the LC changes that were mapped in the MRLC product between 1995 and 2019, we see that the changes are much more important between the 2 products with extrema less than 20%.

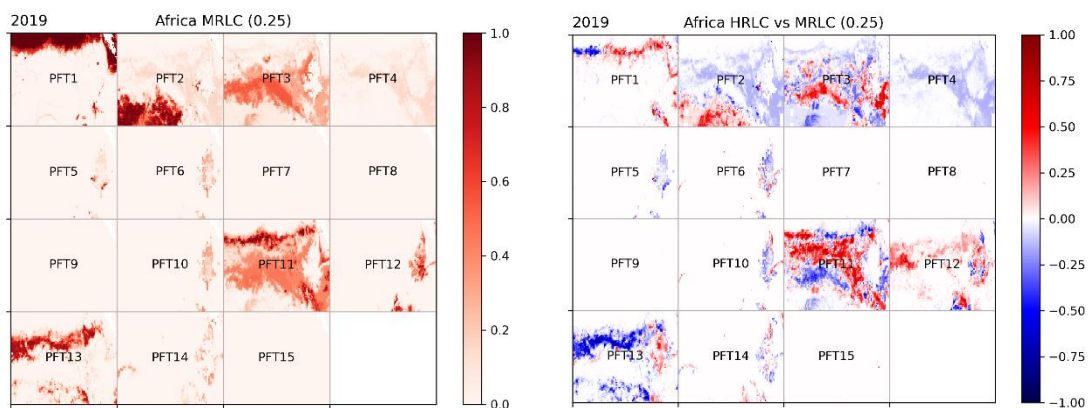


Figure 11.6: ORCHIDEE PFT fractions derived from HRLC product (left) and differences between the HRLC and MRLC products aggregated at 0.25° (right).

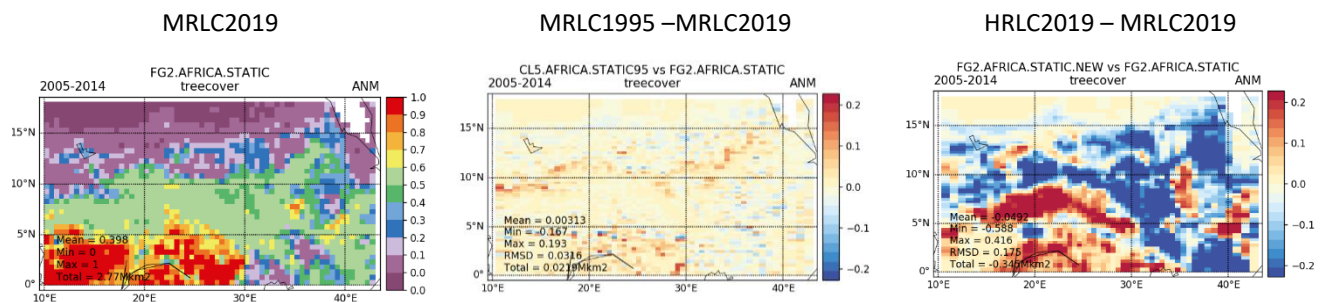


Figure 11.7: from left to right, tree cover fraction from MRLC2019 and differences (MRLC1995- MRLC2019) and (HRLC2019-MRLC2019)

## 11.2.2 Land cover impacts on surface variables

Figure11.8 shows how these LC differences translated in surface processes in prescribed atmospheric conditions. The albedo difference map shows lower values up to 4% in absolute values where the tree fraction is larger and opposite variations where tree increased. In consequence, turbulent fluxes vary following the energy budget variations, soil moisture follows the evapotranspiration changes and GPP the tree cover changes and the changes between C3 and C4 grasslands/crops differences, as what was observed in Amazonia.

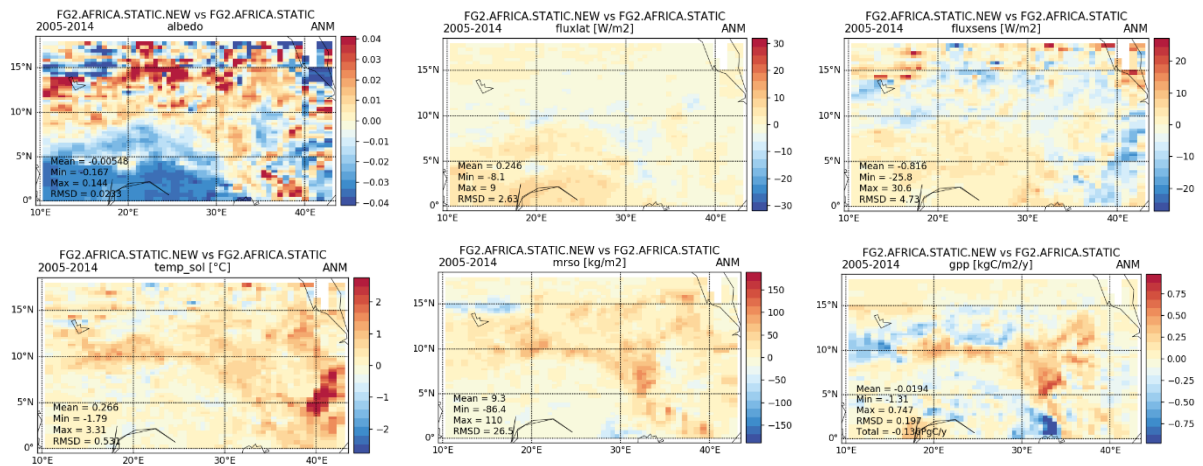


Figure 11.8: Upper panel: surface albedo, latent heat and sensible heat fluxes simulated by ORCHIDEE; Lower panel: soil temperature, soil water content and GPP; all variables are annual averages for the period (2005-2014)

### 11.2.3 Land cover – atmosphere feedback analysis

The impacts on the atmosphere are shown on Figure 11.9, and display different features. The soil temperature presents similar variations compared to the forced simulations but the latent heat flux appears more impacted with a larger RMSD (4.63W/m<sup>2</sup> compared to 2.63 in annual mean) and larger extrema, whereas sensible heat flux presents about the same statistics. Air temperature, wind speed, LAI and rainfall presents variations explained by the tree cover variations with larger impacts on the convective precipitation which dominates the rainfall contribution compared to the large scale one in the regions impacted by the tree cover changes (central Africa).

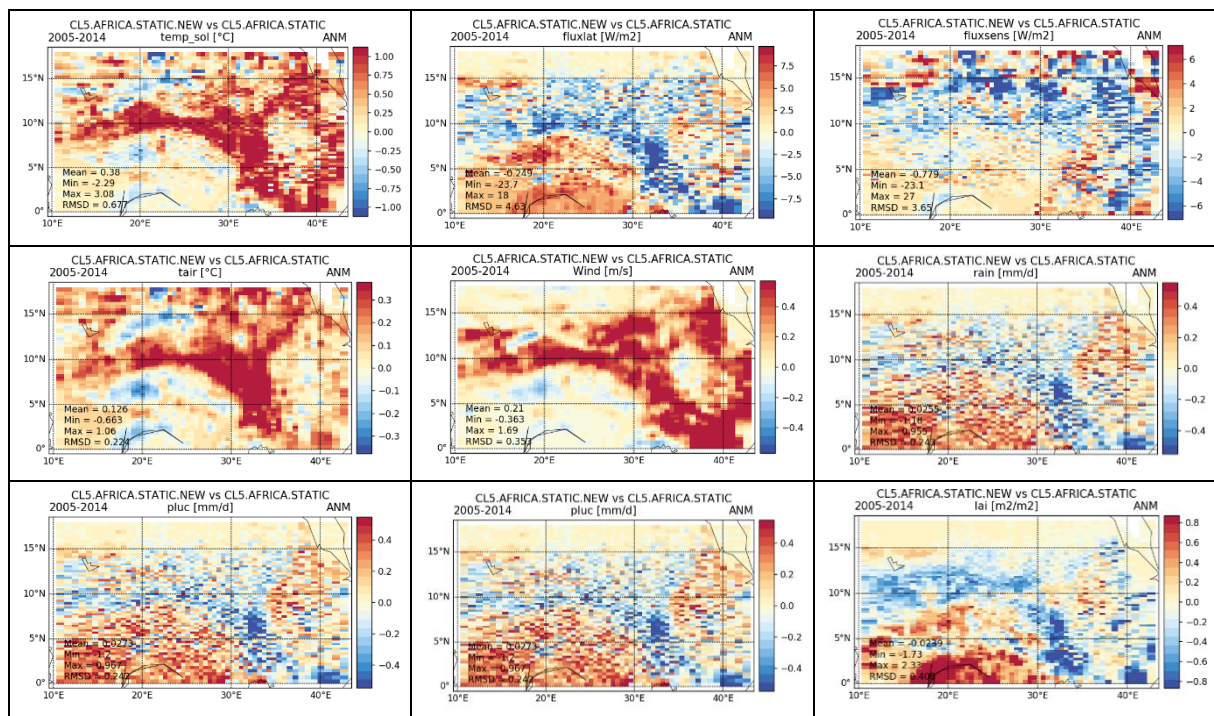


Figure 11.9: Upper panel: soil temperature, latent heat and sensible heat fluxes simulated by LMDZ; Middle panel: air temperature, wind speed and rainfall; Lower panel: large scale precipitation, convective precipitation and LAI; all variables are annual averages for the period (2005-2014)

### 11.2.4 Comparison with observations

Comparison to observations do not highlight much improvements, the errors on LAI and GPP are about the same, slight improvement could be seen in the northern part of the domain (between 10°N and 15°N) where the tree cover decreased to the benefit of grasslands. Albedo is slightly improved in the 5°N -10°N latitudinal band but degraded in the northern part of the region probably linked to the revision of the background albedo which contributes a lot in this zone presenting a large fraction of bare soils. This point will require further analysis in the next future.

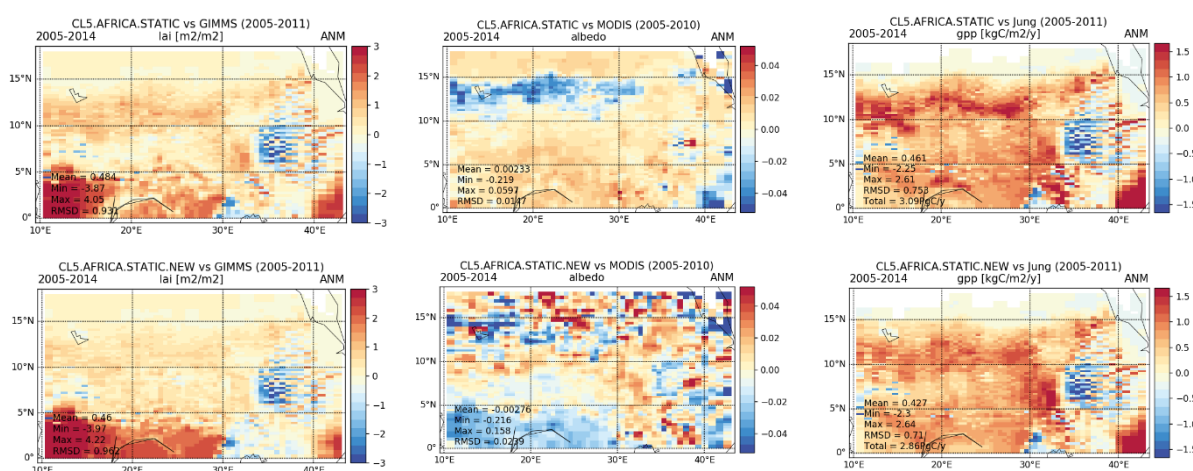


Figure 11.10: Differences (simulated- observations) for LAI, albedo and GPP obtained for 2 LMDZ simulations based on the former MRLC land cover map (upper panel) and with the new HRLC product (lower panel).

## 11.3 Siberia

The resized Siberian static map covers the region 75.75N-51.25N, 64.5E-93.5E. It covers the north-western part of Siberia and the vegetation vary from crops in the south to boreal forests, grasslands and bare soils in the extreme north.

### 11.3.1 PFT maps used in the simulations

The comparison of the HRLC and MRLC PFTs maps (Figure 11.11) shows differences in the various fractions of tree amounts with slightly less trees in the northern part to the benefit of grasslands, less crops and more grasslands in the south. After aggregation of tree PFTs, we can see that overall, the tree fraction is reduced up to 20% in the northern part and mostly increased southern with an increase of broadleaf summer green trees. Here again, if we compare with the LCC mapped by the MRLC product between 1995 and 2019, these changes are much more consequent and expected to lead to stronger impacts on the atmosphere.

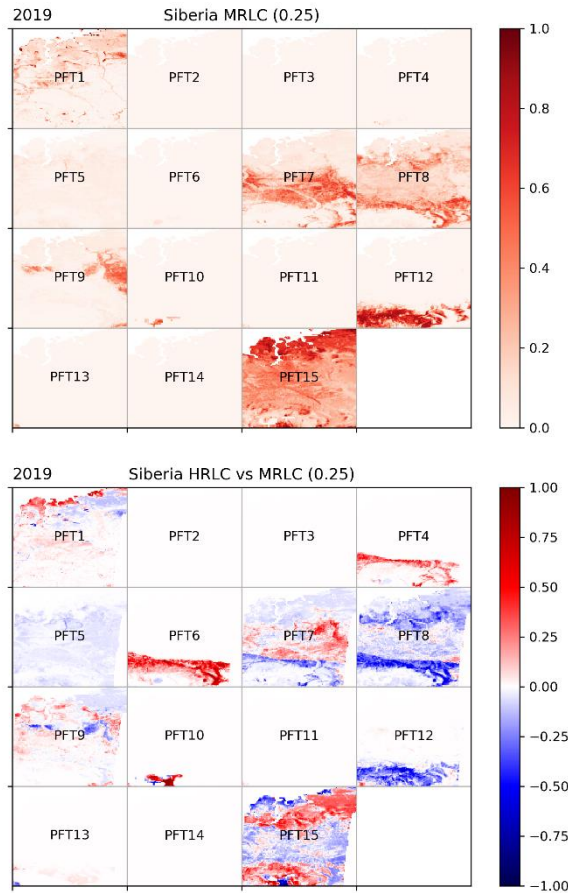


Figure 11.11: ORCHIDEE PFT fractions derived from HRLC product (left) and differences between the HRLC and MRLC products aggregated at 0.25° (right).

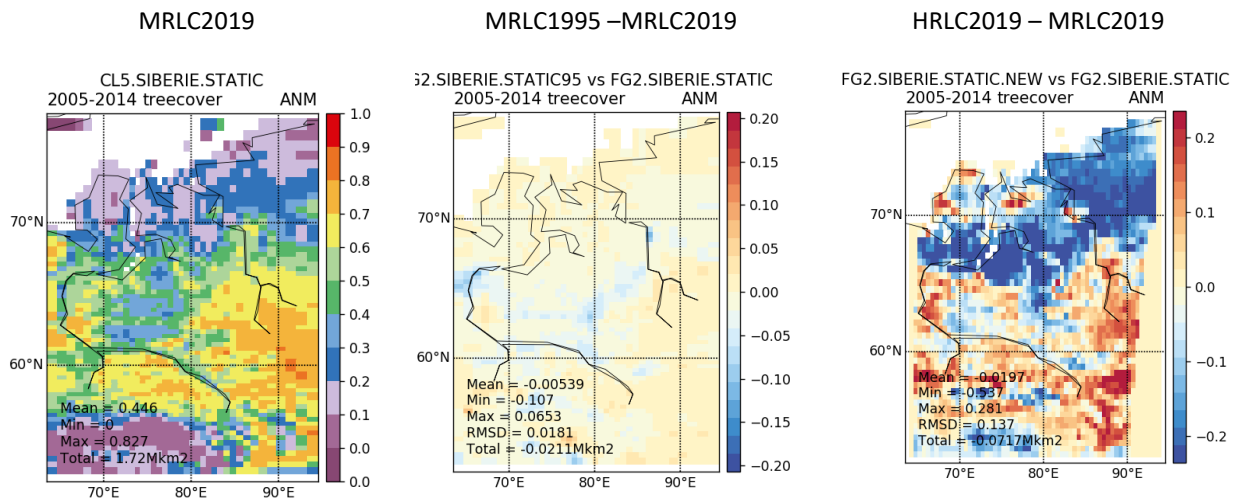


Figure 11.12: from left to right, tree cover fraction from MRLC2019 and differences (MRLC1995- MRLC2019) and (HRLC2019-MRLC2019)

### 11.3.2 Land cover impacts on surface variables

Because of the smaller albedos of trees compared to grasslands and the albedo revisions, the tree cover difference in the north leads to larger albedo values and the opposite is observed southern (Figure 11.13). Consequently, the net energy is smaller, the turbulent fluxes and the surface temperature reduced (up to 0.3°C), same for LAI and soil moisture is increased because of the lower evapotranspiration.

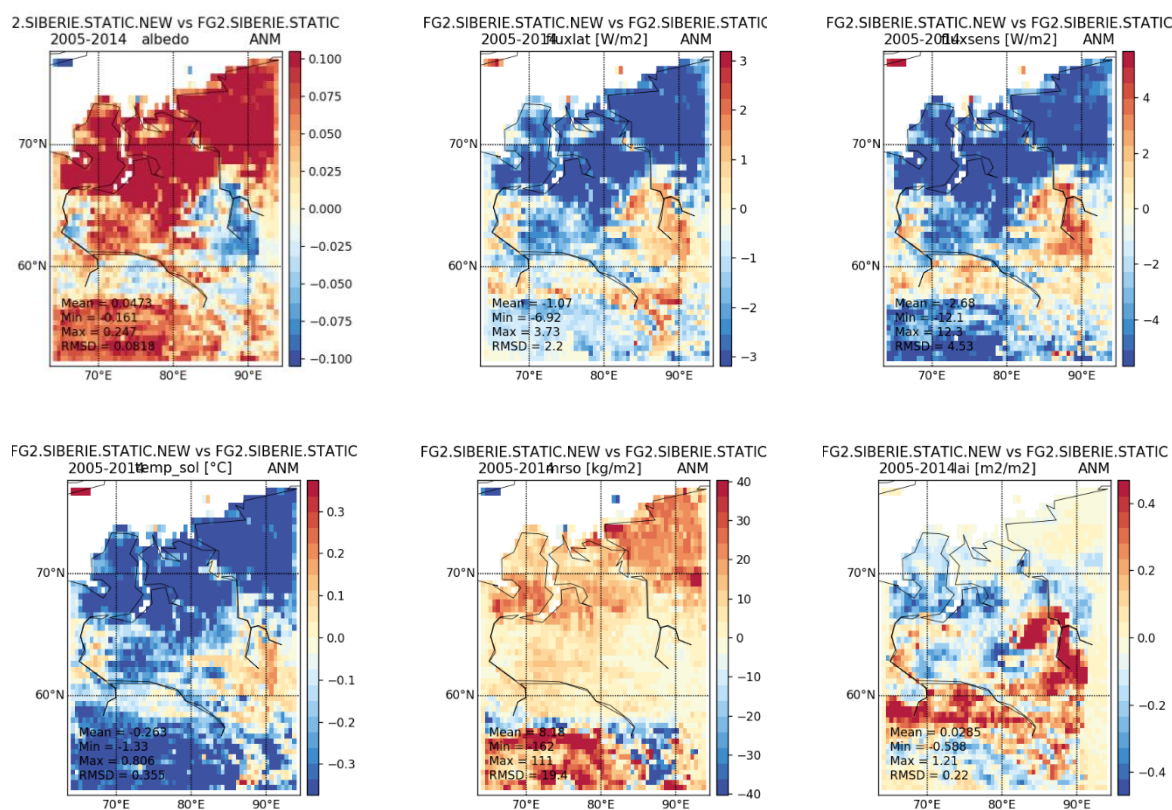


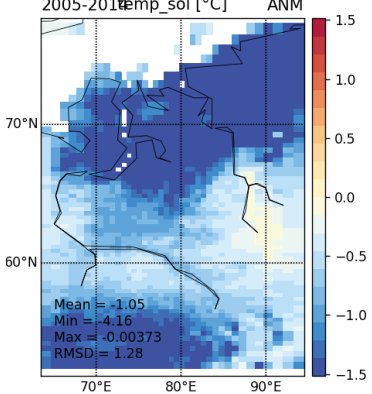
Figure 11.13: Upper panel: surface albedo, latent heat and sensible heat fluxes simulated by ORCHIDEE; Lower panel: soil temperature, soil water content and GPP; all variables are annual averages for the period (2005-2014)

### 11.3.3 Land cover – atmosphere feedback analysis

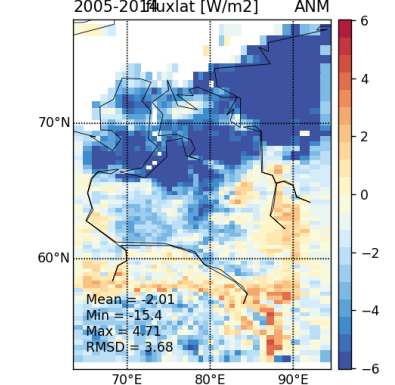
When coupled with the atmosphere, we observe that the albedo and energy budget changes impacted the surface temperature and the air temperature which are colder by about 1°C in average mean, the wind speed is larger where tree cover is smaller and the other way round. Precipitation is impacted (large scale and convective components) and the colder temperatures influenced the snowfall/rainfall partition with larger snowfall in winter and in spring, especially in the north-eastern part of the region. Despite the larger wind speeds in the north due to less trees/shrubs, the turbulent fluxes are lower by more than 4 W/m<sup>2</sup> in annual mean because of the lower radiation budget at the surface. If we compare to the results of the ORCHIDEE simulations performed with a prescribed atmosphere, we can see that all the changes are amplified especially in winter season because of the snow effects. If we look to the evolution of the snow mass simulated on the region, we can see that the time series present very different features with a positive trend in the simulation with HRLC map, highlighting a positive feedback loop where the snow mass increases because of the colder temperatures, the larger snowfall (especially in spring and early summer), the larger albedos decreasing even more the air temperatures and the rainfall/snowfall partition. This feedback loop is illustrated in Figure 11.16. The analysis of the MRLC1995 and

MRLC2019 simulations do not show the same features since the tree cover and albedo changes on the time period are much smaller. This comparison highlights the well-known non-linearity of the snow processes with threshold effects that can converge to completely different states when temperature thresholds are reached, modifying the rainfall/snowfall partition and the surface processes. The availability of high-resolution land cover maps, albedo and snow observations is crucial to better understand these vegetation-snow-atmosphere processes and better quantify the impacts of environmental changes and climate warming on the regional climates.

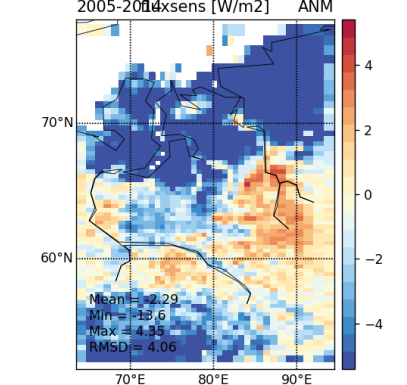
.SIBERIE.STATIC.NEW vs CL5.SIBERIE.STATIC



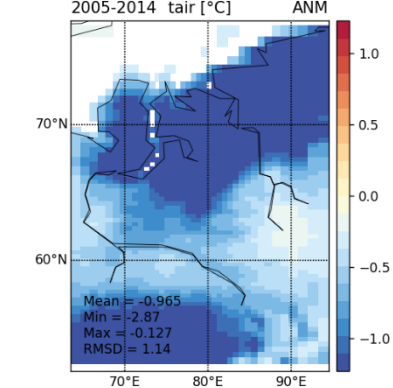
CL5.SIBERIE.STATIC.NEW vs CL5.SIBERIE.STATIC



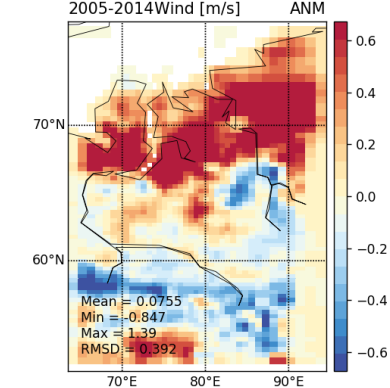
CL5.SIBERIE.STATIC.NEW vs CL5.SIBERIE.STATIC



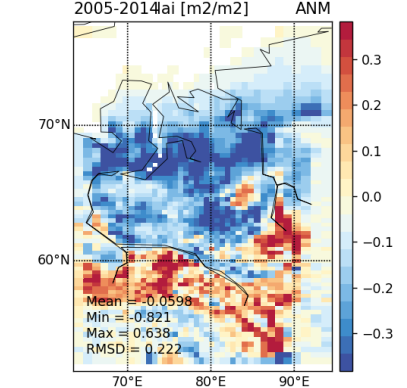
CL5.SIBERIE.STATIC.NEW vs CL5.SIBERIE.STATIC



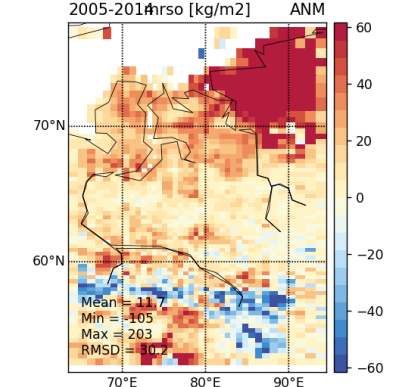
CL5.SIBERIE.STATIC.NEW vs CL5.SIBERIE.STATIC



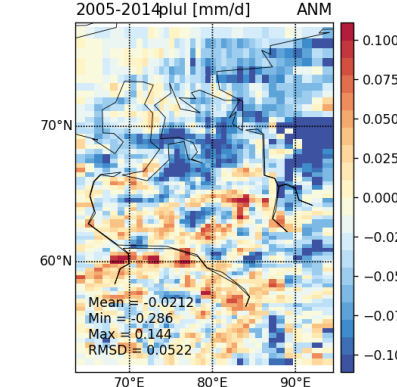
CL5.SIBERIE.STATIC.NEW vs CL5.SIBERIE.STATIC



CL5.SIBERIE.STATIC.NEW vs CL5.SIBERIE.STATIC



CL5.SIBERIE.STATIC.NEW vs CL5.SIBERIE.STATIC



CL5.SIBERIE.STATIC.NEW vs CL5.SIBERIE.STATIC

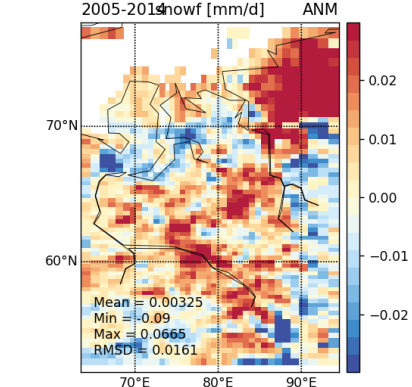


Figure 11.14: Upper panel: soil temperature, latent heat and sensible heat fluxes simulated by LMDZ; Middle panel: air temperature, wind speed and LAI; Lower panel: soil moisture, large scale precipitation and snowfall; all variables are annual averages for the period (2005-2014)

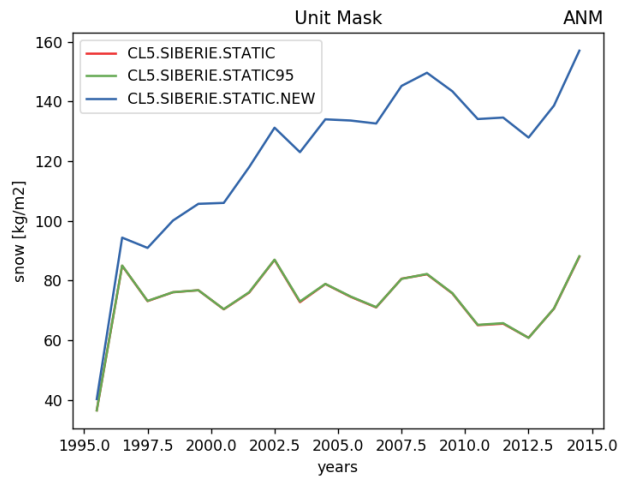


Figure 11.15: Snow mass simulated by LMDZ-ORCHIDEE on the time period 1995 to 2015, for 3 simulations performed based on MRLC products (1995 et 2019, the red and green curves are superimposed) and the new product in blue.

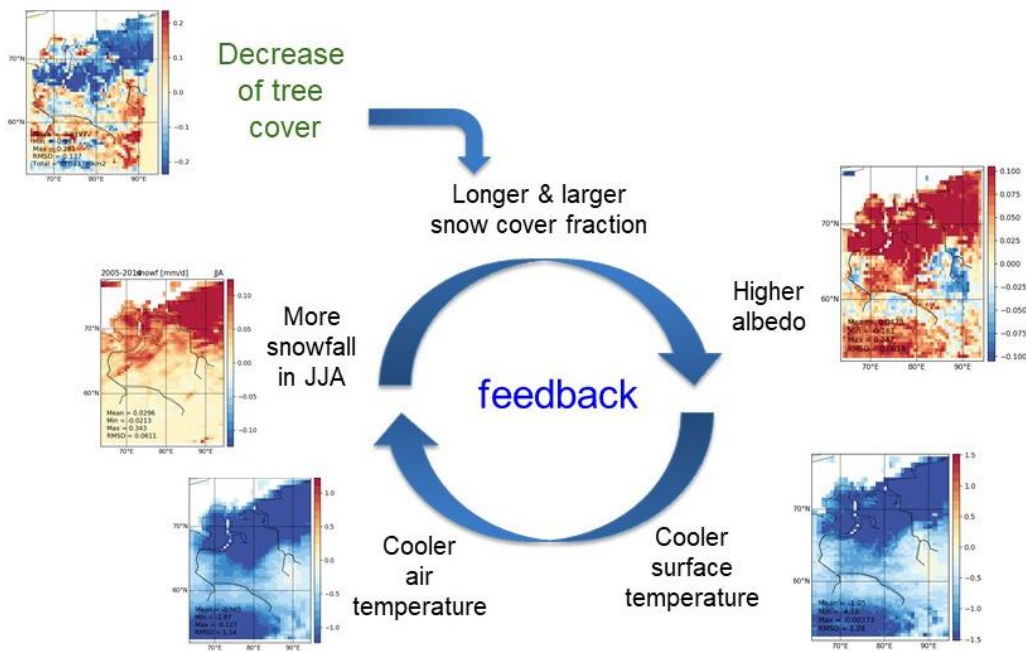


Figure 11.16: Snow-atmosphere feedback loop simulated in ORCHIDEE-LMDZ when comparing MRLC and HRLC simulations over Siberia

### 11.3.4 Comparison with observations

The comparison of some of the surface variables simulated to observations, show degraded performances probably because of the snow feedback processes that have been triggered. The albedo is too large in the northern part of the domain, the LAI and GPP present about the same errors.

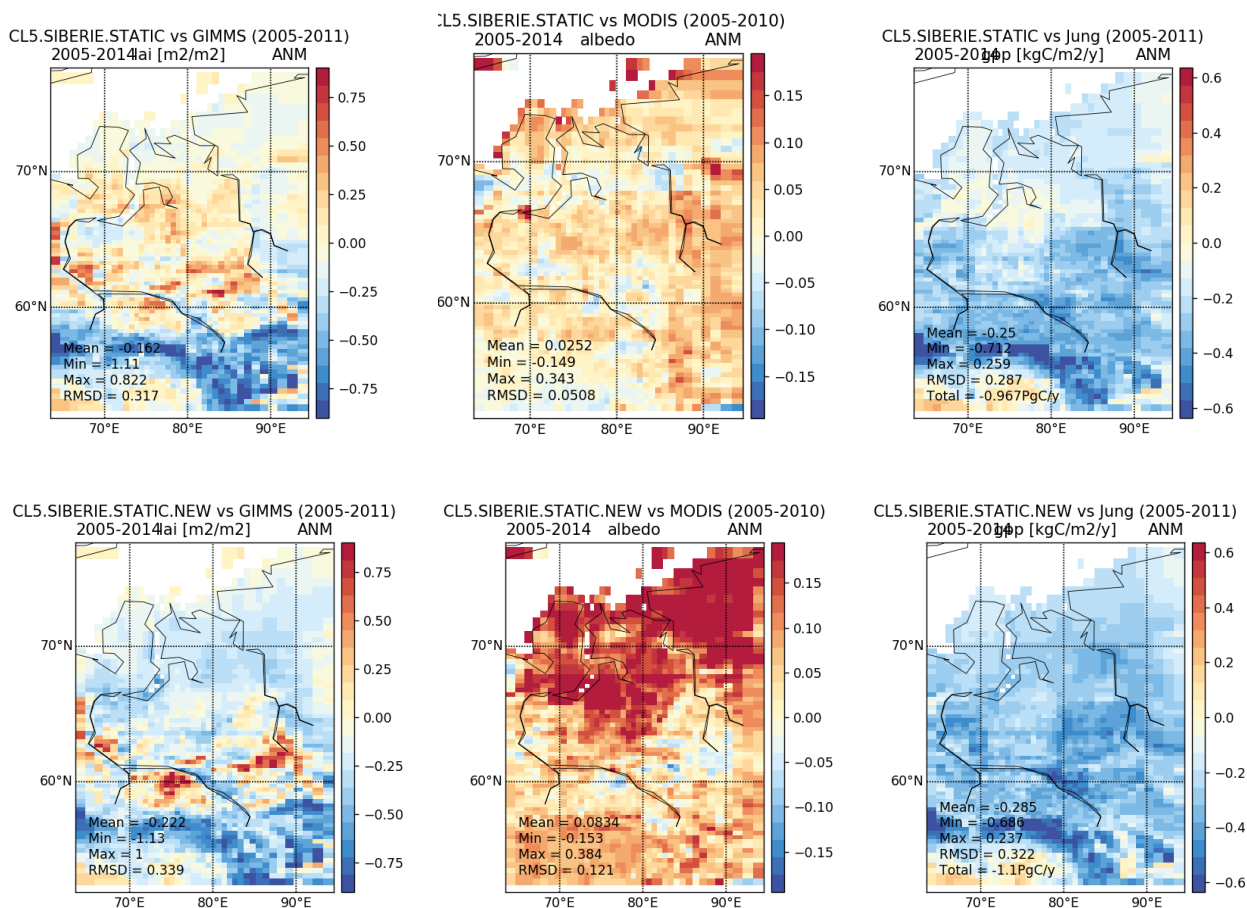


Figure 11.17: Differences (simulated- observations) for LAI, albedo and GPP obtained for 2 LMDZ simulations based on the former MRLC land cover map (upper panel) and with the new HRLC product (lower panel).

## 12 Analysis of the land cover change product on 3 regions

The land cover change datasets have been produced on the 3 regions following the priorities defined in Appendix D. The LSCE team worked as a first step, on the Amazon and Siberia regions. Figure 11.18 presents the gross changes detected between 1990 and 2019 in these regions. These changes are more important on Amazonia compared to Siberia and can reach 20% when aggregated at 0.25° (less than 10% in Siberia). Over Amazonia, they concern mainly the replacement of forests with grasslands and crops. In Siberia, the main feature appears to be the increase of flooded vegetation. In the following, we focus on the Amazonian region and have analysed the impacts of these changes in the ORCHIDEE simulations and the benefit to map land cover each 5 years.

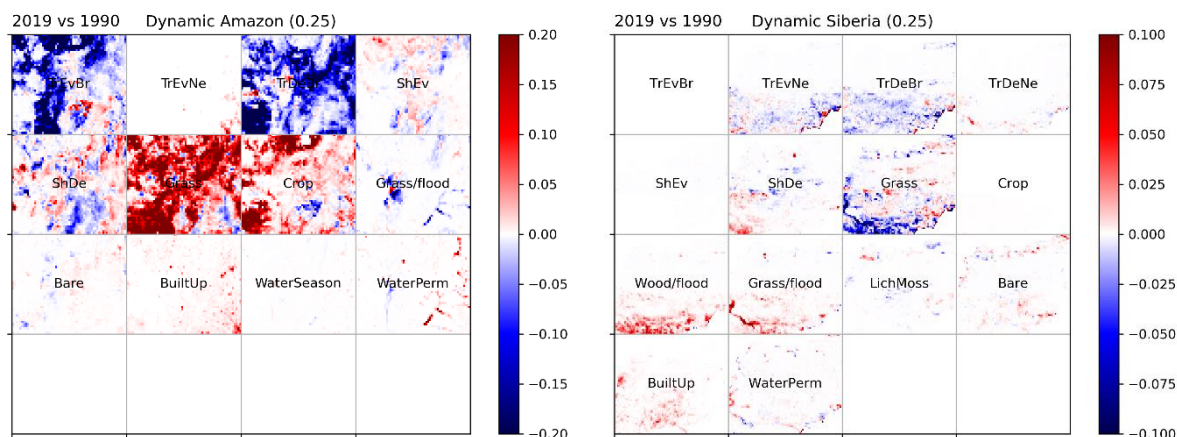


Figure 11.18: Land cover changes mapped over Amazon (left) and Siberia (right) regions between 1990 and 2019

### 13 Sensitivity of ORCHIDEE to LCC on Amazonia

To assess the benefit of the historical product and of updating the land cover map each 5 years in ORCHIDEE, we run the model in 3 configurations with prescribed atmosphere given by the CRU-JRA reanalysis at 0.5° resolution and over the time period 1979-2019:

- With the land cover map obtained for Year 1990
- With the land cover map of Year 2019
- With the land cover map updated each 5 years between 1990 and 2019

We have first analysed the differences in the surface fluxes and variables simulated and compared the simulations with the observations available at this scale. All the results are visible on our dedicated web site (<https://orchidas.lscce.ipsl.fr/mapper/time-series.php?set=ESA.HRLC&mode=FR.AMAZON.DYNAMIC&group=0&freq=0&reg=0>). They show significant differences in the regions where land cover has changed as expected, especially in the deforested zones. We present in Figure 11.19, the comparison of albedo, latent heat flux and LAI to observations, which indeed show slight improvements with slight decrease of the RMSD compared to observations, especially for the simulated LAI which show better agreement in the regions impacted by the deforestation and where grasslands and crops replace trees during the simulated period.

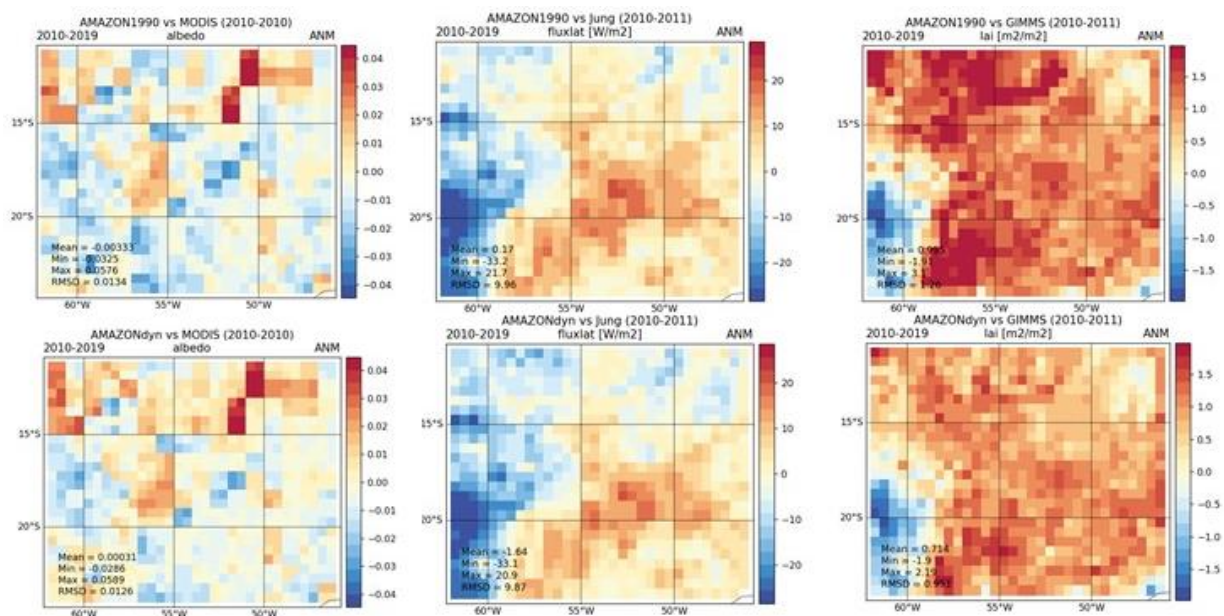


Figure 11.19: Albedo, latent heat flux and LAI simulated by ORCHIDEE in two configurations: in the upper panel, the model was forced by the land cover map of Year 1990, in the lower panel, the land cover was updated each 5 years.

To better highlight the added value of the land cover updates, we have extracted the results obtained on one grid point as an example, where the fraction of tree cover changes at different times from 1995. The coordinates of this point is [lat=12.25S, lon=55.75W], it is located in Mato Grosso, a region in Central Brazil much influenced by deforestation to the benefit of grasslands and croplands. Figure 11.20, shows how the fraction of tree cover varies regularly from 0.8 in 1995 to 0.3 in 2019. In this pixel, the land cover changes concern essentially the conversion of tropical broadleaf evergreen forest to croplands C3 type. The resulting fluxes and surface impacts are clearly shown on Figure 11.21, where the time series are compared to observations. The plots show clearly how the albedo increased during that period by about 2% in the dynamic simulation in agreement with the observations provided by the MODIS and Globalbedo products, the GLASS-AVHRR product showing a positive bias of about 2% (in absolute value) and larger temporal variability. The surface temperature increased slightly in the simulations, in agreement with the SAF Land product even if the observations show a much larger positive trend. Evapotranspiration show also a negative trend that is not present in the GLEAM product. This could be explained by the fact that GLEAM product is based on too simple evapotranspiration model (Priestley & Taylor) and a one bucket root zone, that leads to a larger sensitivity to soil moisture compared to vegetation type. Therefore, the transpiration of forests and crops are not so different for a same amount of soil water available, contrary to the ORCHIDEE model where trees and low vegetation will show very different transpiration capacities given also their different root profiles. If we now look to the LAIs modelled, they show a negative trend whereas COPERNICUS product appears quite stable. This is may be the result of a scale effect, given that the observations are provided at 1 km scale and are compared to a 0.25° pixel.



Figure 11.21: Tree cover, albedo, surface temperature, soil moisture, evapotranspiration and LAI simulated by ORCHIDEE in three configurations: in red, the model was forced by the land cover map of Year 1990, in blue, the land cover was updated each 5 years and in green, the model was forced with the land cover map of 2019. Observations are plotted in orange colour. For albedo, 3 different products are plotted.

The seasonal cycles simulated in the 3 configurations have been also compared to the observed products and are plotted in Figure 11.22. They have been calculated on the last 10 years when the deforestation and land cover are quite stabilized. The plots highlighted some model deficiencies like the too low variability of the albedo along the year compared to the observations, explaining part of the lower variability of the surface temperature

compared to the SAF product. The seasonal cycle of the evapotranspiration is larger in the dynamic and 2019 simulations because of the larger amount of crops (presenting a seasonality opposite to evergreen trees), and leading to a better agreement with the GLEAM product. In the same way, soil moisture presents a larger variability in better agreement with the GLEAM product.

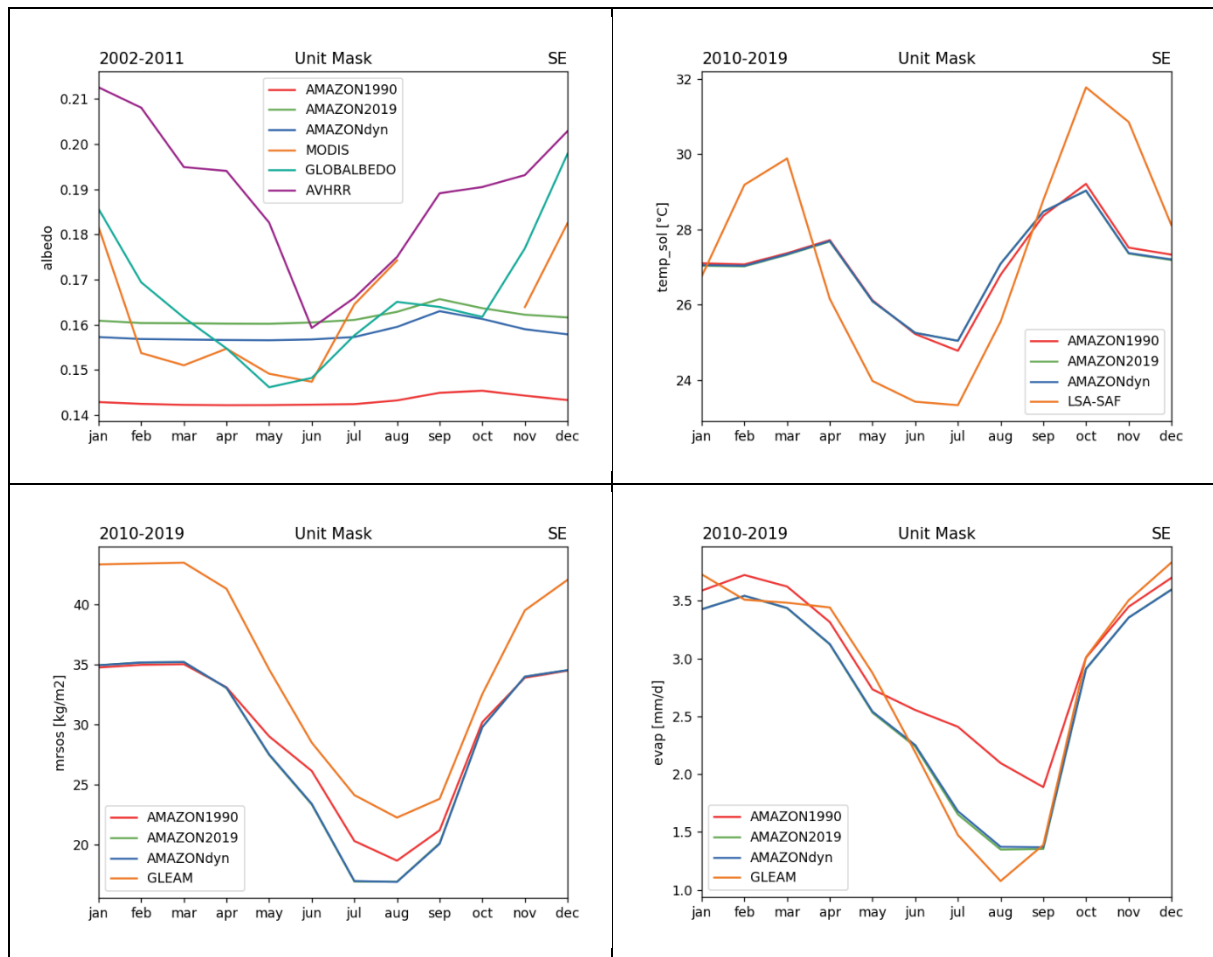


Figure 11.22: Albedo, surface temperature, soil moisture, evapotranspiration seasonal cycles simulated by ORCHIDEE in three configurations: in red, the model was forced by the land cover map of Year 1990, in blue, the land cover was updated each 5 years and in green, the model was forced with the land cover map of 2019. Observations are plotted in orange colour. For albedo, 3 different products are plotted.

In conclusion, the benefit of updating regularly land cover in land surface models has been demonstrated. More validation of the HRLC product is needed to really assess the model deficiencies and improve parameterizations.

## 14 Ecosystem changes model using VI time series, Medium Resolution (MR) land cover maps and climate variables

Global change affects ecosystem functionalism and biodiversity through land-use and climate alteration (Vitousek 1997). The characterization of the ecosystem in functional units and the monitoring of their dynamics allows assessing the effects of climate change and LCC. With this aim, Ecosystem Functional Types (EFT) are defined as a group of ecosystems sharing functional characteristics that include the amount and timing of matter and energy exchanged between the biotic community and the environment (Alcaraz 2006).

EFT relies on the use of seasonal dynamics analysis of vegetation indices derived from Earth Observation (EO) data that can provide key functional aspects of ecosystems. Remote sensing time series provides an integrated measure of ecosystem responses to climatic factors that are also land cover dependent (Ivits 2012). Thus, this section explains the approach used to combine land cover maps and its changes and drought climate models coupled with the dynamic model of the Ecosystem Functional types and its changes. Comparisons of results using medium resolution and high resolution maps have been conducted to evaluate the role of Land cover maps spatial resolution for climate-ecosystem coupled modelling (see Section 15 and 16).

## 14.1 Materials

The presented approach uses three types of variables:

- Remote sensing images and its derived products
- Land cover maps
- Drought Climate outputs

The remote sensing dataset availability is a key factor for the pilot area and study years' selection (see section 14.2.1).

### 14.1.1 Remote sensing images and derived products

The time series of Envisat MERIS Full Resolution 7-day composites surface reflectance product [AD5] provided by the MR Land Cover CCI project have been used. From the available MERIS time series (2003-2012) and according to the historical case study regions of defined in the project, a selection of tiles and regions to explore has been performed, as shown in Table 14.1:

	Tiles	Years
Sahel	h42v15; h43v15	2004;2005;2010;2011
Siberia	h49v05; h50v05; h51v05; h52v05;	2004;2005;2010;2011
Amazonia	h24v21; h25v21	2004;2005;2010;2011

*Table 14.1: Selected tiles and years for MERIS time series in the project pilot regions*

The tiles code follows the tiling system used in the MR project [AD5].

The data used has been the provided composites of the vegetation index product that corresponds to the Normalized Difference Vegetation Index (NDVI), although derived Enhanced Vegetation Index (EVI) has been also prepared from the original composites of reflectance bands for some verification and exploratory purposes.

### 14.1.2 Land cover maps

For this analysis the ESA Land Cover CCI Product at MR [AD5] for the tiles and years detailed in Table 14.1 has been used

Regarding the Land Cover map, the analysis has been focused on the changes of the first level of the Land Cover Classification System (LCCS) between 2005 and 2011.

### 14.1.3 Drought climate models and its derived variables

Climate models and its derived drought climate variables are indeed one of the possible drivers affecting the land cover and specifically land cover changes. In order to monitor anomalies of temperature and precipitation and analyse its role on specific changes of different land cover types, some multiscale indices can be used. Specifically, we model such anomalies using the Standardized Precipitation - Evapotranspiration Index (SPEI). The SPEI index is a multiscale index based on precipitation and evapotranspiration, thus climate data. It is used to

determine the onset, duration and magnitude of drought conditions with respect to normal conditions in a variety of natural and managed systems. Therefore, its characteristics make it a perfect candidate to be combined with the LCC to determine which EFT changes might be driven by extreme climatic conditions. The level of the anomaly is usually classified into several categories, like the ones described in the following Table 14.2:

Index Value	Drought Class	Probability (%)
$\geq 2.0$	Extreme wet	2.3
1.5~2.0	Very wet	4.4
1.0~1.5	Moderate wet	9.2
-1.0~1.0	Near normal	68.2
-1.5~-1.0	Moderate dry	9.2
-2.0~-1.5	Severe dry	4.4
$\leq -2.0$	Extreme dry	2.3

*Table 14.2. SPEI-based thresholds for classifying drought condition and probability of occurrence.*

Negative SPEI values indicate less than average precipitation, i.e., dry events, while positive values indicate greater than average precipitation, thus wet events. A threshold of -1 or lower is selected to identify the drought condition, which ends as soon as the SPEI becomes positive again. The scale of the departure from the mean is therefore a probabilistic indicator of intensity for each event, either dry or wet.

As pointed out in the introduction of this section, the main advantage of this index is that it can be calculated for several timescales. The most commonly-used timescales are monthly and yearly, being the first most appropriate for monitoring effects of drought conditions on vegetation (Mishra and Singh 2010). Short time lags, i.e. 3-months are indicators of short drought events with immediate impact on the agricultural sector mainly. Longer time lags, i.e. 48-months, are indicators of persistent drought events (Domingo-Marimon et al., 2015).

These two extreme time lags allow identification of climate patterns related to local meteorology as well as identification of resilient drought waves that are not directly and locally perceived by scientists or population but that are affecting the area.

The database used for this preliminary analysis was provided by Begueria et al 2010, through <https://spei.csic.es/index.html>. The SPEI Global Drought monitor distributes global maps of drought conditions with a 1-degree spatial resolution and a monthly time resolution. SPEI time-scales between 1 and 48 months are provided. Data from March 1950- June 2020 has been downloaded for time lags of 3, 6, 12, 24 and 48 months, although only data from January 2005 - January 2011 has been used.

## 14.2 Methodology

### 14.2.1 Spatio-temporal selection

The selection of the study regions and the temporal period of the presented analysis should maximize:

- Free cloud cover images availability: for a complete description of annual vegetation index profile
- Maximum length of time period analysis: in order to identify clear ecosystem, climate and land cover changes

The preliminary information was obtained from the MERIS density maps at MERIS Full Resolution Full Swath site: <https://earth.esa.int/web/guest/data-access/browse-data-products/-/article/meris-full-resolution-full-swath-6015>. There is global information for the complete period (Figure 14.1) and density maps for each year.

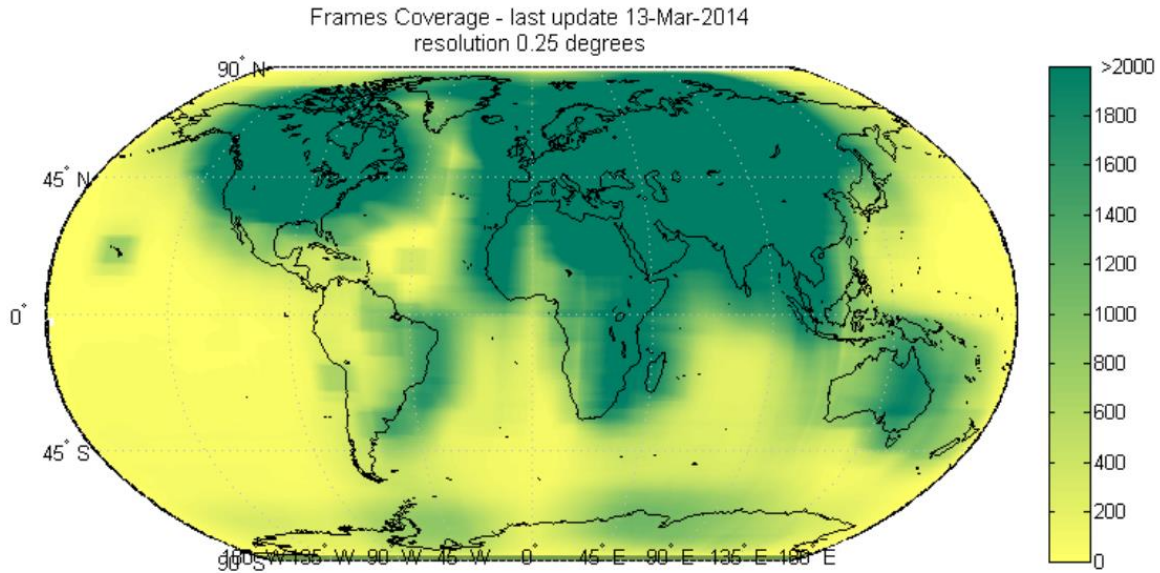


Figure 14.1: MERIS images availability. Source ESA.

Density maps indicate a lack of data specifically at South America region. This results in a low-quality dataset and jeopardizes the probability of achieving successful analysis results in the Amazonia region.

After this preliminary verification, other tiles apparently presenting more data density were selected for each region (Table 14.1) and an analysis of the spatial and temporal distribution of images was performed. The main condition to fulfil in order to select a given scene was that it should be able to present a complete seasonal time series of vegetation indexes that would allow extracting a phenology temporal profile. The main criteria used was based on the first (low) quartile (Q1) and median (Q2) of a raster counting the valid values for each pixel (300 m) during one year. Figure 14.2 shows one valid scene with high density availability of data (Q1=29; Q2=32) and one poor density availability of data scene (Q1=11; Q2=12), both in the Sahel region.

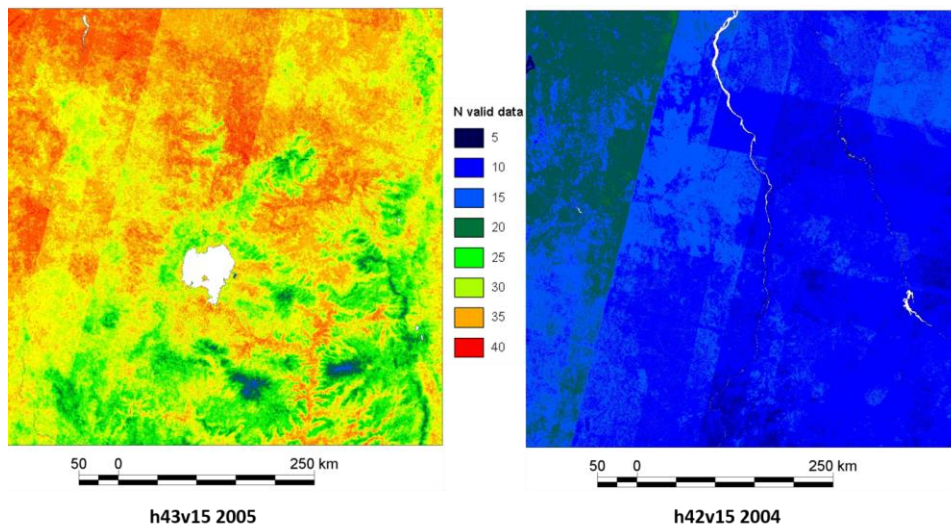


Figure 14.2 Raster with the number of available valid data of 7-day composite vegetation index. Sahel region

Tile h42v15 2004 example presents a significant area located in the northeast part of the region with very low availability of images. For most of the region, data availability suits around the median (12 images).

This low availability implies relevant gaps of information on the annual VI profile.

Unfortunately, all explored tiles and years in the Amazonia region present poor availability conditions similar to the ones of Figure 14.2 (right).

Therefore, the final decision on selecting the best study areas for this approach was:

	MERIS tile	Boundary box	Extension	Years
Sahel	h43v15	35E,10N; 40E,15N	524 km x 579 km	2005-2011
Siberia	h50v05	70E, 60N; 75E,60N	374 km x 615 km	2005-2011

Table 14.3: Main properties of ECM pilot regions

Concerning the Amazonia region, alternative VI time series will be explored and included in future analysis if available.

### 14.2.2 EFT generation

EFTs are obtained from the combination of three quantitative components of time series' variables derived from vegetation indices, NDVI in the current study: productivity (NDVI-I), seasonality (sCV) and phenology (MMAX). Productivity is the annual mean of the VI; seasonality is computed as the coefficient of variation of the NDVI seasonal curve (standard deviation / mean), while phenology is represented by the date of the maximum NDVI (Figure 14.3)

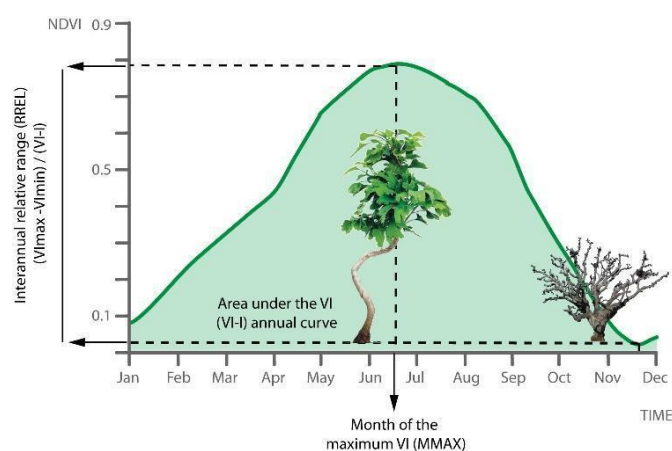


Figure 14.3: NDVI annual profile and EFT component

These quantitative components are later reclassified to usually 4 categories (Alcaraz et al 2013, Pesquer et al. 2019), but other options can be chosen for specific studies (Paruelo et al. 2001). The reclassification is defined following the frequency distribution of the NDVI-I and sCV, and a climate criterion for MMAX. Table 14.4 shows these interval definitions based on 1/3 and 2/3 percentiles of 2005 NDVI-I and sCV and the periods for MMAX. NDVI-I needed a previous saturation step for correcting a few over range values. Figure 14.4 shows the map reclassification process.

			Sahel		Siberia		Amazonia	
			from	to	from	to	from	to
NDVI-I	L	Low	0.000	0.356	0.000	0.550	0.000	0.613
	M	Mid	0.356	0.432	0.550	0.647	0.613	0.683

	<b>H</b>	<b>High</b>	0.432	1.000	0.647	1.000	0.683	1.000
<b>sCV</b>	<b>l</b>	<b>low</b>	0.000	0.328	0.000	0.101	0.000	0.200
	<b>m</b>	<b>mid</b>	0.328	0.426	0.101	0.310	0.200	0.268
	<b>h</b>	<b>high</b>	0.426	8.500	0.310	9.000	0.268	20.000
<b>MMAX (Sahel &amp; Amazonia)</b>	<b>1</b>	<b>wet</b>	01/06	31/08			1/10	30/04
	<b>2</b>	<b>post-wet</b>	01/09	30/11			1/05	14/06
	<b>3</b>	<b>dry</b>	1/12	31/05			15/06	30/09
<b>MMAX (Siberia)</b>	<b>1</b>	<b>spring</b>			15/04	14/06		
	<b>2</b>	<b>summer</b>			15/06	14/09		
	<b>3</b>	<b>winter</b>			15/09	14/04		

Table 14.4: Interval definitions for transforming quantitative to categorical MR EFT components

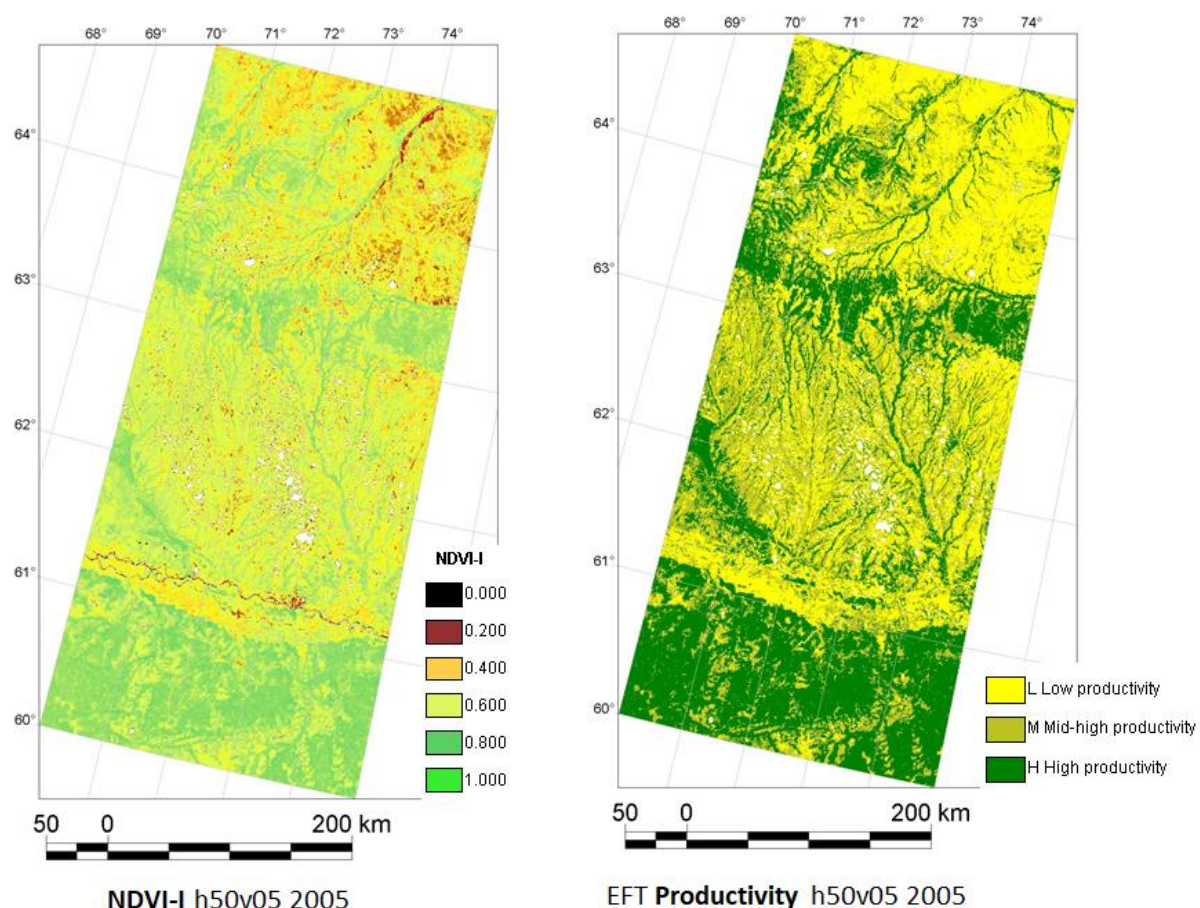


Figure 14.4: Quantitative MR NDVI-I map and the reclassified productivity EFT component. Siberia region

The spatial and thematic combination of the three categorical components generates the final EFT map. Figure 14.5 and Figure 14.6 show EFT maps for years 2005 and 2011 for Sahel and Siberia regions (detailed in Table 14.2).

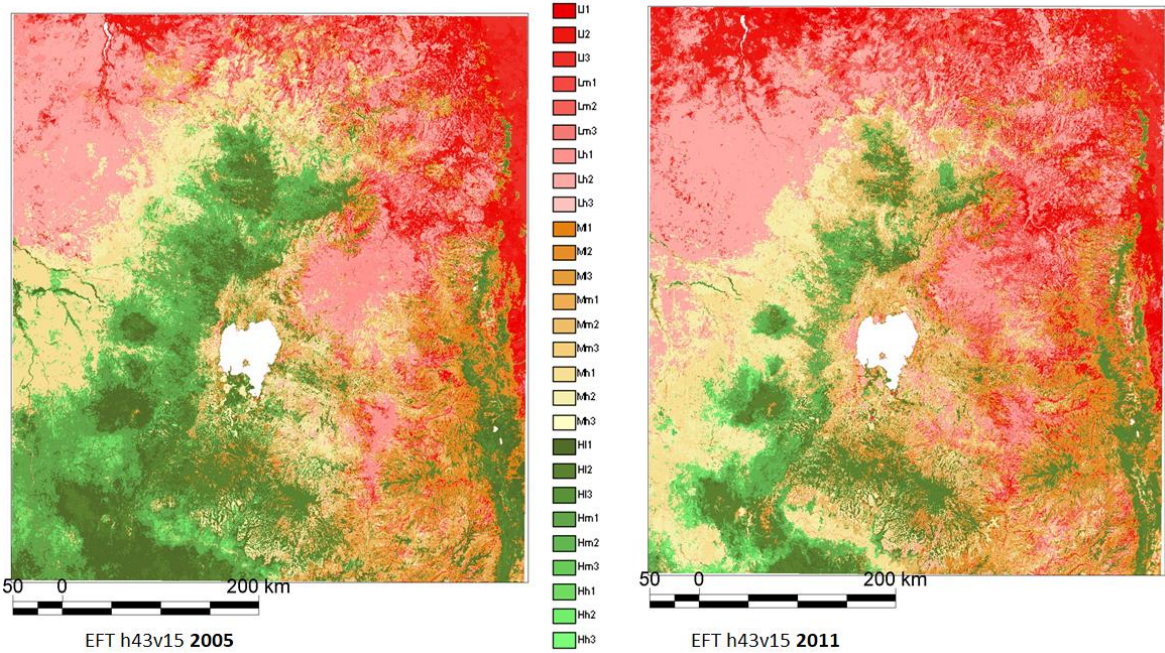


Figure 14.5: MR EFT map for Sahel region.

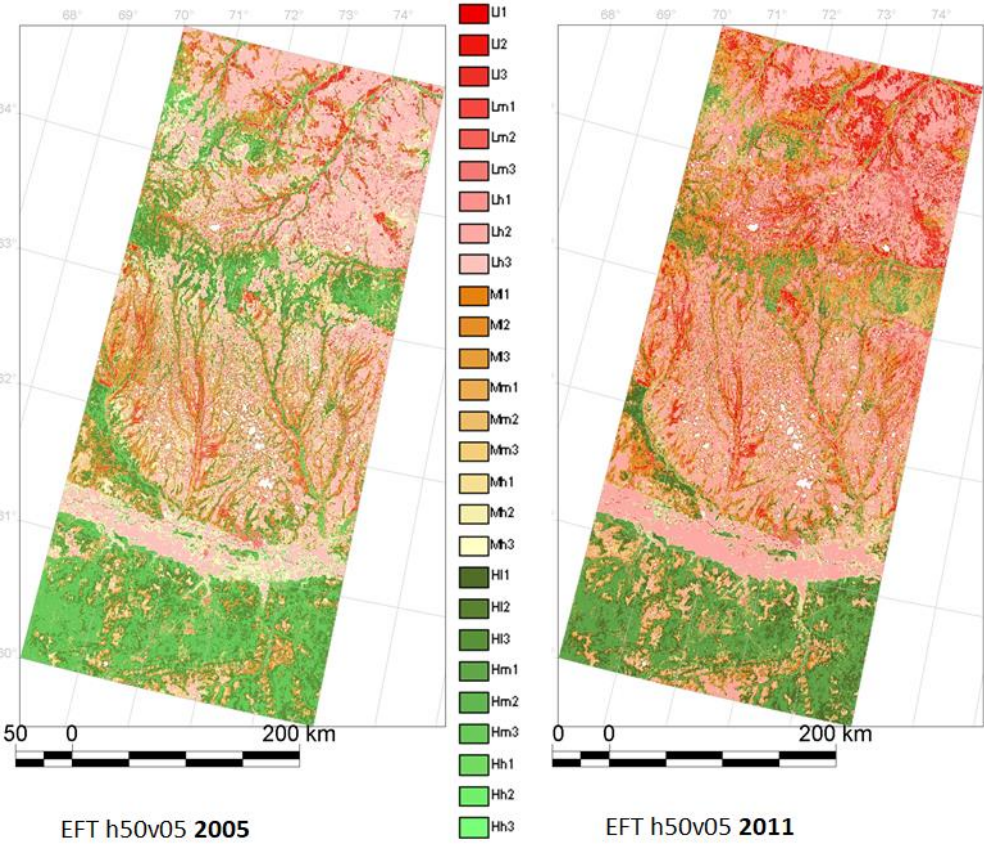


Figure 14.6: MR EFT map for Siberia region

Appendix B shows the three categorical EFT components for the two selected years and regions. They are the base of these EFT maps.

#### Cartographic projection considerations:

In order to avoid the distortions in area calculations on geographic coordinates (latitude, longitude), we reprojected these maps to a projected coordinate reference system (CRS) based on an **equivalent projection** (Albers Conic Equal Area) before any processing step of the analysis. These distortions are very important in Siberia, because they increase for high latitudes [Snyder 1997], moreover it is also an accurate solution for the Sahel region. As a clear example, both pilot regions are tiles of 5x5 degrees latitude/longitude however the dimensions (detailed in Table 14.2) and shown region extensions in Figure 14.5 and Figure 14.6 illustrate the area distortions in using a coordinate reference system (CRS) based on geographic coordinates.

The chosen CRS are:

- Siberia: Asia North Albers Equal Area Conic (EPSG:102025): see all parameters at <http://epsg.io/102025>
- Sahel: Africa Albers Equal Area Conic (EPSG: 102022): see all parameters at <https://epsg.io/102022>
- Amazonia: Brazil Albers Equal Area Conic (SR-ORG: 7390): see all parameters at <https://spatialreference.org/ref/sr-org/brazil-albers-equal-area-conic-wgs84/html/>

### 14.2.3 Selected Land Cover Changes

Analyses of Land cover changes between 2005 and 2011 for both regions have been performed. All the combinations of the LC types between 2005 and 2011 years result in a highly fragmented and complex map with 142 crossed categories (as an example see a subset of these combinations in Figure 14.7). The global LC changed area corresponds to a 1.13% of total extension in Sahel pilot region and 1.96% in Siberia pilot region.

32 (Mosaic natural vegetation (tree, shrub, herbaceous cover) (>50%) / cropland (<50%)) and (Shrubland)
33 (Mosaic natural vegetation (tree, shrub, herbaceous cover) (>50%) / cropland (<50%)) and (Grassland)
34 (Mosaic natural vegetation (tree, shrub, herbaceous cover) (>50%) / cropland (<50%)) and (Sparse vegetation (tree, shrub, herbaceous cover) (<15%))
35 (Mosaic natural vegetation (tree, shrub, herbaceous cover) (>50%) / cropland (<50%)) and (Tree cover, flooded, saline water)
36 (Mosaic natural vegetation (tree, shrub, herbaceous cover) (>50%) / cropland (<50%)) and (Urban areas)
37 (Mosaic natural vegetation (tree, shrub, herbaceous cover) (>50%) / cropland (<50%)) and (Bare areas)
38 (Mosaic natural vegetation (tree, shrub, herbaceous cover) (>50%) / cropland (<50%)) and (Water bodies)
39 (Tree cover, broadleaved, evergreen, closed to open (>15%)) and (Cropland, rainfed)
40 (Tree cover, broadleaved, evergreen, closed to open (>15%)) and (Mosaic cropland (>50%) / natural vegetation (tree, shrub, herbaceous cover) (<50%))
41 (Tree cover, broadleaved, evergreen, closed to open (>15%)) and (Mosaic natural vegetation (tree, shrub, herbaceous cover) (>50%) / cropland (<50%))
42 (Tree cover, broadleaved, evergreen, closed to open (>15%)) and (Tree cover, broadleaved, evergreen, closed to open (>15%))
43 (Tree cover, broadleaved, evergreen, closed to open (>15%)) and (Mosaic tree and shrub (>50%) / herbaceous cover (<50%))
44 (Tree cover, broadleaved, evergreen, closed to open (>15%)) and (Shrubland)
45 (Tree cover, broadleaved, evergreen, closed to open (>15%)) and (Shrub or herbaceous cover, flooded, fresh/saline/brakish water)
46 (Tree cover, broadleaved, evergreen, closed to open (>15%)) and (Water bodies)
47 (Tree cover, broadleaved, deciduous, closed to open (>15%)) and (Cropland, rainfed)
48 (Tree cover, broadleaved, deciduous, closed to open (>15%)) and (Mosaic cropland (>50%) / natural vegetation (tree, shrub, herbaceous cover) (<50%))

*Figure 14.7: Examples of the LC combination categories from LC 2005 and LC 2011 maps. For example, change 39 passes from Mosaic natural, vegetation in 2005 to Cropland, rainfed in 2011*

In order to focus the analysis, relevant changes have been grouped in 4 land cover more general transitions:

- Tree loss
- Tree gain
- Urban growth
- Crop expansion

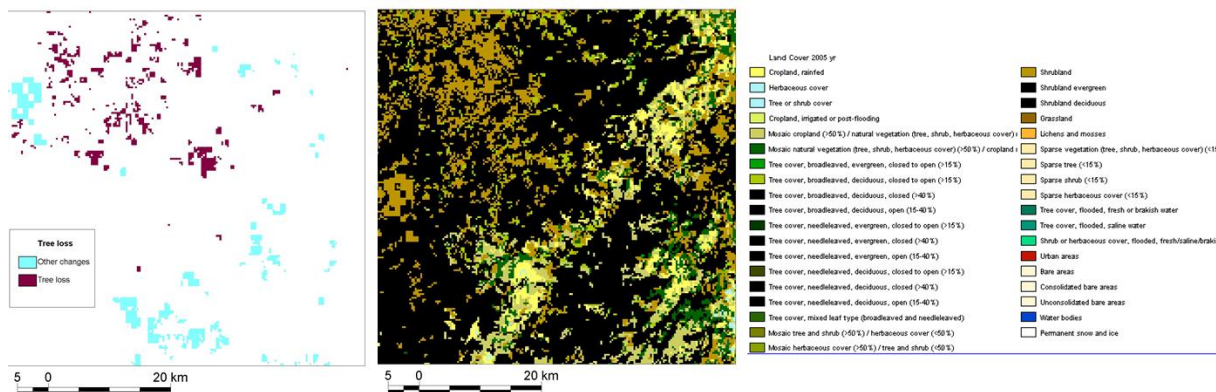


Figure 14.8: Sahel region. Left: zoom (36.280E,11.447N to 36.825E,11.941N) to a tree loss (burgundy red) example region during 2005-2011. Center: map of MR LC 2015 and legend (right)

The extension affected by these transitions in both regions are:

- Tree loss: 62892 ha in Sahel (corresponding to the 18.35% of LC changes); 156951 ha in Siberia (corresponding to the 55.74% of LC changes)
- Tree gain
- Crop expansion: 160407 ha in Sahel (corresponding to the 46.81 % of LC changes); 125559 ha in Siberia (corresponding to the 44.59% of LC changes)
- Urban growth: 5229 ha in Sahel (corresponding to the 1.5% of LC changes); 11187 ha (corresponding to the 3.97% of LC changes)

Note that some changes can be classified as more than one transition. For example, some LC changes could be considered Tree loss transition and Crop expansion transition simultaneously.

### 14.3 Analysis and conclusions

The following preliminary analysis aims at explaining the contribution of LCC and climate models (specifically drought) (coupled and separated) in the identification of the most relevant EFT changes.

Four different coupled results are expected (in order of probability):

- LC change between 2005-2011 and EFT change between 2005-2011
- NO LC change and stable EFT
- NO LC change and EFT change between 2005-2011
- LC change between 2005-2011 and stable EFT

These 4 coupled results are also analysed with the SPEI tendency at 3-month time span and 48-month time span to verify if drought is one of the drivers' changes.

First, comparisons of EFTs between 2005 and 2011 have been carried out. The combination of 32 EFT classes in 2005 with 32 EFTs classes in 2011 generates 1024 possible EFT changes. For instance, change *Hh1 to Hm2* means a change from an EFT of high productivity (H), high seasonality (h) and wet season maximum phenology phase (1) (see Table 14.4 definitions) to an EFT of high productivity (H), mid seasonality (m) and post-wet season maximum phenology phase. The analysis of all combinations is too complex but above all senseless, because some of these combinations represent a very tiny area (just a few pixels). For this reason, the analysis is focused on main change patterns and selected LC transitions.

The global EFT changes trends observed in Sahel (see EFT comparison in Figure 14.5 and related EFT components in Appendix B) indicate a decreasing of productivity (from high to mid productivity, green colors to red colors in Figure 14.5), clearer in Sahel than in Siberia, although Siberia shows an increase of low productivity EFT classes.

The discrepancies and agreements between EFT changes and LC changes in both regions are presented in Figure 14.9.

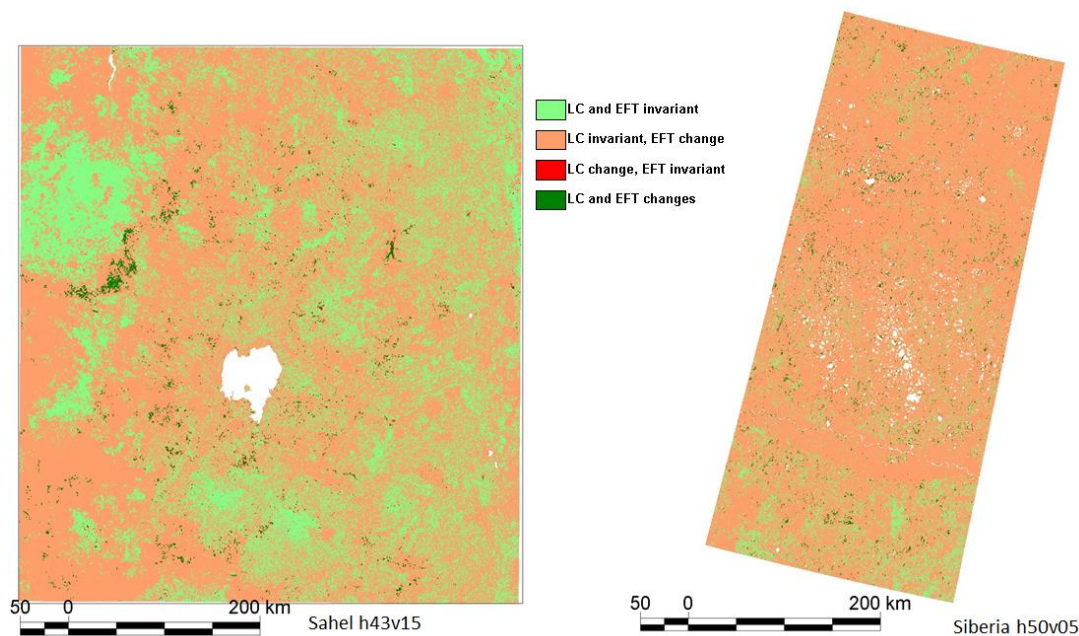


Figure 14.9: Combinations of MR LC and MR EFT changes in Sahel and Siberia

	Sahel		Siberia	
	Area (ha)	%	Area (ha)	%
<b>LC and EFT invariant</b>	1551078 ha	11.06 %	9051147 ha	30.43 %
<b>LC invariant, EFT change</b>	12197880 ha	86.95 %	20349396 ha	68.42 %
<b>LC change, EFT invariant</b>	27522 ha	0.20 %	62955 ha	0.21 %
<b>LC and EFT changes</b>	252270 ha	1.80 %	278649 ha	0.94 %

Table 14.5: Proportions of LC and EFT changes

Results (Table 14.5) show that in general Siberia less land cover change dynamics than Sahel, 30.43% vs. 11.06% (both LC and EFT remain invariant between 2005 and 2011). This indicates Siberia as a quite stable area in terms of Land cover and ecosystem functionalism.

Following results point out an interesting situation to analyse: when LC remains invariant but EFT changes between 2005 and 2011. This result does not indicate a discrepancy between both models but highlights the fact that the changes on ecosystem functionalism are not explained by land cover change. In this case is where the climate model has a relevant role, given that these changes might be explained by climate change extreme situations (otherwise it could indicate errors in any of the maps). This part of the analysis shows that an 86.95 % of the Sahel experimenting EFT changes although the LC remains constant. Contrary, in Siberia only 68.42 % (not negligible) of the area corresponds to this result.

Regarding the changes on LC that are coupled with stable EFT results show a very low representation (0.20% and 0.21% of the area in Table 14.5, red colour in Figure 14.9) and it's 10 times lower than LC changes coupled with EFT changes.

Finally, the combination of LC and EFT changes, although corresponding to a small area (1.80 % for Sahel and 0.94 % of Siberia) is the most interesting one to assess, because LCC is the main driver of this EFT change.

### 14.3.1 Tree loss analysis

Specific analysis results for Tree loss transitions for Sahel area are included in Table 14.6 (results in % of total area). The first column of the table contains the name of the EFT transitions between 2005 and 2011, (see beginning of section 14.3 for more details). For each EFT transition, its corresponding LC behaviour has been analysed so each EFT transition is explained by a LC change related to Tree loss (second column), other LC changes (third column) or non LC changes (fourth column). List is ordered according to the % of total area corresponding to Tree loss LC changes. This Table 14.6 shows the EFT transitions over the 2.5% of the total area in the Tree loss LC implied changes at the Sahel pilot region. The sum of the area of the most relevant Tree loss EFT transitions between 2005 and 2011 is 34.42 %, the total number of EFT transitions is 582, thus the top ranked ones are really relevant. The sum of the area of the same subset of EFT transitions is significantly low for other types of LCC changes and when LC is invariant.

MR EFT transitions (2005-2011)	Tree loss (% total area)	Other LCC (% total area)	LC invariant (% total area)
Hm1 to Mh2	8.43	2.14	1.93
Hm1 to Mh1	5.62	2.59	1.87
Hm1 to Mm2	5.44	1.14	0.99
Hm2 to Mm2	5.19	2.20	1.86
Hm2 to Mh2	3.53	0.78	0.82
HI2 to HI2	3.39	4.74	4.73
HI1 to Hm2	2.82	0.58	1.54
<b>Sum</b>	<b>34.42</b>	<b>14.17</b>	<b>13.74</b>

Table 14.6: Relevant MR EFT transitions mainly explained by Tree loss land cover change. Sahel region

The most relevant EFT transitions show a clear tendency to:

- decrease (H to M) or preservation (H to H) of productivity levels
- increase of seasonality levels (m to h, l to m) or preservation (m to m)
- shift of maximum phenology phase (1 to 2) or preservation (1 to 1, 2 to 2)

Most of the area of EFT transitions that indicate a change of the ecosystem functionalism are also explained by LC transitions related to tree loss (34.42% of the area), while LC transitions corresponding to other types of LC changes explain changes of ecosystem functionalism for an area of approximately 14%. Finally, note that indeed, the combination *HI2 to HI2* (in italics in the table) is not an EFT transition between 2005-2011 so the % of area presenting this false transition are better explained by none LC changes (invariant LC, 4.73 %) or LC changes corresponding to other LCC (4.74 %) rather than by tree loss transition (3.39 %)

For each of these EFT transitions covering a major area explained by Tree loss, a preliminary analysis using drought climate models have been performed in order to verify if these EFT and tree loss changes could be driven by extreme drought events. Figure 14.10 shows the dynamics of SPEI 3- and 48-months index for the first fifth most relevant EFT transitions explained by tree loss.

Results of SPEI-3 show short term events of drought combined with rainy events along the period 2005-2011 with a clear regime shift starting at the end of 2008. From that moment on, the region went under constant drought events, more critical in some specific areas, such as the ones corresponding to *Hm2\_Mh2* EFT transitions. Instead, the second graph, corresponding to a time span of 8 months, shows a persistent a long-term drought event starting earlier than 2005, at least 4 years, that was smoothed by the short-term rainy periods of 2006, 2007 and beginning of 2008, achieving an almost normal climatic behaviour by mid 2008 that was rapidly worsen by the short-term drought persisting event starting at the end of 2008.

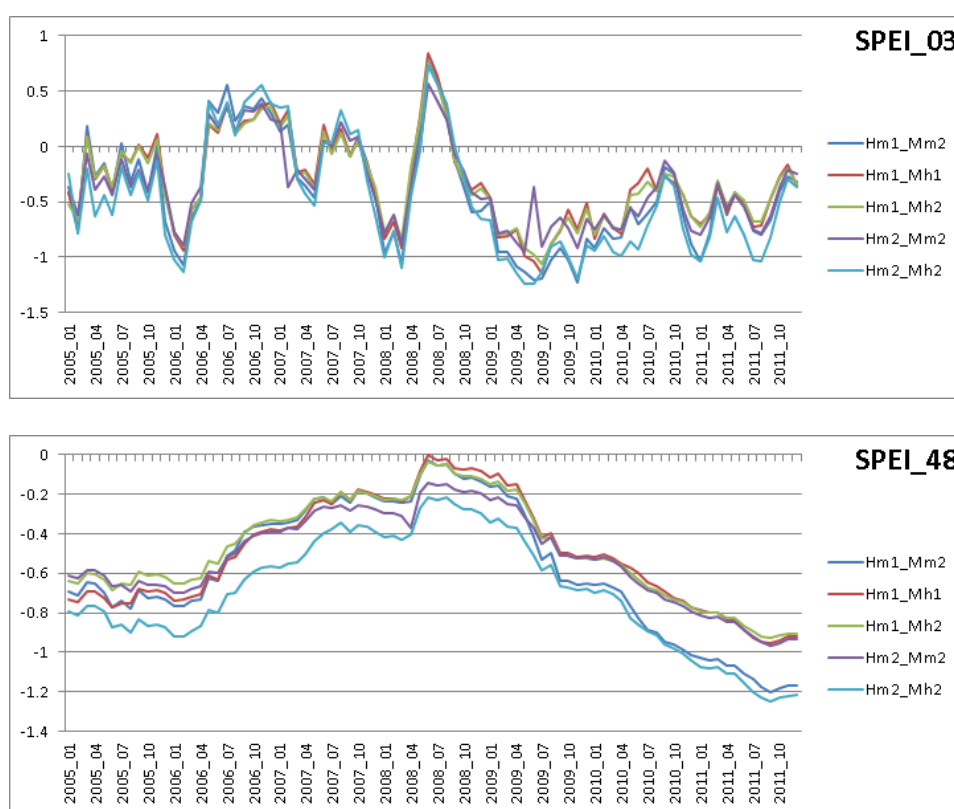


Figure 14.10: Drought index time plot for relevant EFT transitions. Sahel region

Therefore, in Sahel, tree loss LC changes that result in ecosystem functionalism changes for the period 2005-2011 are mainly explained by short-term drought extreme events but mainly by a persisting drought wave difficult to be perceived by regular meteorological observations other than specific drought climate models. Indeed, this tree loss changes driven by a severe drought event derived with a decrease in vegetation productivity, changes in seasonality (vegetative period is shorter and higher) and in a shift of the maximum phenological phase depending on the vegetation local availability of water (local precipitation events).

Results of EFT transitions related to Tree loss land cover changes for Siberia area are shown in Table 14.7 EFT dynamics are similar to the ones for Sahel, but with some singularities:

- decrease of productivity is more frequent but without changes in seasonality or phenology: *HI2 to MI2*, *Hm2 to Mm2*, *Mm2 to Lm2*, *Mh2 to Lh2*.

- seasonality is generally preserved although some changes in both directions (m to h, but also h to m) might be observed
- phenology is preserved in all cases

MR EFT transitions (2005-2011)	Tree loss (% total area)	Other LCC (% total area)	LC invariant (% total area)
Lh2 to Lh2	14.47	6.69	10.06
Mm2 to Mm2	6.21	6.06	2.41
HI2 to HI2	4.78	8.35	3.88
MI2 to MI2	4.64	7.22	3.7
Lm2 to Lm2	4.56	1.88	1.34
Hm2 to Hm2	4.37	10.5	6.43
HI2 to MI2	4.25	4.51	2.4
Hm2 to Mm2	4.13	7.26	1.72
Lh2 to Lm2	3.82	1.2	1.65
Mm2 to Lh2	3.53	1.75	1.6
Mm2 to Lm2	3.18	1.18	0.77
Mh2 to Lh2	2.92	1.58	2.21
<b>Sum</b>	<b>60.86</b>	<b>58.18</b>	<b>38.17</b>

Table 14.7: Relevant EFT transitions mainly explained by Tree loss land cover change. Siberia region

Due to the climatic conditions of the area, mainly frozen areas and with low amount of sun days during the year, SPEI analysis is not recommended in this case.

### 14.3.2 Tree gain analysis

Tree gain, considered as the opposite transition to tree loss, it was also analysed. Table 14.8 shows Sahel dynamics for relevant EFT transition between 2005-2011 mainly explained by Tree gain Land cover changes.

MR EFT transitions (2005-2011)	Tree gain (% total area)	Other LCC (% total area)	LC invariant (% total area)
Mh2 to Lh2	11.94	11.54	2.76
Mh1 to Lh2	11.02	9.39	2.12
HI2 to HI2	6.26	1.69	4.73
Hm1 to Mh1	3.42	2.73	1.87
Hm1 to Mh2	2.71	4.2	1.93
Hh1 to Mh1	2.59	0.96	0.89
Mh1 to Mh2	2.55	1.17	1.85

Hm2 to Mm2	2.53	3.09	1.86
<b>Sum</b>	<b>43.02</b>	<b>34.77</b>	<b>18.01</b>

*Table 14.8: Relevant MR EFT transitions explained by Tree gain land cover change. Sahel region*

In this case, most of the area identified as tree gain presents a decrease in productivity and remains constant for seasonality and phenology components. This decrease in productivity might be explained due to the fact that vegetation productivity is lower for young trees than for prairies that present some bushes. Therefore, understanding this transition as a natural vegetation succession, productivity of a prairie with some small trees/bushes is higher than productivity of a prairie with some young trees that could have grown up during the period 2005-2011.

Table 14.9 shows Siberia dynamics for relevant EFT transition between 2005-2011 mainly explained by Tree gain Land cover changes. The general tendencies in this area are less evident. In general, areas presenting Tree gain do not present EFT transitions or if so, the transitions are towards a lower productivity and a higher seasonality, although only 3 out of 10 cases present these dynamics. This might be explained by the type of aboveground biomass of the area, which is usually rather sparse and small and its productivity changes might not be captured at a 300 m spatial resolution..

MR EFT transitions (2005-2011)	Tree gain (% total area)	Other LCC (% total area)	LC invariant (% total area)
Hm2 to Hm2	11.95	5.05	6.43
HI2 to HI2	9.11	5.21	3.88
Hm2 to Mm2	7.87	4.53	1.72
MI2 to MI2	7.39	5.11	3.70
Mm2 to Mm2	6.32	6.07	2.41
HI2 to Hm2	5.86	1.68	1.69
HI2 to Mm2	5.58	2.45	1.41
Lh2 to Lh2	5.48	13.35	10.06
HI2 to MI2	4.56	4.28	2.40
MI2 to Mm2	2.67	1.88	1.42
<b>Sum</b>	<b>66.79</b>	<b>49.61</b>	<b>35.12</b>

*Table 14.9: Relevant transitions explained by Tree gain land cover change. Siberia region*

### 14.3.3 Urban growth

The dynamics of EFT in areas where urban growth has occurred is complex to be analysed (Table 14.10 and Table 14.11). First, EFTs should be only computed in areas presenting vegetation or natural surface, because EFT of areas corresponding to impervious surfaces is not properly possible to monitor ecosystem functionalism nor possible to analyse the EFT transition. However, the pixel size of MR implies that some urban areas can include a subregion of vegetated cover into the pixel dimensions. With these considerations, some specific characteristics allow us to identify and understand many existing cases.

Indeed, for the Sahel area, most of the areas involving urban growth correspond to types of cover presenting low or mid vegetation productivity, thus the urban expansion is not affecting land surface with mature or high

productivity vegetation from an ecosystem point of view. In these processes with EFT changes (many of them are EFT invariants), phenology is the main change involved.

In any case, EFT transitions for urban growth areas might vary according to the type or urbanization performed, but in general, decreasing in productivity should be observed, like for example transitions *HI2 to MI2* or *MI2 to Lm2*. This LC change coupled with the EFT transition is also relevant to detect which hot spots suitable to be urbanized are more interesting to be protected in terms of ecosystem functionalism.

The same pattern is observed in the Siberia region (Table 14.11).

MR EFT transitions (2005-2011)	Urban growth (% total area)	Other LCC (% total area)	LC invariant (% total area)
MI2 to MI2	12.22	0.7	2.73
LI2 to LI2	6.71	0.45	1.68
HI2 to MI2	4.82	0.89	1.04
MI2 to MI1	4.65	0.35	0.77
LI1 to LI2	4.48	0.20	1.03
LI1 to Lm2	3.79	0.21	1.17
MI1 to MI2	3.61	0.33	1.16
MI2 to LI2	3.61	0.04	0.32
LI2 to LI1	2.75	0.40	0.91
Lm1 to LI2	2.75	0.09	0.63
MI1 to MI1	2.75	0.29	0.47
LI1 to LI1	2.58	0.20	0.70
<b>Sum</b>	<b>54.72</b>	<b>4.15</b>	<b>12.61</b>

Table 14.10: Relevant MR EFT transitions explained by urban growth land cover change. Sahel region

MR EFT transitions (2005-2011)	Urban growth (% total area)	Other LCC (% total area)	LC invariant (% total area)
Lh2 to Lh2	13.92	10.91	10.06
LI2 to LI2	8.93	1.52	0.98
MI2 to MI2	7.64	5.71	3.70
Lm2 to Lm2	6.11	3.26	1.34
Hm2 to Hm2	4.67	7.18	6.43
Lm2 to LI2	3.54	0.66	0.34
Lh2 to Lm2	3.22	2.64	1.65
Lm2 to Lh2	3.14	1.70	0.73
LI2 to Lm2	2.98	0.59	0.31
MI2 to Lm2	2.90	1.18	0.65

Lh2 to Ll2	2.82	1.55	1.12
<b>Sum</b>	<b>59.87</b>	<b>36.90</b>	<b>27.31</b>

Table 14.11: Relevant EFT transitions explained by urban growth land cover change. Siberia region

### 14.3.4 Crop expansion

Sahel and Siberia pilot regions present very different EFT transitions explained by crop expansion LC change:

In Sahel, two high dominant EFT transitions explained by crop expansion occur: *Mh2 to Lh2* and *Mh1 to Lh2* (Table 14.12). Both EFT changes present high seasonality and change from mid to low productivity functionality while preserving the phenology (post-wet in Sahel). The decrease in the productivity may be explained by the deforestation or reduction of mature tree cover to grow crops.

MR EFT transitions (2005-2011)	Crop expansion (% total area)	Other LCC (% total area)	LC invariant (% total area)
Mh2 to Lh2	23.58	1.40	2.76
Mh1to Lh2	21.48	0.63	2.12
Mh2 to Mh2	3.66	1.35	1.46
Mh1 to Mh2	3.48	0.72	1.85
<b>Sum</b>	<b>52.20</b>	<b>4.10</b>	<b>8.19</b>

Table 14.12: Relevant EFT transitions explained by crop expansion land cover change. Sahel region

On the other hand, in Siberia, the EFT dynamics in areas where crop expansion has occurred (Table 14.13) present:

- decrease of productivity
- increase of seasonality
- preservation of phenology in all cases
- most EFTs remain invariant

MR EFT transitions (2005-2011)	Crop expansion (% total area)	Other LCC (% total area)	LC invariant (% total area)
Lh2 to Lh2	15.31	7.58	10.06
MI2 to MI2	5.30	6.18	3.70
Lm2 to Lm2	5.29	1.83	1.34
Hm2 to Hm2	5.20	8.6	6.43
HI2 to HI2	4.95	7.5	3.88
Mm2 to Mm2	4.74	7.27	2.41
Mm2 to Lh2	3.91	1.81	1.60
Hm2 to Mm2	3.66	7.01	1.72
Lh2 to Lm2	3.50	1.98	1.65
HI2 to Hm2	3.34	2.57	1.69
HI2 to Mm2	3.28	3.46	1.41

Mm2 to Lm2	3.18	1.58	0.77
HI2 to MI2	2.97	5.49	2.40
Lm2 to Lh2	2.91	0.83	0.73
Mh2 to Lh2	2.54	2.15	2.21
Sum	<b>70.08</b>	<b>65.84</b>	<b>42.00</b>

Table 14.13: Relevant EFT transitions explained by crop expansion land cover change. Siberia region

The fact that although crop expansion there is no EFT change may be explained accordingly to the type of cover that is eliminated to grow crops. In this case, areas transformed to crops are not mature forests but rather low vegetation extensions of meadows or small bushes that present a similar ecosystem functionality than a crop system, especially in an area with a short vegetative period limited by light and cold climatic conditions.

## 15 Ecosystem changes model with HR land cover final product

The analysis using the final HR product version has been focused on the interaction between Land Cover changes and EFT changes.

### 15.1 Materials

The current HR study mainly uses:

- Remote sensing vegetation indices
- Final HR Land cover maps and quality layers

#### 15.1.1 Remote sensing images and derived products

The NDVI times series obtained from Landsat Collection 1 Surface Reflectance have been used. According to the historical case study regions defined in the project, a selection of tiles (WRS2 path-row tiling system) has been performed, as shown in Table 15.1:

	Tiles	Years
Sahel	169-51, 169-52, 170-51, 170-52	2005, 2010, 2015
Siberia	158-16, 158-17, 159-16, 159-17	2005, 2010, 2015
Amazonia	227-72, 227-73, 228-72, 228-73,	2005, 2010, 2015

Table 15.1: Selected tiles and years for Landsat time series in the project pilot regions

#### 15.1.2 Land cover maps

The ESA High Resolution Land Cover CCI Product final version has been used. This collection includes 4 layers:

- best class land cover
- second best class land cover
- best class posterior probability
- second best class posterior probability

The spatial resolution of HR LC for the historical (times series) product is 30 m.

## 15.2 Methodology and results

The approach applied is the same used for the MR testing (section 14.2) with some adaptations to the new spatial resolution. The generation of the annual NDVI profiles directly from remote sensing images with time resolution

of 16 days (8 days in some small regions of path overlapping) presents a few artefacts in spatial continuity between tiles and some relevant temporal gaps caused by a significant cloud cover (Amazonia), large snow periods (Siberia) and lower time resolution than MR products.

HR EFT generation requires a high detailed annual vegetation profile and we attempted to increase this time resolution by:

- For a given year, addition of selected images from the previous or following year to cover some relevant temporal gaps
- Addition of selected images with partial cloud cover other than the collection of images used for the classification by the Earth Observation team of the project. Obviously, these images present many cloud cover areas and their contribution is low, however they complement a little bit the initial collection.

Figure 15.1 left shows an example of the addition of images from close years for Siberia: some images from 2009 and 2011 helps to fill some gaps on the 2010 and to obtain an improved 2010 HR EFT (Pesquer et al. 2019). However, for year 2005 at Siberia, this addition process is not enough (see 15.1 right) since 2004-2005-2006 presents a longer snow cover period and we could not achieve a valid NDVI profile for the winter.

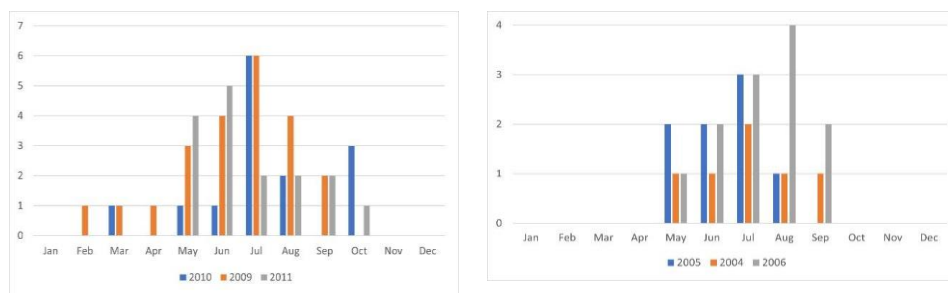


Figure 15.1. Number of used (valid) images (Y axis) per months of the year (X axis). Left: Quasi optimal distribution of valid images for 2010 with the additional ones from closer years. Right: Example 2005 series complemented with images from 2004 and 2006 for which the number of images is still insufficient, above all during winter and spring.

## 15.2.1 EFT generation

Despite the above mentioned barriers for the generation of HR EFTs, feasible HR EFT maps have been obtained (selection of results in Figure 15.2, and Figure 15.3).

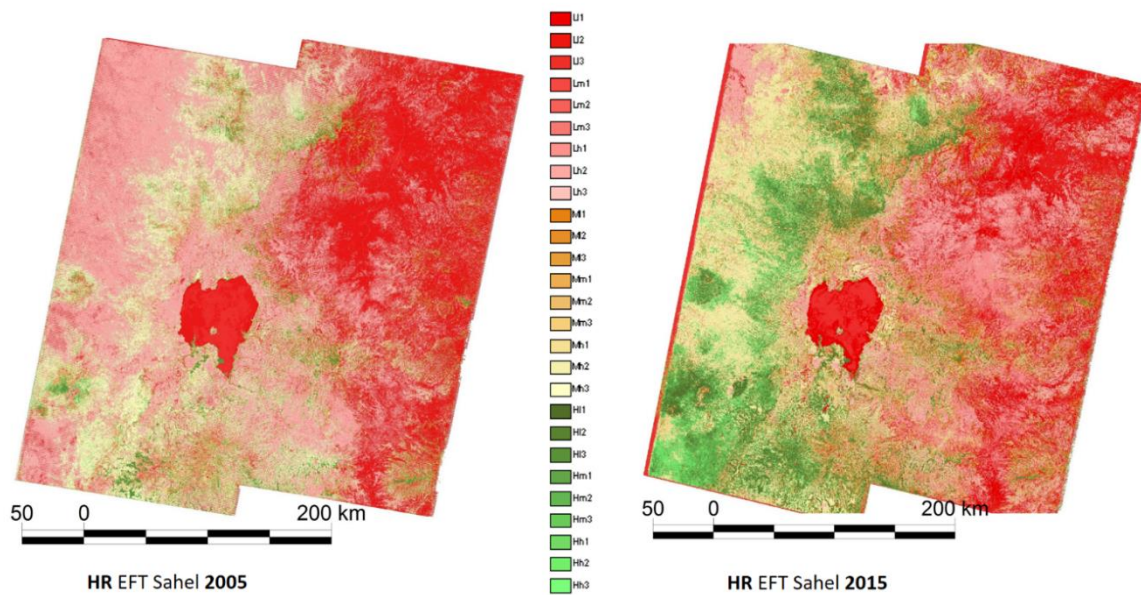


Figure 15.2: 2005 and 2015 EFT maps at HR for the 4-tiles region in **Sahel** (see Table 15.1)

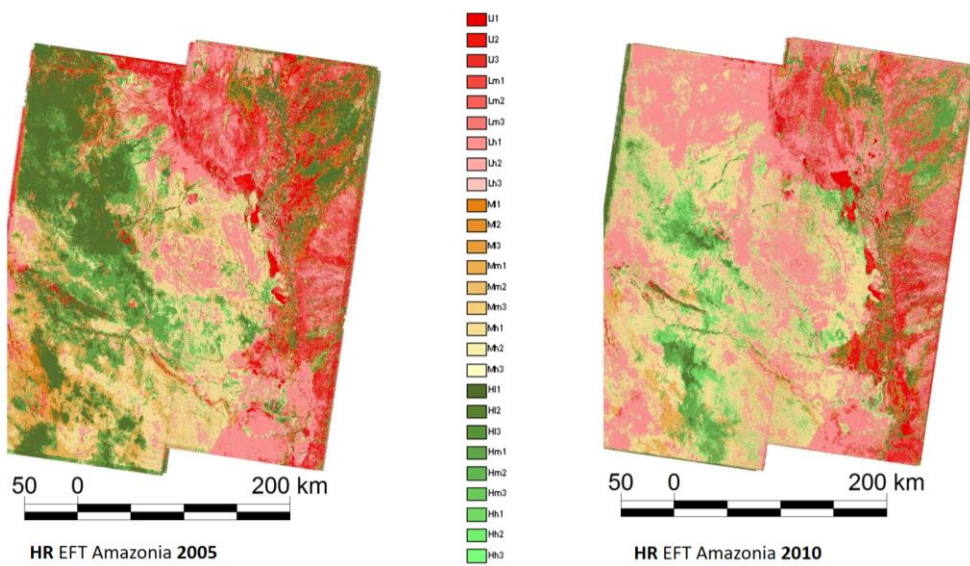


Figure 15.3: 2005 EFT and 2010 maps at HR for the 4-tiles region in **Amazonia** (see Table 15.1)

Complete results in Appendix C. Still, such results present different artefacts: in Sahel and Amazonia artefacts are not significant for the analysis, but for Siberia the presence of gaps is significant in terms of map visualization and analysis. Figure 15.4 compares the spatial detailed ecosystem information between HR and MR. This example is a zoom of the area presenting poorest quality EFT but still we see that this HR EFT is useful for characterizing ecosystem functionalities even considering its spatial continuity problems.

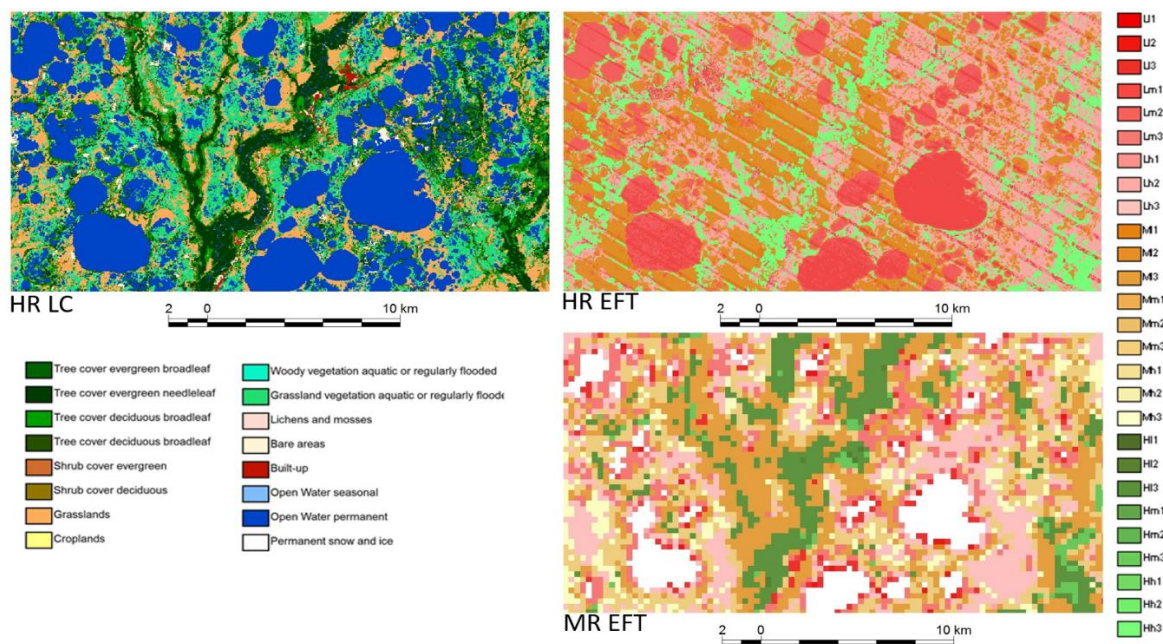


Figure 15.4: Zoom at coordinates 73° 54' 41.48"E, 62° 29' 3.13"N of 2005 HR LC and EFT maps. On the left HR maps (clean of artifacts) HR EFT (top right) and MR EFT (bottom right) at Siberia. Differences in EFT classes (ex. water mass) and spatial resolution are evident.

## 15.2.2 Correlation between LC changes and EFT changes at HR

The analysis of HR LC changes compared to EFT changes and climate drivers performed using MR data (see section 14.3) has been replicated. In order to clearly identify the role of LC maps spatial resolution, the comparison have been done using the same MR EFT maps resampled to 30 m. Moreover, EFT generated directly at 30 m present artefacts (see section 15.2.1) that may introduce noise to the analysis of changes. This final HRLC product has been filtered using the four ancillary layers distributed with the product (classes and probabilities, see section 15.1.2).

The normal identification of a LC change between year1 and year2 is defined by:

$$(best\ class\ year1 \neq best\ class\ year2)$$

However, we added two specific conditions in order to consider a LC change and reduce the misclassifications :

- Strictly different (STRICT):  
 $(best\ class\ year1 \neq 2nd\ best\ class\ year2) \text{ AND } (best\ class\ year2 \neq 2nd\ best\ class\ year1)$
- 5% threshold in difference of the probabilities (GT\_5):  
 $((prob\ best\ year1 - prob\ 2nd\ best\ year2) > 5) \text{ AND } ((prob\ best\ year2 - prob\ 2nd\ year1) > 5)$

Figure 15.5 shows an example of these quality layers for the Sahel region.

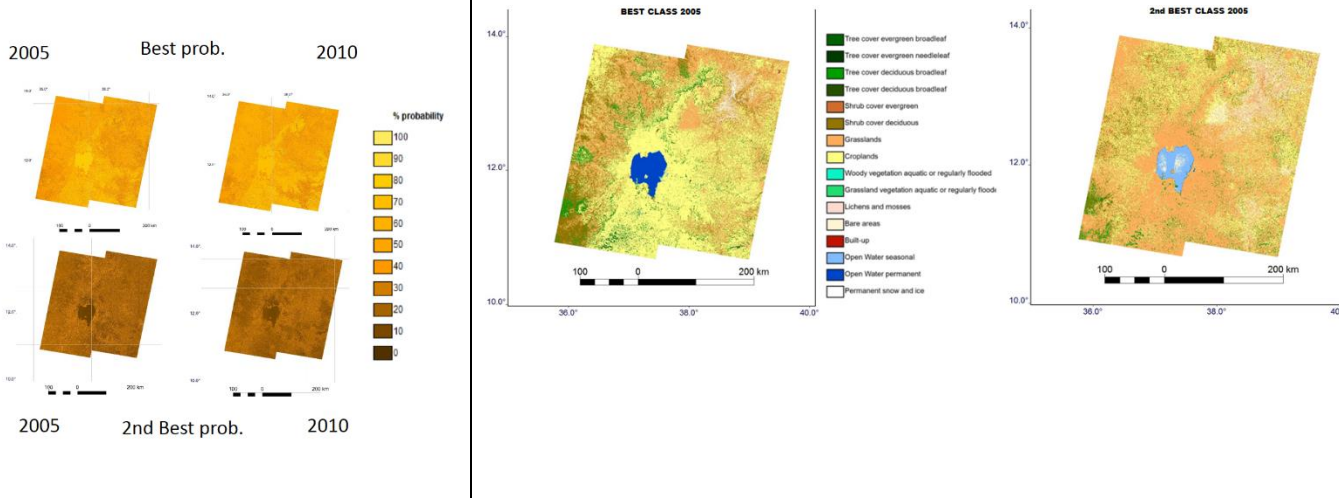


Figure 15.5: Left: HR maps of posterior probabilities of the best and second-best classes at 2005 and 2010 in Sahel region. Right: HR maps of LC classes at Sahel: the first and the second classes, the first is the usual LC map.

At Sahel, the number of changes is reduced from an initial affected area of 4.1% to an area of 0.8 % for 2005-2010, respectively. Moreover, a comparison analysis of the agreement between LC changes and MR EFT changes was carried on with and without these filters. Figure 15.6 shows its statistical representation.

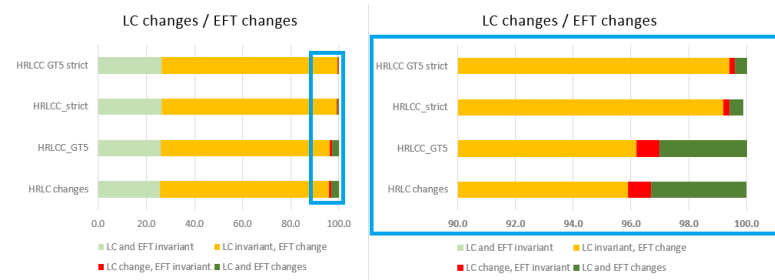


Figure 15.6: Different proportions of the cross classes LC/EFT changes considering (or not) the defined additional criteria.

In addition, analysis of relevant changes have been performed. Four different coupled results are expected (in order of probability):

- LC change between 2005-2010 and EFT change between 2005-2010
- NO LC change and stable EFT
- NO LC change and EFT change between 2005-2010
- LC change between 2005-2010 and stable EFT

	Sahel		Siberia	
	Area (ha)	%	Area (ha)	%
<b>LC and EFT invariant</b>	2725294.8	23.80	70989132	51.08
<b>LC invariant, EFT change</b>	8258514.5	72.11	67292278	48.42
<b>LC change, EFT invariant</b>	90098.7	0.79	279503	0.20

<b>LC and EFT changes</b>	379035.4	3.31	425309	0.31
---------------------------	----------	------	--------	------

Table 15.2: Proportions of LC and EFT changes

Results (Table 15.2) show that, in general, Siberia less land cover and EFT changes than Sahel, 51.08% vs. 23.80% (both LC and EFT remain invariant between 2005 and 2010). Siberia is more stable in terms of dynamics of Land cover and ecosystem functionalism. These results are more consistent than those obtained from the MR analysis (section 14.3). Coherence of invariant changes and both variables changes has increased compared to MR maps.

Moreover, these results point out an interesting situation to analyse: when LC remains invariant but EFT changes between 2005 and 2010. This result does not indicate a discrepancy between both models but highlights the fact that the changes on ecosystem functionalism are not explained by land cover change. In this case is where the climate model has a relevant role, given that these changes might be explained by climate change extreme situations, (otherwise it could indicate errors in any of the maps) for which ecosystems need functionalism adaptation without changing necessarily the land cover type. This part of the analysis shows that a 72.11% of the Sahel is experimenting EFT changes although the LC remains constant. Contrary, in Siberia only 48.42% (not negligible) of the area corresponds to this result. Regarding the changes on LC that are coupled with stable EFT, results show a very low representation (0.79% and 0.20% of the area).

Finally, the combination of LC and EFT changes, although corresponding to a small area (3.31% % for Sahel and 0.31 % of Siberia) is the most interesting one to assess, because LCC is the main driver of this EFT change.

### 15.2.3 Tree/shrub loss analysis

Specific analysis results for Tree/shrub loss transitions based on final HR LC maps for Sahel area are included in Table 15.3 (results in % of total area). The first column of the table contains the name of the EFT transitions between 2005 and 2010, (see section 15.2.2 for more details). For each EFT transition, its corresponding LC behaviour has been analysed so each EFT transition is explained by a LC change related to Tree/shrub loss (second column), other types of LC changes (third column) or non LC changes (fourth column). List is ordered according to the % of total area corresponding to Tree/shrub loss LC changes. This Table 15.3 shows the EFT transitions over the 2.5% of the total area in the Tree/shrub loss LC implied changes at the Sahel pilot region. The sum of the area of the most relevant Tree/shrub loss EFT transitions between 2005 and 2010 is 52.69 % and the top ranked ones are really relevant. The sum of the area of the same subset of EFT transitions is significantly low for other types of LCC changes and when LC is invariant.

HR LCC and MR EFT transitions (2005-2010)	Tree/ shrub loss (% total area)	Other LCC (% total area)	LC invariant (% total area)
(Hm1) to (Mh2)	17.43	5.20	6.25
(Hm2) to (Mh2)	11.99	4.16	5.78
(Hh1) to (Mh2)	6.52	1.20	1.73
(Mh1) to (Mh2)	6.41	0.39	1.82
(Hl1) to (Hm2)	3.51	5.89	2.25
(Hh2) to (Mh2)	3.50	0.36	0.89
(Hm1) to (Mh1)	3.33	0.54	1.37

Sum	<b>52.69</b>	<b>17.74</b>	<b>20.09</b>
-----	--------------	--------------	--------------

Table 15.3: Relevant EFT transitions mainly explained by Tree loss land cover change. Sahel region

The most relevant EFT changes for the selected land cover transitions (dark blue cells in Table 15.3) show a clear tendency to:

- decrease (H to M or M to L) of productivity levels, a clear indicator of woody vegetation degradation or loss
- increase of seasonality levels (m to h, l to m) or preservation (h to h)
- shift of maximum phenology phase (1 to 2) or preservation (1 to 1, 2 to 2)

Most of the area of EFT transitions that indicate a change of the ecosystem functionalism are also explained by LC transitions related to tree loss (52.69% of the area), while LC transitions corresponding to other types of LC changes explain changes of ecosystem functionalism for an area of approximately 18%. These changes are a clear indicator of vegetation cover degradation, corresponding to vegetation that is losing productivity while keeping seasonality or losing productivity while increasing seasonality (covers corresponding to herbaceous vegetation instead of woody vegetation). Changes in shift of maximum phenology may be related to drought events as indicated in section 14.3.1.

Results of EFT changes for the selected land cover transitions for Siberia area are shown in Table 15.4. EFT dynamics are similar to the ones for Sahel, but with some singularities:

- decrease of productivity and increase of seasonality is more frequent
- phenology is preserved in all cases

HR LCC and MR EFT transitions (2005-2010)	Tree/shrub loss (% total area)	Other LCC (% total area)	LC invariant (% total area)
(Mm2) i (Lh2)	11.86	23.06	12.82
(Mh2) i (Lh2)	10.36	20.80	13.42
(Hm2) i (Mm2)	7.48	1.09	1.96
(Ml2) i (Lh2)	7.14	14.17	9.06
(Hl2) i (Hm2)	5.22	2.04	9.86
(Lm2) i (Lh2)	3.71	1.92	4.35
(Ml2) i (Mm2)	3.53	2.89	4.52
(Hl2) i (Mm2)	3.41	2.33	1.66
(Hl2) i (Lh2)	2.92	5.40	2.98
(Hm2) i (Lm2)	2.73	0.23	0.06
(Hl2) i (Mh2)	2.50	4.38	3.81
Sum	<b>60.86</b>	<b>78.31</b>	<b>64.5</b>

Table 15.4: Relevant EFT transitions mainly explained by Tree loss land cover change. Siberia region

## 15.2.4 Tree/shrub gain analysis

Tree/shrub gain, considered as the opposite transition to tree/shrub loss, it was also analysed. Table 15.5 shows Sahel dynamics for relevant EFT changes between 2005-2010 mainly explained by Tree /shrub gain Land cover changes.

HR LCC and MR EFT transitions (2005-2010)	Tree/shrub gain (% total area)	Other LCC (% total area)	LC invariant (% total area)
(H11) to (Hm2)	10.38	3.22	2.25
(H12) to (Hm2)	9.56	2.16	2.40
(Hm1) to (Mh2)	8.92	15.97	6.25
(Hm2) to (Mh2)	7.23	10.97	5.78
(H11) to (H12)	4.78	1.58	2.10
(H12) to (Mh2)	3.04	1.18	0.69
(H11) to (Hh2)	2.57	0.43	0.34
Sum	<b>46.48</b>	<b>35.51</b>	<b>19.81</b>

Table 15.5: Relevant MR EFT transitions explained by Tree/shrub gain land cover change. Sahel region

In this case, most of the area identified as tree/shrub gain maintains the productivity and increase or maintain the seasonality. Phenology also is maintained or change in some cases from pre-wet season to post-wet season.

Table 15.6 shows Siberia dynamics for relevant EFT changes between 2005-2010 mainly explained by Tree/shrub gain Land cover changes. The general tendencies in this area are unexpected. In general, areas presenting Tree/shrub gain are towards a lower productivity and a higher seasonality. This might be explained by the type of regeneration occurring, with sparse woody vegetation and dense aboveground biomass, which is usually small and with higher seasonality than trees, or by the type of trees appearing in the regeneration (mostly deciduous with lower productivities).

HR LCC and MR EFT transitions (2005-2010)	Tree gain (% total area)	Other LCC (% total area)	LC invariant (% total area)
(Mm2) i (Lh2)	24.82	16.05	12.82
(Mh2) i (Lh2)	19.63	16.48	13.42
(M12) i (Lh2)	15.03	9.96	9.06
(H12) i (Lh2)	6.48	3.31	2.98
(H12) i (Mh2)	5.86	2.27	3.81
(M12) i (Mh2)	5.01	2.32	3.16
(Mm2) i (Mh2)	3.29	2.19	2.87

(MI2) i (Mm2)	2.71	3.36	4.52
(HI2) i (Mm2)	2.61	2.66	1.66
Sum	<b>90.35</b>	<b>64.30</b>	<b>66.62</b>

Table 15.6: Relevant transitions explained by Tree/shrub gain land cover change. Siberia region

### 15.2.5 Urban growth analysis

The dynamics of EFT in areas where urban growth has occurred is complex to be analysed (Table 15.7 and Table 15.8). First, EFTs should be only computed in areas presenting vegetation or natural surface, because EFT of areas corresponding to impervious surfaces is not properly possible to monitor ecosystem functionalism nor possible to analyse the EFT transition. At this spatial resolution, results show more coherence than using the MR LC maps because the increase of pure classes pixels.

Indeed, for the Sahel area, most of the areas involving urban growth correspond to types of cover presenting low or mid vegetation productivity, thus the urban expansion is not affecting land surface with mature or high productivity vegetation from an ecosystem point of view.

In any case, EFT changes for urban growth areas might vary according to the type or urbanization performed, but in general, decrease in productivity is observed. This LC change coupled with the EFT transition is also relevant to detect which hot spots suitable to be urbanized are more interesting to protect in terms of ecosystem functionalism although usually, areas that are converted into urban areas are already suffering a degradation process.

The same pattern is observed in the Siberia region (Table 15.8).

HR LCC and MR EFT transitions (2005-2010)	Urban growth (% total area)	Other LCC (% total area)	LC invariant (% total area)
(HI2) i (MI2)	9.25	81.96	3.16
(Mm2) i (MI2)	5.68	0.34	1.88
(Lh2) i (Lm2)	5.65	0.71	1.16
(Mh2) i (Lm2)	5.12	1.00	1.06
(Mh2) i (Lh2)	4.82	0.62	4.90
(Mm2) i (Lm2)	3.91	1.02	2.47
(LI1) i (LI2)	3.59	1.05	0.68
(MI1) i (MI2)	3.59	0.81	1.18
(MI2) i (LI2)	3.25	0.35	0.85
(Hm2) i (Mm2)	2.58	0.22	4.01
Sum	<b>47.44</b>	<b>88.08</b>	<b>21.35</b>

Table 15.7: Relevant MR EFT transitions explained by urban growth land cover change. Sahel region

HR LCC and MR EFT transitions (2005-2010)	Urban growth (% total area)	Other LCC (% total area)	LC invariant (% total area)
(Mm2) i (Lh2)	12.43	20.72	12.82
(MI2) i (Lh2)	9.53	12.48	9.06
(Lm2) i (Lh2)	8.69	1.74	4.35
(Hm2) i (Mm2)	8.53	2.27	1.96
(Mh2) i (Lh2)	7.72	18.96	13.42
(HI2) i (Mm2)	4.35	2.45	1.66
(Hm2) i (Lm2)	4.32	0.56	0.06
(HI2) i (Lh2)	3.41	4.84	2.98
(MI2) i (Mm2)	3.13	3.07	4.52
(Mm2) i (Lm2)	3.07	0.56	0.59
(HI2) i (Hm2)	3.05	2.92	9.86
<b>Sum</b>	<b>68.23</b>	<b>70.57</b>	<b>61.28</b>

Table 15.8: Relevant EFT transitions explained by urban growth land cover change (HR LC maps v2). Siberia region

## 15.2.6 Crop expansion analysis

In Sahel, EFT changes explained by crop expansion are characterized by a reduction or maintenance of productivity and seasonality is kept either invariant or increase for all cases (Table 15.9). These results are consistent with the tree/shrub loss analysis since many deforested areas are transformed to crops. Therefore, the decrease in the productivity may be explained by the deforestation or reduction of mature tree cover to grow crops.

HR LCC and MR EFT transitions (2005-2010)	Crop expansion (% total area)	Other LCC (% total area)	LC invariant (% total area)
(HI2) i (MI2)	8.66	0.77	3.16
(Hm1) i (Mh2)	6.56	16.74	6.25
(HI1) i (Hm2)	5.26	3.71	2.25
(Hm2) i (Mh2)	5.12	11.53	5.78
(HI1) i (HI2)	5.06	1.36	2.10
(HI2) i (Mm2)	3.61	1.25	3.32
(Mh1) i (Mh2)	2.99	5.75	1.82
(MI1) i (MI2)	2.85	0.70	1.18
(HI2) i (Hm2)	2.73	2.93	2.40

Sum	<b>42.84</b>	<b>44.74</b>	<b>28.26</b>
-----	--------------	--------------	--------------

Table 15.9: Relevant EFT transitions explained by crop expansion land cover change. Sahel region

On the other hand, in Siberia, the EFT dynamics in areas where crop expansion has occurred (Table 15.10) present:

- Mainly decrease of productivity
- Mainly increase of seasonality
- preservation of phenology in all cases

HR LCC and MR EFT transitions (2005-2010)	Crop expansion (% total area)	Other LCC (% total area)	LC invariant (% total area)
(Mm2) i (Lh2)	10.56	20.24	12.82
(Hm2) i (Mm2)	9.59	2.65	1.96
(MI2) i (Lh2)	8.11	12.33	9.06
(Lm2) i (Lh2)	7.96	2.23	4.35
(Mh2) i (Lh2)	4.93	18.32	13.42
(MI2) i (Mm2)	4.42	3.02	4.52
(LI2) i (Lm2)	4.20	0.80	1.29
(Hm2) i (Lm2)	3.87	0.83	0.06
(HI2) i (Mm2)	3.33	2.61	1.66
(Mm2) i (Lm2)	3.15	0.72	0.59
(MI2) i (Lm2)	2.93	0.65	0.46
(Lh2) i (Lm2)	2.90	0.82	2.14
(LI2) i (Lh2)	2.81	0.85	1.22
Sum	<b>68.76</b>	<b>66.07</b>	<b>53.55</b>

Table 15.9: Relevant EFT transitions explained by crop expansion land cover change. Siberia region

### 15.3 Discussion

On the one hand, the spatial detail of the provided collection of HR LC maps (based on Landsat Collection) and its derived HR EFT is very valuable; however, its time resolution is not enough for some applications and locations compared to MR products. One image every 16 days together with the cloud cover affections (and snow at Siberia) in some cases becomes a challenge for a correct identification of some LC classes (i.e., deciduous or evergreen), increasing its associated uncertainty and generating too much heterogeneity (salt and pepper texture). Moreover, it's the main reason for an overestimation of LC changes. Other problems are detected when generating HR EFT, given that EFT classes are vegetation index annual profile depending. Also, when the LC map is based on Landsat 7 ETM+ data, the artefacts derived from SCL-off problem, are slightly transferred to the final products.

In order to enrich temporal information for the EFTs profiles, some initial discarded images (by decrease the cloud free threshold) from previous and following year of the selected study year were added.

On the other hand, the quality layers of the LC product help to filter some classified pixels that not have a clear decided category.

Finally, the analysis performed of the areas where tree loss, tree gain, urban expansion or crop expansion is occurring according to final historical maps of HR LC shows that results obtained using the HR products are more consistent than the ones performed using MR data, since HR maps present better defined categories (instead of mixed categories). Vegetation phenology is better related to these type purer categories.

## 16 Comparison between MR and HR LC products

### 16.1 KPIs on ORCHIDEE

The KPIs proposed to use for the assessment of the HRLC data in our climate model are all statistical metrics based on the output model errors calculated against independent observations. The simulated surface variables for which observations at a comparable scale to the model grid one are available, are the following:

- Land surface temperatures (LSTs), which can be estimated from space with thermal infrared radiometers (e.g., Landsat, ASTER, MODIS, AATSR, SEVIRI, Sentinel-3, CCI-LST products...)
- Soil moisture (SM), provided by CCI-SM, SMOS, SMAP, ...
- Leaf Area Index (LAI) from solar sensors (MODIS, SEVIRI, VGT, Copernicus, ...)
- Surface Albedo, (GlobAlbedo, MODIS, Sentinel-2 products...)
- Snow mass and extent (GlobSnow, CCI-Snow, ...)
- Evapotranspiration (FLUXNET, GLEAM, Jung et al., 2009, ...)
- GPP (FLUXNET, Jung et al., 2009, MODIS)

The KPIs will quantify the discrepancies (model-observations) and improvement factors based on the reduction of the model errors. All the evaluation datasets that will be used in the project have been processed globally and in our 3 studied regions and upscaled to the various model grids used in the simulations.

### 16.2 KPIs on Landscape metrics

The benefits of HR LC product compared to MR one were evaluated using landscape metrics. These regular metrics are used in Landscape Ecology.

#### 16.2.1 Shannon diversity index

Shannon diversity index (Shannon and Weaver, 1949) is used as a relative index for comparing different landscapes or the same landscape at different time or spatial scales. This study compares the MR LC (300 m) and final HR static product (10m) for 2019 and the historical product (30 m). This index can be evaluated as a global indicator for the study region or it can be regionalized, calculated in any subregion of a defined grid size, 10 km, 20 km and 30 km in this study. This regionalized form allows the analysis of the spatial distribution of the landscape diversity. In addition, for the regionalized form, a layer of Shannon index Differences between HR and MR is generated. Table 16.1 shows the Shannon for 2019 for the static map and two years, 2005 and 2010 and two regions.

Siberia 2019		Amazonia 2019	
MR	HR	MR	HR
2.19	2.53	2.82	2.08

	Siberia		Amazonia		Sahel	
Year	MR	HR	MR	HR v1	MR	HR
2005	2.14	2.79	2.70	2.44	2.84	2.04
2010	2.14	2.80	2.71	2.69	2.85	2.01

Table 16.1: Global I Shannon for the Siberia and Sahel regions for the static and historical maps

It's important to note that, despite MR has more classes (37) than HR level 1 (14), the results of Shannon diversity index at HR are similar or higher than MR, thus HR maps present more diversity than MR ones, as a consequence of its higher spatial detail and the absence of the mix classes. These MR mix classes generate higher spatially aggregated patches.

In addition, Figure 16.1 shows one regionalized example of this metrics, in MR we can see more dark patches (lowest value), and also some yellow (value 1.0) that turn to orange or brown (1.5; 2.0 values) at HR.

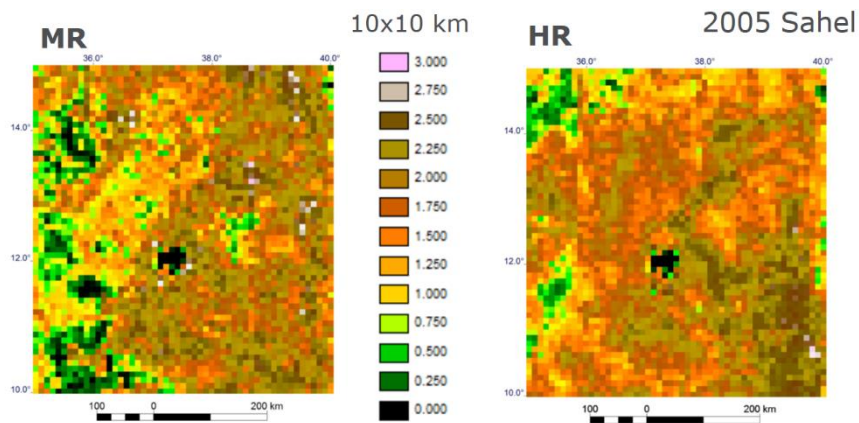


Figure 16.1: 10 km regionalized Shannon Index at MR (left) and HR (right) for 2005 Sahel.

Additionally, the differences between MR and HR have been map and a zoom area with significant Differences has been analysed (Figure 16.2):

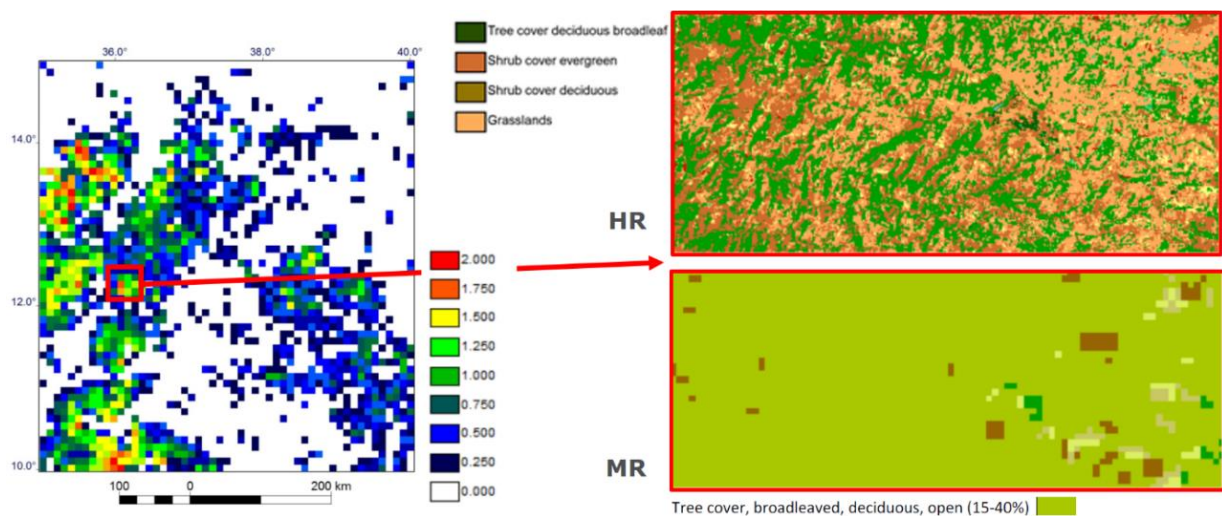


Figure 16.2: Left: map differences HR - MR I. Shannon at 10 km grid. Right: Zoom at 36°5' 13.5"E, 12°10' 20.23" for the HR LC (top) and for the MR LC map (bottom) for 2005 Sahel region.

## 16.2.2 Edge density

The Edge density (McGarigal and Marks 1995) is a measure of fragmentation and it is obtained as the sum of length of all edge segments divided by total landscape area (in ha). It means that the LC maps are converted to a vector model and those segments closing the polygons corresponding to the entities of LC classes are obtained (Table 16.2).

This metric has currently been calculated for the static maps and also the historical.

Siberia 2019		Amazonia 2019		
MR	HR	MR	MR	HR
20.81	217.11		14.94	201.14

	Amazonia		Sahel	
Year	MR	HR v1	MR	HR v1
2005	14.34	96.67	19.03	123.47
2010	14.58	117.56	19.15	81.77

Table 16.2: Edge density indicator at MR and HR for static and historical maps.

## 16.3 KPI's on Ecosystem functional metrics

### 16.3.1 Confusion matrix

As explained in Section 14.2, changes on EFT are mainly caused by Land Cover changes and by climate change adaptation mechanisms. A simple correlation matrix between changes and non-changes of both variables are analysed in two resolutions: MR and HR. Table 16.3 shows more agreement (values on the diagonal) for HR than for MR for Siberia, while Table 16.4 shows the same results for Sahel:

MR		Land Cover		HR		Land Cover	
		No-change %	Change %			No-change %	Change %
EFT	No-change	0.90	0.02	EFT	No-change	0.59	0.33
	Change	97.32	1.75		Change	57.88	41.29

Table 16.3: Confusion / agreement matrix between LC and EFT changes 2005-2010 at Siberia

MR		Land Cover		HR		Land Cover	
		No-change %	Change %			No-change %	Change %
EFT	No-change	0.68	0.01	EFT	No-change	0.41	0.28
	Change	97.85	1.46		Change	56.99	42.32

Table 16.4: Confusion / agreement matrix between LC and EFT changes 2005-2010 at Sahel

### 16.3.2 Detrended Correspondence Analysis

LC classes and EFT classes correspond to two different but not independent perspectives of the land surface status and processes. Some of their cross classes are expected to be very related and grouped in a two dimensional analysis. Therefore, a KPI for evaluating the modification of this correlation/ correspondence to pass from MR LC to HR LC is carried out. This KPI is based on Detrended Correspondence Analysis (DCA) (Hill and Gauch, 1980). It is a multivariate statistical technique widely used by ecologists to find the main factors in species-richness. It is recommended instead of Principal components analysis (PCA) or the Correspondence Analysis (CA) when the lack of linear response to environmental gradients.

This KPI is an ongoing analysis at this current version in which preliminary results are generated at Sahel 2005 (Table 16.5 and Figure 16.3) collected by the two first axes of the DCA eigenvalues, the ones that, like PCA, collect the main contributions.

LC & EFT	DCA1	DCA2	DCA1+DCA2
MR LC	0.438	0.152	0.590
HR-LC	0.556	0.197	0.753

Table 16.5: DCA of correspondence of LC changes and EFT changes at Sahel 2005-2010.

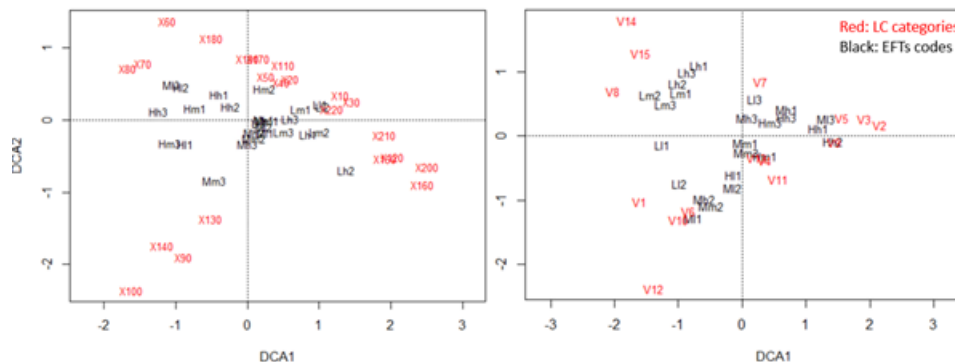


Figure 16.3: Ordination plot of dimension 1 and dimension 2 of the DCA with the contingency matrix between on left: MR-EFT (black), MR-LC (red); right: MR-EFT (black); HR-LC (red)

These first results of the DCA indicate that HR LC maps collect more correlated information than MR (the sum of the two first eigenvalues in Table 16.5 are 0.753 and 0.590, respectively) and the plot (Figure 16.3) show a slightly clearer clusters in some LC / EFT eigenvalues correspondences.

## 17 References

Alcaraz, D., Paruelo, J. and Cabello, J., (2006) Identification of current ecosystem functional types in the Iberian Peninsula. *Global Ecology and Biogeography* 15, 200–212.

Alcaraz-Segura, D.; Paruelo, J.M.; Epstein, H.E.; Cabello, J. (2013) Environmental and Human Controls of Ecosystem Functional Diversity in Temperate South America. *Remote Sens.* 5, 127-154.

Bastrikov, V., P. Peylin, C. Ottlé, Calibration of albedo parametrisation in ORCHIDEE based on various satellite products, in preparation for *Geosci. Model Dev.*

	Ref	CCI_HRLC_Ph1-CAR		
	Issue	Date	Page	
	3.0	28/10/2022	79	

Beguería, S., Vicente-Serrano, S. M., & Angulo-Martínez, M. (2010). A Multiscalar Global Drought Dataset: The SPEIbase: A New Gridded Product for the Analysis of Drought Variability and Impacts. *Bulletin of the American Meteorological Society*, 91(10), 1351-1356.

Bontemps, S., Defourny, P., Radoux, J., Van Bogaert, E., Lamarche, C., Achard, F., Mayaux, P. 2013. Consistent global land cover maps for climate modelling communities: current achievements of the ESA's land cover CCI. *Proceedings of the ESA Living Planet Symposium*, Edinburgh, UK, 9–13 Septembre 2013, pp. 9–13.

Bouvet, A., Mermoz, S., Le Toan, T., Villard, L., Mathieu, R., Naidoo, L. and Asner, G. (2018). An above-ground biomass map of African savannas and woodlands at 25 meters resolution derived from ALOS PALSAR. *Remote Sensing of Environment*, 206, 156-173.

Cheruy, F., Campoy, A., Dupont, J. C., Ducharne, A., Hourdin, F., Haeffelin, M., ... & Idelkadi, A. (2013). Combined influence of atmospheric physics and soil hydrology on the simulated meteorology at the SIRTA atmospheric observatory. *Climate dynamics*, 40(9-10), 2251-2269.

Cheruy F., A. Ducharne, F. Hourdin, I. Musat, E. Vignon, G. Gastineau, V. Bastrikov, N. Vuichard, B. Diallo, J.L. Dufresne, J. Ghattas, J.Y. Grandpeix, A. Idelkadi, L. Mellul, F. Maignan, M. Menegoz, C. Ottlé, P. Peylin, F. Wang, Y. Coindreau, O., Hourdin, F., Haeffelin, M., Mathieu, A., & Rio, C. (2007). Assessment of physical parameterizations using a global climate model with stretchable grid and nudging. *Monthly weather review*, 135(4), 1474-1489.

Di Gregorio, A. (2005). Land cover classification system: classification concepts and user manual: LCCS (Vol. 2). Food & Agriculture Org.

Domingo-Marimon, C., Pons, X., Cristóbal, J., Ninyerola, M., & Wardlow, B. (2015). Integration of climate time series and MODIS data as an analysis tool for forest drought detection. In J. Andreu, A. Solera, J. Paredes-Arquiola, D. Haro-Monteagudo, & H. A. J. Van Lanen (Ed.), *Drought. Research and Science-Policy Interfacing* (p. 514). CRC Press, Taylor & Francis Group (<https://books.google.es/books?hl=es&lr=&id=zka3BgAAQBAJ&oi=fnd&pg=PA97&ots=GELcyQirJT&sig=qDP6B3Q1WwI0m6w8zvmB-QCluj8#v=onepage&q&f=false>).

Dyukarev, E. A., Pologova, N. N., Golovatskaya, E. A., & Dyukarev, A. G. (2011). Forest cover disturbances in the South Taiga of West Siberia. *Environmental Research Letters*, 6(3), 035203.

Fetene, A., Hilker, T., Yeshitela, K., Prasse, R., Cohen, W., & Yang, Z. (2016). Detecting trends in landuse and landcover change of Nech Sar National Park, Ethiopia. *Environmental management*, 57(1), 137-147.

Forbes, B. C., Fauria, M. M., & Zetterberg, P. (2010). Russian Arctic warming and 'greening' are closely tracked by tundra shrub willows. *Global Change Biology*, 16(5), 1542-1554.

Harris, I. C. (2019). CRU JRA v1. 1: A forcings dataset of gridded land surface blend of Climatic Research Unit (CRU) and Japanese reanalysis (JRA) data; Jan. 1901-Dec. 2017. Published by: University of East Anglia Climatic Research Unit, Centre for Environmental Data Analysis, 2905.

Hill, M.O., Gauch H.G. (1980) Detrended Correspondence Analysis: an improved ordination technique. *Vegetation* 42:47-58.

Ivits, E., Cherlet, M., Horion, S. and Fensholt, R., (2013) Global Biogeographical Pattern of Ecosystem Functional Types Derived From Earth Observation Data. *Remote Sensing* 5, 3305-3330.

Kobayashi, S., Ota, Y., Harada, Y., Ebata, A., Moriya, M., Onoda, H., ... & Miyaoka, K. (2015). The JRA-55 reanalysis: General specifications and basic characteristics. *Journal of the Meteorological Society of Japan. Ser. II*, 93(1), 5-48.

	Ref	CCI_HRLC_Ph1-CAR		
	Issue	Date	Page	
	3.0	28/10/2022	80	

Liang, S., Cheng, C., Jia, K., Jiang, B., Liu, Q., Xiao, Z., Yao, Y., Yuan, W., Zhang, X., Zhao, X., & Zhou, J. (2020). The Global LAnd Surface Satellite (GLASS) products suite. *Bulletin of the American Meteorological Society*, DOI: 10.1175/BAMS-D-18-0341.1

Lurton Thibaut, Y. Balkanski, V. Bastrikov, S. Bekki, L. Bopp, P. Braconnot, P. Brockmann, P. Cadule, C. Contoux, A. Cozic, D. Cugnet, J.L. Dufresne, Ch. Éthé, MA Foujols, J. Ghattas, D. Hauglustaine, RM. Hu, M. Kageyama, M. Khodri, N. Lebas, G. Levvasseur, M. Marchand, C. Ottlé, Ph. Peylin, A. Sima, S. Szopa, R. Thiéblemont, N. Vuichard and O. Boucher, Implementation of the CMIP6 forcing data in the IPSL-CM6A-LR model, 2020, *Journal of Advances in Modeling Earth Systems*, 12, e2019MS001940.

Macias-Fauria, M., Forbes, B. C., Zetterberg, P., & Kumpula, T. (2012). Eurasian Arctic greening reveals teleconnections and the potential for structurally novel ecosystems. *Nature climate change*, 2(8), 613-618.

Martens, B., Miralles, D.G., Lievens, H., van der Schalie, R., de Jeu, R.A.M., Fernández-Prieto, D., Beck, H.E., Dorigo, W.A., and Verhoest, N.E.C.: GLEAM v3: satellite-based land evaporation and root-zone soil moisture, *Geoscientific Model Development*, 10, 1903–1925, doi: 10.5194/gmd-10-1903-2017, 2017.

McGarigal, K. and Marks, B. (1995). FRAGSTATS: Spatial analysis program for quantifying landscape structure. USDA Forest Service Gen. Tech. Rep. PNW-GTR–351.

Miles, V. V., & Esau, I. (2016). Spatial heterogeneity of greening and browning between and within bioclimatic zones in northern West Siberia. *Environmental Research Letters*, 11(11), 115002.

Mishra, A. K., & Singh, V. P. (2010). A review of drought concepts. *Journal of Hydrology*, 391(1–2), 202-216.

Muller, J.-P., et al. (2012), The ESA GlobAlbedo Project for mapping the Earth's land surface albedo for 15 Years from European Sensors., paper presented at *IEEE Geoscience and Remote Sensing Symposium (IGARSS) 2012*, IEEE, Munich, Germany, 22-27.7.12.

Paruelo, J., Jobbágy, E. & Sala, O. (2001) Current Distribution of Ecosystem Functional Types in Temperate South America. *Ecosystems* 4, 683–698.

Peel, M. C., Finlayson, B. L., & McMahon, T. A. (2007). Updated world map of the Köppen-Geiger climate classification. *Hydrology and earth system sciences*, 11(5), 1633-1644.

Pesquer, L., Domingo-Marimon, C., Cristóbal, J., Ottlé, C., Peylin, P., Bovolo, F., Bruzzone, L. (2019) Comparison of ecosystem functional type patterns at different spatial resolutions in relation with FLUXNET data. *Proceedings SPIE Remote Sensing, Remote Sensing for Agriculture, Ecosystems, and Hydrology* Vol. 11149: 1114908

Poulter, B., MacBean, N., Hartley, A., Khlystova, I., Arino, O., Betts, R., ... & Hagemann, S. (2015). Plant functional type classification for earth system models: results from the European Space Agency's Land Cover Climate Change Initiative. *Geoscientific Model Development*, 8, 2315-2328.

Vitousek, P.M., Mooney, H.A., Lubchenco, J. & Melillo, J.M. (1997) Human domination of Earth's ecosystems. *Science*, 277, 494–499.

Shannon, C. E, Weaver, W. (1949). *The Mathematical Theory of Communication*. Urbana, IL: The University of Illinois Press, 1-117.

Schaaf, Crystal - University of Massachusetts Boston, Zhuosen Wang - NASA GSFC and MODAPS SIPS - NASA. (2015). MCD43C3 MODIS/Terra+Aqua BRDF/Albedo Snow-free Model Parameters Daily L3 0.05Deg CMG. NASA LP DAAC. <http://doi.org/10.5067/MODIS/MCD43C3.006>

Snyder J. P. (1997) *Map Projections, A Working Manual*, U.S. Geological Survey professional paper 1395.

	Ref	CCI_HRLC_Ph1-CAR		
	Issue	Date	Page	
	3.0	28/10/2022	81	

Still, C. J., Berry, J. A., Collatz, G. J., & DeFries, R. S. (2003). Global distribution of C3 and C4 vegetation: carbon cycle implications. *Global biogeochemical cycles*, 17(1), 6-1.

Still, C. J., Pau, S., & Edwards, E. J. (2014). Land surface skin temperature captures thermal environments of C3 and C4 grasses. *Global ecology and biogeography*, 23(3), 286-296.

Trigo, I. F., C. C. DaCamara, P. Viterbo, J.-L. Roujean, F. Olesen, C. Barroso, F. Camacho-de Coca, D. Carrer, S. C. Freitas, J. García-Haro, B. Geiger, F. Gellens-Meulenberghs, N. Ghilain, J. Meliá, L. Pessanha, N. Siljamo, and A. Arboleda, 2011: The Satellite Application Facility on Land Surface Analysis. *Int. J. Remote Sens.*, 32, 2725-2744, doi: 10.1080/01431161003743199

Verger, A., Baret, F., Weiss, M., Smets, B., Lacaze, R., & Camacho, F. (2014b). Near real time estimation of biophysical variables within Copernicus global land service. In, *Global vegetation monitoring and modeling (available at <https://colloque.inra.fr/gv2m/Poster-Sessions/Poster-S7>)*. Avignon (France)

Zhao. Improved near surface continental climate in IPSL-CM6 by combined evolutions of atmospheric and land surface physics, *JAMES Journal*, in press.

## Appendix A: CWT-ORCH v2

Table A.1: CWT-ORCH v2 (Part 1): Tree PFTs (in brackets: total area in Mkm2 from MRLC).

Source: [https://orchidas.lsce.ipsl.fr/dev/lccci/new\\_protocol.ph](https://orchidas.lsce.ipsl.fr/dev/lccci/new_protocol.ph) (section 6)

GENERIC	KG/Still/LUH	PFT1	PFT2	PFT3	PFT4	PFT5	PFT6	PFT7	PFT8	PFT9	PFT10	PFT11	PFT12	PFT13	PFT14	PFT15
TrBrEv	tropical		1 (13.77)													
TrBrEv	arid_warm		1 (0.1523)													
TrBrEv	arid_cool					1 (0.008954)										
TrBrEv	temp_warm					1 (0.9819)										
TrBrEv	temp_cool					1 (0.9989)										
TrBrEv	boreal_warm							1 (0.002714)								
TrBrEv	boreal_cool							1 (0.03229)								
TrBrDe	tropical			1 (2.176)												
TrBrDe	arid_warm			1 (0.3922)												
TrBrDe	arid_cool						1 (0.04869)									
TrBrDe	temp_warm						1 (1.342)									
TrBrDe	temp_cool						1 (0.7328)									
TrBrDe	boreal_warm						1 (2.135)									
TrBrDe	boreal_cool								1 (0.7625)							
TrNeEv	tropical	1 (0.0549)														
TrNeEv	arid_warm	1 (0.01916)														
TrNeEv	arid_cool				1 (0.06536)											
TrNeEv	temp_warm				1 (1.022)											
TrNeEv	temp_cool				1 (1.029)											
TrNeEv	boreal_warm				1 (1.594)											
TrNeEv	boreal_cool							1 (4.22)								
TrNeDe	tropical		1 (0.01601)													
TrNeDe	arid_warm		1 (0.01041)													
TrNeDe	arid_cool						1 (0.01366)									
TrNeDe	temp_warm						1 (0.02521)									
TrNeDe	temp_cool									1 (0.01768)						
TrNeDe	boreal_warm									1 (0.1219)						
TrNeDe	boreal_cool									1 (2.177)						

Table A.2: CWT-ORCH v2 (Part 2): Shrub Generic PFTs (in brackets: total area in Mkm2 from MRLC).

Source: [https://orchidas.lsce.ipsl.fr/dev/lccci/new\\_protocol.ph](https://orchidas.lsce.ipsl.fr/dev/lccci/new_protocol.ph) (section 6)

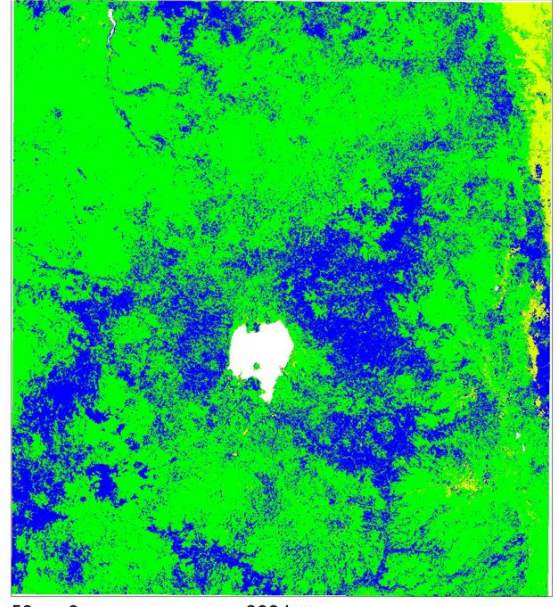
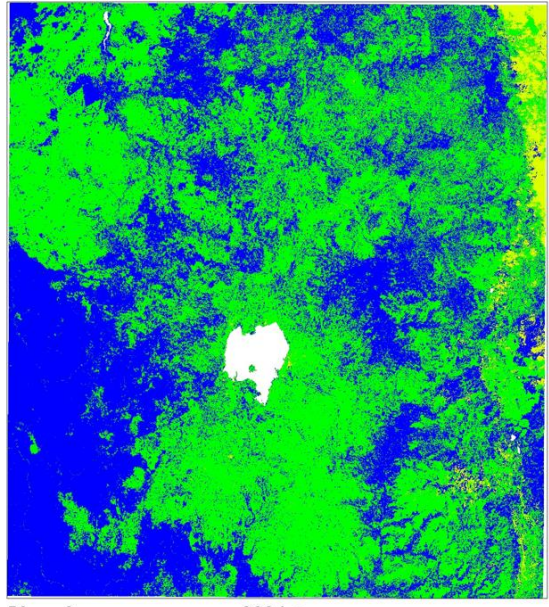
ShBrEv	tropical		1 (0.2985)													
ShBrEv	arid_warm		1 (0.04183)													
ShBrEv	arid_cool					1 (0.02984)										
ShBrEv	temp_warm					1 (0.06789)										
ShBrEv	temp_cool					1 (0.04876)										
ShBrEv	boreal_warm							1 (3.692E-5)								
ShBrEv	boreal_cool							1 (0.01846)								
ShBrDe	tropical			1 (0.8805)												
ShBrDe	arid_warm			1 (1.132)												
ShBrDe	arid_cool						1 (0.1903)									
ShBrDe	temp_warm						1 (0.18)									
ShBrDe	temp_cool						1 (0.08915)									
ShBrDe	boreal_warm						1 (0.0162)									
ShBrDe	boreal_cool								1 (0.04638)							
ShNeEv	tropical	1 (0.001368)														
ShNeEv	arid_warm	1 (0.0458)														
ShNeEv	arid_cool				1 (0.1434)											
ShNeEv	temp_warm				1 (0.06115)											
ShNeEv	temp_cool				1 (0.04497)											
ShNeEv	boreal_warm				1 (0.05666)											
ShNeEv	boreal_cool							1 (0.2603)								
ShNeDe	tropical		1 (0.006356)													
ShNeDe	arid_warm		1 (0.06844)													
ShNeDe	arid_cool						1 (0.03497)									
ShNeDe	temp_warm						1 (0.01333)									
ShNeDe	temp_cool									1 (0.002936)						
ShNeDe	boreal_warm									1 (0.007115)						
ShNeDe	boreal_cool									1 (0.1306)						



■ 1 wet  
■ 2 post-wet  
■ 3 dry

Phenology h43v15 2005

Phenology h43v15 2011



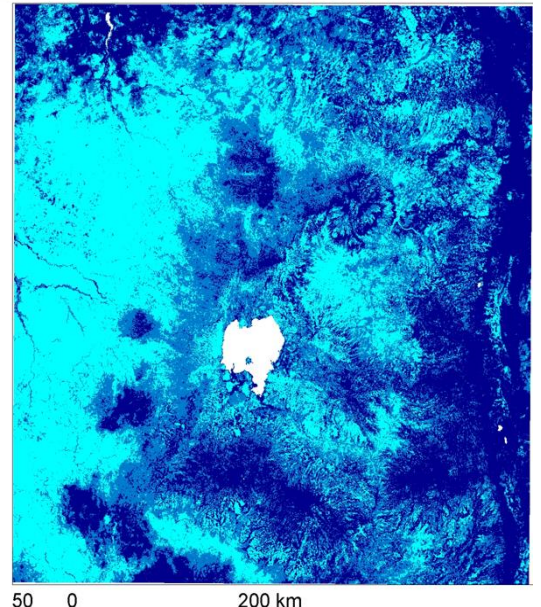
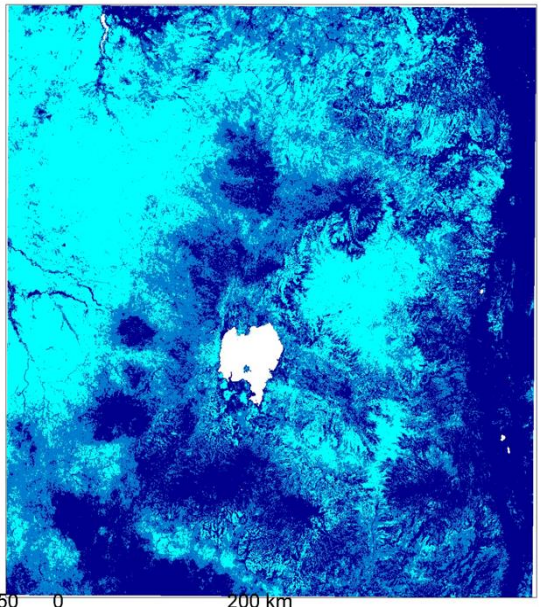
50 0 200 km

50 0 200 km

■ l Low seasonality  
■ m Mid seasonality  
■ h High seasonality

Seasonality h43v15 2005

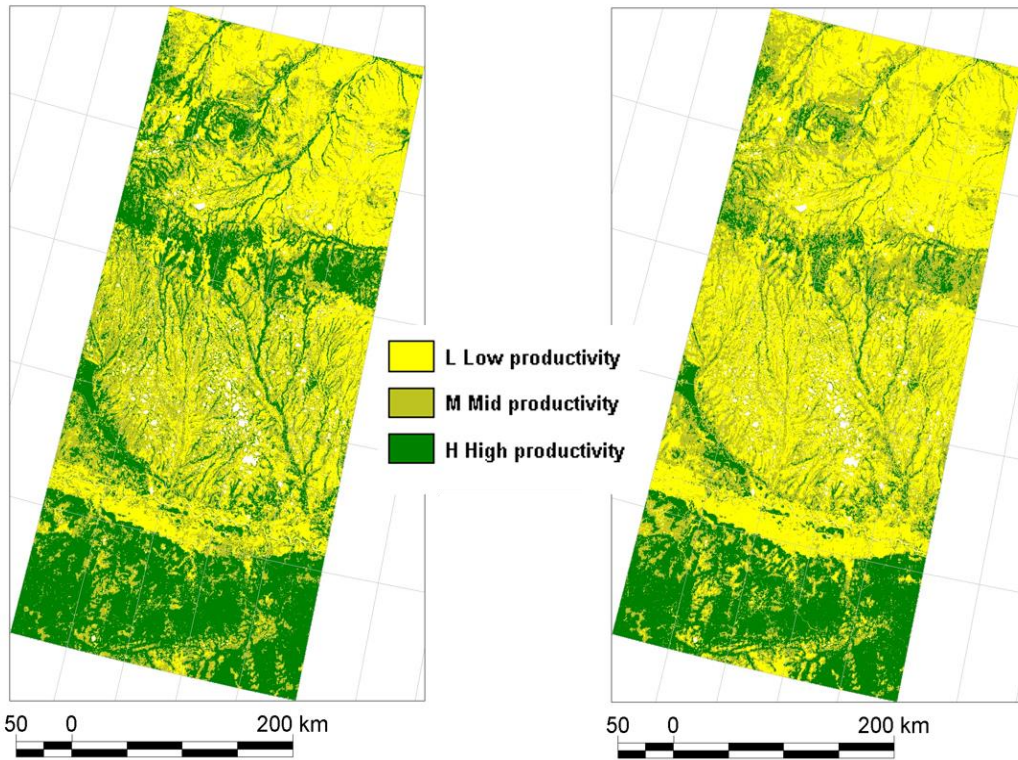
Seasonality h43v15 2011



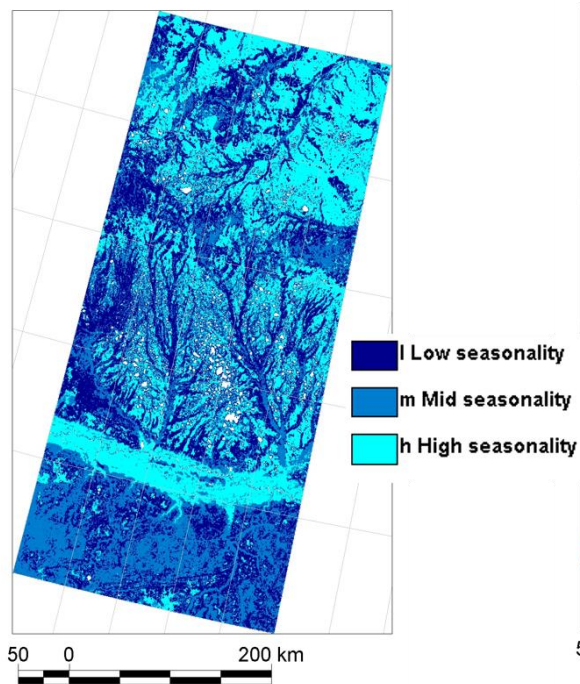
50 0 200 km

50 0 200 km

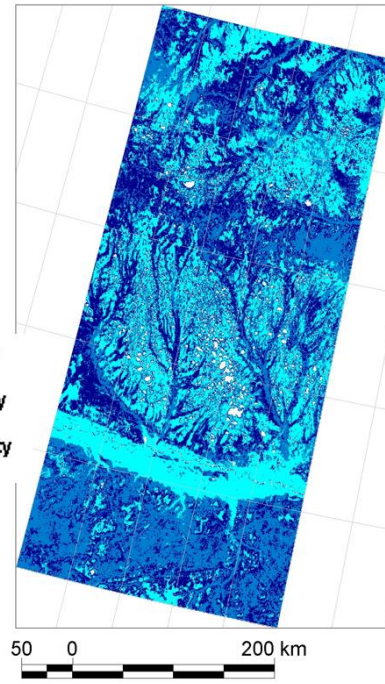
Productivity h50v05 2005



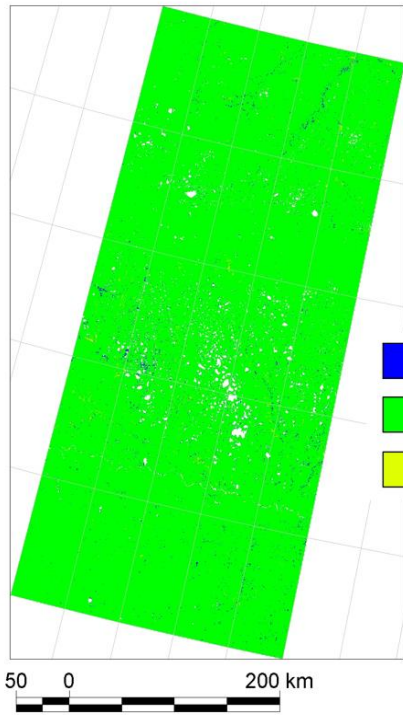
Seasonality h50v05 2005



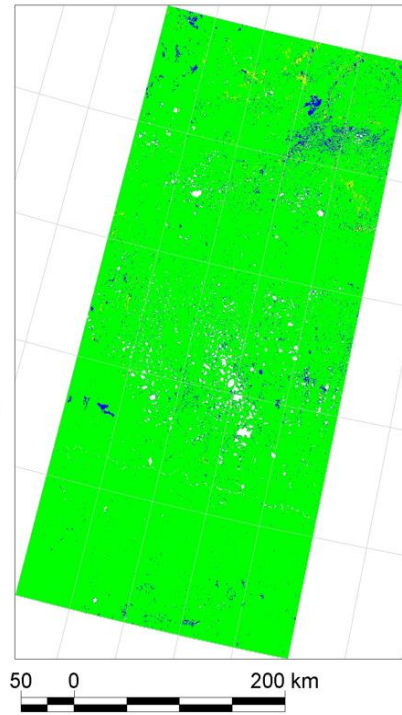
Seasonality h50v05 2011



Phenology h50v05 2005

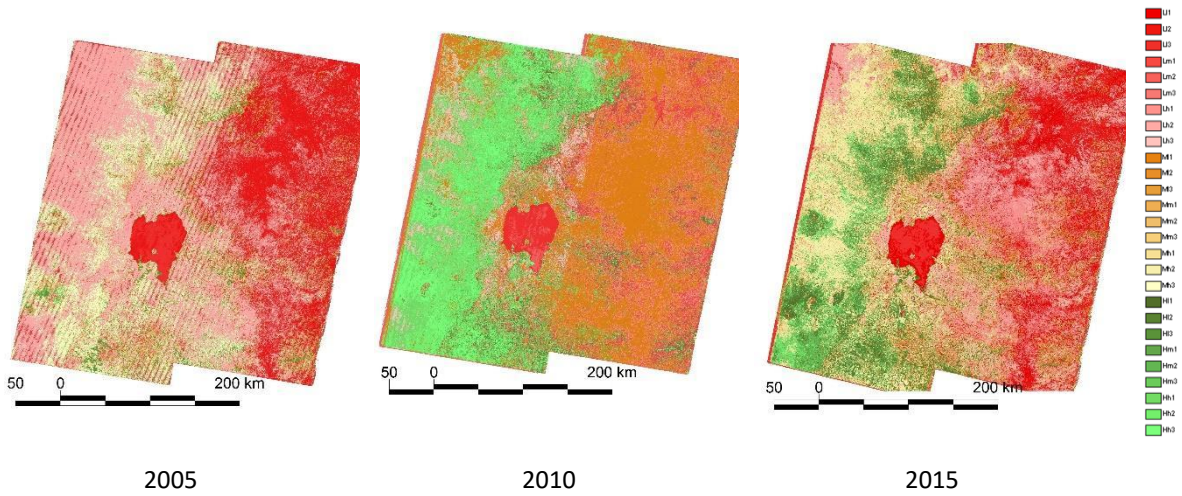


Phenology h50v05 2011

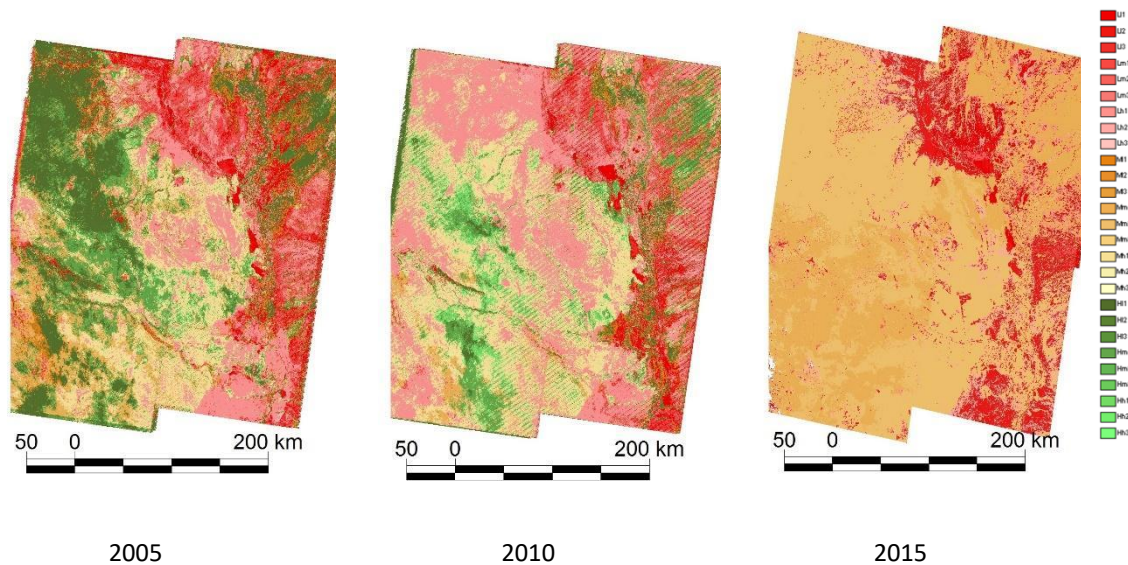


### Appendix C: EFT maps at HR

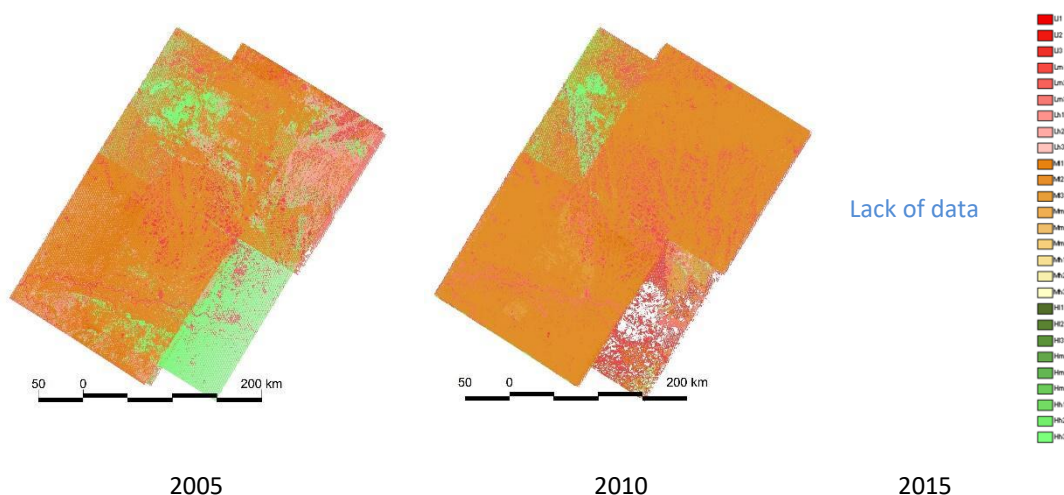
Sahel: WRS2 tiles: 169-51, 169-52, 170-51, 170-52



Amazonia: WRS2 tiles: 227-72, 227-73, 228-72, 228-73



Siberia: WRS2 tiles: 58-16, 158-17, 159-16, 159-17



## Appendix D: Land Cover Changes Mapping priorities

Some LCC have been prioritized for the generation of the LCC maps. Since the purpose of this yearly product was to focus on abrupt changes, the climate teams have defined for each region the main abrupt changes that can occur and could affect the regional climate. The report of this work is given in the following.

Abrupt changes or land disturbances could be the consequence of extreme meteorological events (storms, drought, high precipitation, fires) or human disturbances (deforestation/afforestation, crop plantation, urban/industry settlements ...). These land disturbances may be different in each region and they are summarized in the following table based on a quick bibliography. The transitions which should be dominant and are the more significant for climate modellers are highlighted in bold.

	South Brazil	Ethiopia	Western Siberia
<b>Land disturbances</b>	<ul style="list-style-type: none"> <li>- deforestation, land clearing by fires or cutting</li> <li>- afforestation</li> <li>- crop plantation</li> <li>- floodings linked to heavy precipitation or dam construction</li> </ul>	<ul style="list-style-type: none"> <li>- drought events</li> <li>- deforestation</li> <li>- afforestation</li> <li>- crop plantation</li> <li>- floodings linked to heavy precipitation or dam construction</li> </ul>	<ul style="list-style-type: none"> <li>- landslides linked to heavy precipitation on thawed permafrost areas</li> <li>- floodings linked to extreme precipitation events or dam construction</li> <li>- longer freezing periods during cold years</li> <li>- fires/storm/tree cuttings leading to land clearing</li> <li>- infrastructure developments for gas exploitation in the arctic zone</li> </ul>

Given these land disturbances and keeping in mind that what really matters for climate modelling is to account for the fraction of bare soil and to separate woody from grass/low vegetation, we have revised the tables and come to the modifications highlighted with a blue code. We have made the assumptions that some tropical crops like coffee/cacao/palm tree will be classified as shrubs evergreen and that frozen rivers will be detected and classified in ice/snow. We did not account for built areas/roads since they are not modeled in many climate models but they could be of interest for some users. These assumptions need to be discussed with the processing team accounting for their detection capabilities and classification rules. We need also to know what will be done for the transitions which are not defined as priorities: if the changes are detected, will they be flagged and not interpreted or not detected at all?

BRAZIL														
Year N	EBT	DBT	ShrE	ShrD	Grass	Crop	WoFlo	GrFlo	Li&Mo	Bare	Build	OpWs	OpWp	Sn&Ic
Year(N+1)														
EBT			X			X								
DBT				X										
ShrE	X	X			XX	XX	X	X		XX				
ShrD	X	X			X	X	X	X		XX				
Grass	XX	XX	XX	XX		X	X	X		XX				
Crop	XX	XX	XX	XX	XX		X	X		XX				
WoFlo	XX	X	X	X										
GrFlo					X	X								
Li&Mo														
Bare	XX	XX	XX	XX	X	X				XX				
Build	XX	XX	XX	XX	XX	XX				XX				
OpWs													XX	
OpWp												XX		
Sn&Ic														

X interesting change      XX relevant change      ○ Drastic change      Highest priority change

The transitions from any kind of trees to grasslands and croplands correspond to the deforestation from agricultural developments (managed grasslands and croplands).

The transitions from grasslands to evergreen shrubs correspond to woody crops plantations like cacao, coffee, palm trees which will be identified as shrubs. It corresponds also to afforestation in protected areas (which can occur also with deciduous species), but we considered that the transitions from grass to evergreen shrubs is more important to detect than the transitions from grass to deciduous shrubs which have both a seasonal cycle.

The transitions from all type of woody vegetation to bare soil (deforestation/fires) are also all important to map and date in the model with expected largest impacts for woody to bare soils.

On the other way round, all the transitions from bare soil to shrubs and crops (afforestation and crop plantation) are important but we put a priority to evergreen shrubs, compared to deciduous for which the fraction of bare soil will differ the most compared to the other classes.

ETHIOPIA															
Year N	EBT	DBT	ShrE	ShrD	Grass	Crop	WoFlo	GrFlo	Li&Mo	Bare	Build	OpWs	OpWp	Sn&Ic	
YearN+1															
EBT			X		X	X									
DBT				X	X	X									
ShrE	XX	XX				XX				XX					
ShrD	XX	XX				XX				XX					
Grass	XX	XX	XX	XX		X				XX					
Crop	XX	XX	XX	XX	XX					XX					
WoFlo												X			
GrFlo															
Li&Mo															
Bare	XX	XX	XX	XX	XX	XX									
Build	XX	XX	XX	XX	X	X				XX					
OpWs								X						X	
OpWp								X				X			
Sn&Ic															

X interesting change      XX relevant change      (o) Drastic change      (■) Highest priority change

As in Brazil, the deforestation/afforestation transitions are important to detect. Therefore, the transitions from any kind of trees to grasslands and croplands correspond to the deforestation from agricultural developments (managed grasslands and croplands).

The transitions from grasslands to evergreen shrubs correspond to woody crops plantations like cacao, coffee, palm trees which will be identified as shrubs. It corresponds also to afforestation which is almost done with deciduous species as we saw in our bibliography.

The transitions from all type of woody vegetation to bare soil (deforestation/fires) are also all important to map and date in the model. Compared to Brazil, we add here the transitions from grass/crops to bare soil which could occur during drought events as Ethiopia experienced some years.

On the other way round, all the transitions from bare soil to shrubs and crops (afforestation and crop plantation) are important but we put a priority to shrubs for which the fraction of bare soil will differ the most compared to crops.

SIBERIA																
Year N	EBT	ENT	DBT	DNT	ShrE	ShrD	Grass	Crop	WoFlo	GrFlo	Li&Mo	Bare	Build	OpWs	OpWp	Sn&Ic
YearN+1																
EBT																
ENT					XX											
DBT																
DNT						XX										
ShrE	XX	XX	X			XX	X			X				XX		
ShrD	XX	XX	X			XX	X			X				XX		
Grass	XX	XX	X	X	X			XX			XX	X		XX		
Crop	XX	XX	X	X	X		X									
WoFlo																
GrFlo																
Li&Mo																
Bare	X	X	X	X	X	X	XX	X								
Build	X	X	X	X	X	X	X	X								
OpWs					XX	XX	XX	XX				XX			XX	X
OpWp														XX		(X)
Sn&Ic														X	(X)	

X interesting change      XX relevant change      (o) Drastic change      (■) Highest priority change

In western Siberia, we put the priorities on deforestation resulting of fires/cuttings, landslides detection and river freezing (even if some climate models don't simulate this process, but will do in a near future).

The deforestation events correspond to the transitions from woody classes to grasslands.

The transitions from all type of woody and grassland vegetation to bare soil corresponding to landslides which are also all important to map and date in the model (it was also a requirement from the permafrost CCI team).

	Ref	CCI_HRLC_Ph1-CAR		
	Issue	Date	Page	
	3.0	28/10/2022	90	

We consider also as a priority, the transitions from permanent water (lakes and rivers) to snow/ice class as the result of cold/warm winter temperatures. We did not consider as a priority the transitions flooded/unflooded since they could be more linked to global warming and follow a gradual process and not abrupt events.